ANALYSIS OF COUPLED BODY MOORING AND FENDER SYSTEM

A Thesis

by

HARISH GIRIJA SASIDHARAN PILLAI

Submitted to the Office of Graduate Studies of
Texas A&M University
in partial fulfillment of the requirements for the degree of

MASTER OF SCIENCE

August 2005

Major Subject: Ocean Engineering

ANALYSIS OF COUPLED BODY MOORING AND FENDER SYSTEM

A Thesis

by

HARISH GIRIJA SASIDHARAN PILLAI

Submitted to the Office of Graduate Studies of
Texas A&M University
in partial fulfillment of the requirements for the degree of

MASTER OF SCIENCE

Approved by:

Chair of Committee,	John M. Niedzwecki
Committee Members,	Richard S. Mercier
	Robert H. Stewart
Head of Department,	David V. Rosowsky

August 2005

Major Subject: Ocean Engineering

ABSTRACT

Analysis of Coupled Body Mooring and Fender System. (August 2005)

Harish Girija Sasidharan Pillai, B.Tech.,

Cochin University of Science and Technology,

Kerala, India

Chair of Advisory Committee: Dr. John M. Niedzwecki

The hydrodynamic excitation and response behavior of multi-body systems with varying degrees of coupling presents many challenges for designers of offshore structures. In this study, attention is focused upon the analysis and interpretation of experimental data obtained for an unmanned deepwater mini-Tension Leg Platform (mini-TLP) coupled to a tender barge. Each body has its own mooring system and the bodies are connected by two breast lines extending from central points on the mini-TLP to central points on the bow and stern of the tender barge. A fender system is located between the two platforms. Thus the two floating bodies are constrained to move together in surge and yaw while they are free to move independently in heave, roll and pitch with some limitations on sway.

The data of the individual records are characterized using statistical moments, including skewness and kurtosis, to examine the degree of non-Gaussian behavior. Correlation analysis and cross spectral analysis are used to investigate the relationships between selected measurements such as the motion of each vessel, tensions in the mooring lines and tendons and the forces on the fenders. The analysis shows that the coupling effects reduce the mooring line and tendon tensions significantly and that the motions of the two vessels influence the line tensions and fender forces. The data distribution patterns followed by the parameters and the corresponding extreme values are also investigated.

DEDICATION

To God and my family for guiding me throughout my life

ACKNOWLEDGMENTS

TABLE OF CONTENTS

LIST OF FIGURES

LIST OF TABLES

1. INTRODUCTION: THE COUPLED BODY SYSTEM

1.1 Problem description

The environmental forces exerted on an offshore structure and the resultant structural responses are generally random in nature and therefore statistical methods are needed to study the effect of these random forces and responses. Most importantly, these methods enable us to predict extreme values which are critical in the design of these structures. Each structure in the ocean presents a unique problem thus making it difficult to generalize the design procedure and hence model testing becomes important in understanding the response behavior of ocean going vessels and offshore structures.

This thesis research will investigate a series of coupled mini-TLP – barge experiments conducted at the OTRC model basin. Statistical methods will be used to characterize the coupled body motions, mooring line tensions, tendon tensions and fender forces. Of particular interest are the cases where the mini-TLP and the barge are held together with a soft mooring connection and a fender system and the uncoupled case where they are in closer proximity with no connection between the bodies. The objective is to investigate the statistical correlation between the forces and responses enabling us to better understand how these parameters affect one another. In addition, the thesis research will review the concepts of detailed static analysis of mooring lines (single and multi-line analyses) and some aspects of dynamic mooring analysis. The basics of fender design will also be covered. These studies are expected to lay the foundation for future experiments involving multiple bodies operating in close proximity such as the LNG carrier –LNG terminal concept.

1.2 Literature review

Technical articles relevant to this study are presented in Table 1-1 with brief comments and are presented in the order of the year in which they were published.

_____

This thesis follows the style of Marine Structures.

The papers reviewed were selected to provide a brief overview on developments in mooring design and analysis and design of fender systems with relation to offshore vessels and statistical data analysis. The effects of mooring line elongation on calculations were included in some of the analyses reported. In particular, articles addressing methods of analysis for vessels held in place by multiple numbers of lines such as barges, Spars etc under regular and random waves were included in this review.

Table 1-1. Summary of literature review

Year	Title	Author(s)	Summary
1973	On Prediction of Extreme Values	Michel K. Ochi	The paper discusses the prediction of the extreme values of a stationary random process having a spectrum of arbitrary bandwidth. Statistical methods are used to predict the extreme values and derive formulas for the same for a given number of observations and time. The most probable extreme value and the probability of exceedance are calculated. These methods and formulas are used to predict the extreme value of the pitching motion and acceleration of a ship in irregular seas. Data from an experiment conducted in a wave tank is used to illustrate the analysis methods. It was shown that the test values compare well with the predicted most probable values.
1988	Application of Extensible Catenary theory to determine the displacement of a moored ship	T.Wren J.N.Fawcett J.S.Burdess	The paper details a simple method of calculating line tensions and cable lengths and arrives at formulas for cable length on floor and critical tension for a single line. Then it addresses the case of multiple mooring lines and calculates the total vessel displacement and line tensions. The analysis method also takes into account elasticity of cables, i.e. line extension and compares values for extensible and inextensible cases. The authors convincingly illustrate that the inclusion of mooring line extensibility significantly influences the results.

Table 1-1. Continued

Year	Title	Author(s)	Summary
1997	Dynamics of a moored barge under regular and random waves	A.P.Shashikala R.Sundaravadivelu C.Ganapathy	The paper presents a comparison of results from experiments conducted on a single point moored (SPM) barge and the numerical analysis of the same with the FLUID software. The paper discusses the principles used behind the program, free surface and body surface boundary conditions and the calculation of the velocity potential Φ based on linear diffraction and refraction analyses. The Bernoulli equation is then used to estimate the hydrodynamic forces acting on the body followed by the calculation of the restoring force on the body. The paper defines the center of gravity of the barge at G and also another point P on the barge that varies. Next, the stiffness matrix due to the mooring member is found and these results are used to solve the equation of motion. The hydrodynamic forces and the exciting forces are derived. These results were validated using experiments on a 1:25 scale model of the SPM barge (conducted at Ocean Engineering center, IIT Madras). Springs were used to replicate the mooring system and separate sets of experiments were run with two different spring stiffnesses (10 and 32 N/mm) each at GP=0 and GP=0.08 m, i.e. P at 80 mm above G. The barge model was tested first in regular waves and then random waves described by the PM spectrum. The mooring line forces and the surge and heave accelerations and the pitch angle are measured. The results showed there was very low surge response in lower frequency ranges if the barge was moored. Surge response was very high if the barge is freely floating. Horizontal mooring lines showed no influence on heave response. Pitch motions were also influenced by mooring, but not significantly. An increase in the height of the mooring point attachment showed an increase in surge and pitch response. Also, higher the mooring stiffness, lesser the surge and higher the mooring point, higher the surge and pitch. The analytical and experimental results were seen to match.

Table 1-1. Continued

Year	Title	Author(s)	Summary
1997	Mars Tension Leg Platform – Use of scale model testing in the global design	R.S.Mercier W.E.Schott C.T.Howell E.B.Denison R.Gopalkrishnan	A comprehensive scale model testing program is studied for the global design of the Mars TLP. Results for tendon tensions, platform offset and underdeck clearances are obtained. The experimental results were compared to a numerical model and were found to be a close match. The high frequency, nonlinear diffraction effects were stronger than expected, causing larger resonant heave, pitch and roll. Larger tendon tensions and larger wave elevations beneath the deck than allowed for in the preliminary design caused significant changes in the final design and sizing of the TLP. The experiment, the calibration of the instruments and the environments considered are explained in detail. The frequency content in the tendon tensions and the extreme value probability distributions are investigated. Based on these observations, the standard design recipes are modified.
1999	Experiments and Analysis with fully coupled Mini-TLP / Barge system	P.Teigen J.M.Niedzwecki	The paper compares Gaussian and Gumbell distributions for extreme values of response data from a Mini-TLP and Barge experiment. Model scale is 1:62. Original TLP has 8 tethers and 12 risers. Model has 4 (1 each corner) equivalent tethers and 12 risers. 3 realizations each of 3 hr duration were run. Then each realization is split into 9 intervals of 20 min each. The maxima of each are taken to obtain 9x3 = 27 maxima (9 maxima each for a 3hr realization). Then the Gumbell (double exponential) and Gaussian distribution for these are compared. 50% exceedance probability level for Gumbell & Gaussian pdfs are calculated, i.e. 50% of realization values are above this. Gaussian method is found to be too conservative and the mean of the measured maxima is consistently on the low side of the Gaussian 50% exceedance probability predictions. Gumbell 50% exceedance probability prediction is closer to the mean of the maxima. The aim was to determine if Gumbell distribution provides a better representation of extreme value predictions when compared to Gaussian distribution. But the results suggest that neither provides an accurate representation and that other distributions may better reflect the data.

Table 1-1. Continued

Year	Title	Author(s)	Summary
2000	Mooring System : From initial design to Offshore Installation	Ricardo B. Portella	The paper deals with the detailed design of a 16 line mooring system for a semi-submersible (converted from a derrick barge) operating in Campos basin (offshore Brazil) at 1080 m water depth. The entire design process is split into 2 stages. The first stage involves the wind tunnel model tests, motion analysis, static riser analysis etc followed by the initial mooring system design and the tank model tests. The 1:240 model for the wind tunnel test is very detailed and involves all details that contribute to the drag. The model tests were used to check the design calculations and to prove the feasibility of the unit to operate at the specified location. A scale model of 1:140 was used. The tests provided information on the total system response, air gaps, mooring line and riser tensions and platform motions. Stage 2 involved corrections to the initial design system based on installation and operating considerations and results from the model tests in Stage 1. Changes to design were made due to restrictions in sizes of available materials.
	Fender System Design		The paper lists methods that are used in fender design. It details the kinetic energy method of fender design where the fender is designed based on the energy to be absorbed by the fender. It takes into account various factors such as the velocity, eccentricity, virtual water mass that moves with the ship when in motion etc and defines coefficients for each. Usually when there is ship motion and the fenders come into play, the vessels are not parallel to each other and hence the entire kinetic energy is not transmitted to the fenders. The paper also looks at different methods of calculations for these coefficients. Methods of determining the fender spacing are also detailed. They are determined from the vessel geometry or equating the environmental forces to the fender reaction forces.

1.3   Objective of research

The basic objective of the thesis research is to use statistical methods to characterize and interpret the data obtained from the coupled mini-TLP – barge experiments. Of particular interest is the identification of correlation patterns between different parameters with particular emphasis on mooring line and tendon tensions and fender forces. Integral to this analysis is the characterization of the environmental forces and the resultant vessel motions and their influence on the mooring and tendon tensions and fender forces.

The experimental setup involved a two-body system with a mini-TLP and a barge coupled to each other with breast lines and separated by a fender system. The mini-TLP was conceived as a more basic and cost effective option to a fully loaded TLP. Since a mini-TLP has a much reduced deck area and storage capacity, supply barges are used to carry the supplies. The concept of a mini-TLP was developed for possible use at a target location in the Gulf of Guinea, off the coast of Nigeria. Model tests of this two-body system were carried out in the OTRC model basin at a scale ratio of 1:62 for a target water depth of 1000 meters. The system was tested both under individual wind, wave and current forces and also in a complete, combined environment (wind + wave + current). Each case was run for two configurations – the head sea condition (0° environmental heading) and the beam sea condition (-90° heading). Fig. 1-1 represents the experimental set-up for the 0° and -90° headings.

Both coupled and uncoupled cases for the different environment headings were investigated as part of the experimental test program. For testing purposes, the mini-TLP design was modified from the original concept. The deck was raised the equivalent of 5 meters in order to allow both West Africa and Gulf of Mexico environments to be studied. The mini-TLP with its deep and slender columns is more sensitive to current than to waves while the barge with a shallower draft and large water plane area is more sensitive to waves.

0° heading   -90° heading
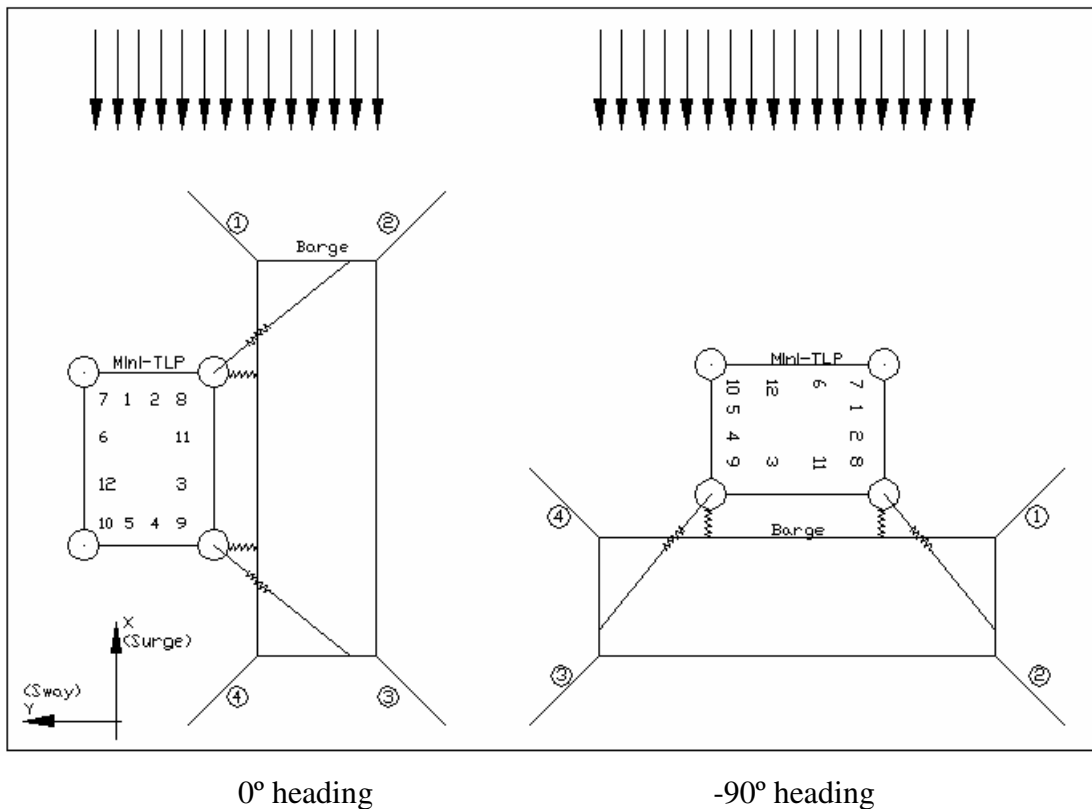
Fig. 1-1. Mini-TLP and barge experimental setup for 0° and -90° headings

Both the prototype design and the model had separate mooring systems. The mini-TLP as designed would have 8 tethers (2 in each corner) and 12 risers, a combination of 3 different types for gas, water injection and production. The spread mooring system for the barge had 8 mooring lines, two in each corner at departure angles of 30° and 60° from the longitudinal axis. To reduce the set up time required when changing model headings, an equivalent spring system of 4 mooring lines (1 in each corner) at a departure angle of 45 deg from the barge's longitudinal axis was used for the experiment. Rather than attempt to model the true catenary system, each equivalent line was made up of 2 in-line linear springs configured so that the global force vs. offset curves would be matched.

The coupling between the TLP and the barge system was achieved by the fender and breast line system. This system was modeled by matching the stiffness between the two bodies in three directions – surge-surge, sway-sway and yaw-yaw. The fender system for the tests was represented by compression springs which were attached to a bar. The compression forces in the springs were measured using a load cell to obtain the fender forces. To avoid friction between the barge and the fender system, paddles were used to support the compression springs. The measurements for each wave heading included:

- The waveheights, fender wave, current and wind data.
- Surge, sway and heave for the TLP and motion in all DOF for the barge.
- The tensions in the 4 barge mooring lines, measured at the fairleads.
- Tensions in all risers measured at the sea floor and
- The compression force between the two bodies, i.e. the fender forces.

The results from the experiments conducted on the floating two body system are analyzed using statistical methods. The focus of this study involves statistical analysis of mooring line and tendon tensions and the fender forces in the system, and determination of how they are related to each other and with the incident environment (wind, current and waves) for the two different environment headings of 0° (head seas) and -90° (beam seas). The coupled and uncoupled cases are analyzed separately and the results are compared to determine how each parameter influences the other. The objective is to investigate how the environmental forces and the body motions affect the mooring line tensions, tendon tensions and the fender forces, as well as to study the coupling effects between the forces and the body motions.

1.4 Methodology

The programming environment, MATLAB – Version 7.0.0.19920 (R14) was used to read the data files containing the experimental measurements and to analyze this data. The analysis of the experimental results involves four parts. The first part of the analysis focuses upon characterization of the data using statistical parameters such as mean,

variance, standard deviation, skewness, kurtosis and the bandwidth of each of the various time series data sets.

The skewness and kurtosis values indicate the Gaussian nature of the distribution function. A Gaussian probability density function (pdf) and its corresponding cumulative density function (cdf) are used and the variation of the data from these curves is studied. Although the data appears to follow a near normal distribution pattern, the extreme values do not necessarily follow a similar distribution. The extremes of the data are generally observed to follow the Weibull distribution pattern. The extreme values including the positive maxima, positive minima, negative maxima and the negative minima are obtained from the time series. Each are superimposed on to ideal Weibull pdf and cdf curves and the conformance of the extreme data values to the Weibull distribution is checked. A curve of probability of exceedance of the values is also used to check the conformance of the extreme values to an ideal Weibull distribution.

Next, the spectral density functions and transfer functions are computed from the data. A spectral analysis of the data is then used to investigate the frequency content. The results obtained for the coupled case for the two headings are compared with the results for the uncoupled case and the variations in the mooring/tendon tensions and the fender forces due to the 2-body interaction are identified.

Finally, the cross spectral and correlation analyses are performed. This step involves evaluation of the cross spectral density, the coherence and the correlation for different parameter combinations. These characterizations provide a true picture of the interaction between the two bodies. These include the influence of the TLP and barge motions and the environmental forces on the mooring line and tendon tensions and fenders forces. The coupled and uncoupled cases are compared to identify the two-body interaction effects on the mooring lines, tendons and fenders.

2. MOORING AND FENDER ANALYSES

Mooring lines are used to hold vessels in relatively fixed positions at an offshore site. Ships drift under the influence of environmental forces due to a combination of wind, wave and current. Often, the functionalities of moored offshore structures call for restrictions in the excursion of the vessel. For example, modern offshore drilling / production platforms cannot be allowed to drift beyond a certain tolerance limit (typically 4 – 6 % of the water depth as a rule of thumb) as such excursions may cause the risers to buckle. Mooring lines are used to constrain the vessel excursions within specified limits.

The most common type of mooring used in ships and other floating platforms is the spread mooring system. For maximum efficiency, each mooring line is divided into a combination of chain and wire segments. Chains are usually used at the segments passing through the chain jack and the fairleads and the end segments at the sea floor. The chain is stored in chain lockers in the vessel and is led through chain jacks and fairleads. The lines are set at a 'pretension' which sets the vessel to the desired location under a certain combination of environmental forces. Then as the force configuration changes (due to changes in wind, wave or current), the lines may be either paid out or hauled in to maintain the vessel position. Mooring analysis involves the calculation of vessel displacement and line tensions for a mooring configuration under a particular environmental force and determination of whether the line tensions are within the permissible limits.

2.1 Static analysis of single mooring lines

Consider a generic floating platform held in position by the spread mooring system shown in Fig. 2-1 with four mooring lines. Fig. 2-2 shows a profile view of the system. Each line has three segments. Assume a flat sea bottom without any slope. Each mooring line under its own weight takes on a catenary curve shape. A catenary is defined as the curve assumed by a perfectly inextensible chord of uniform density and cross section hanging freely from two fixed points as shown in Fig. 2-3.
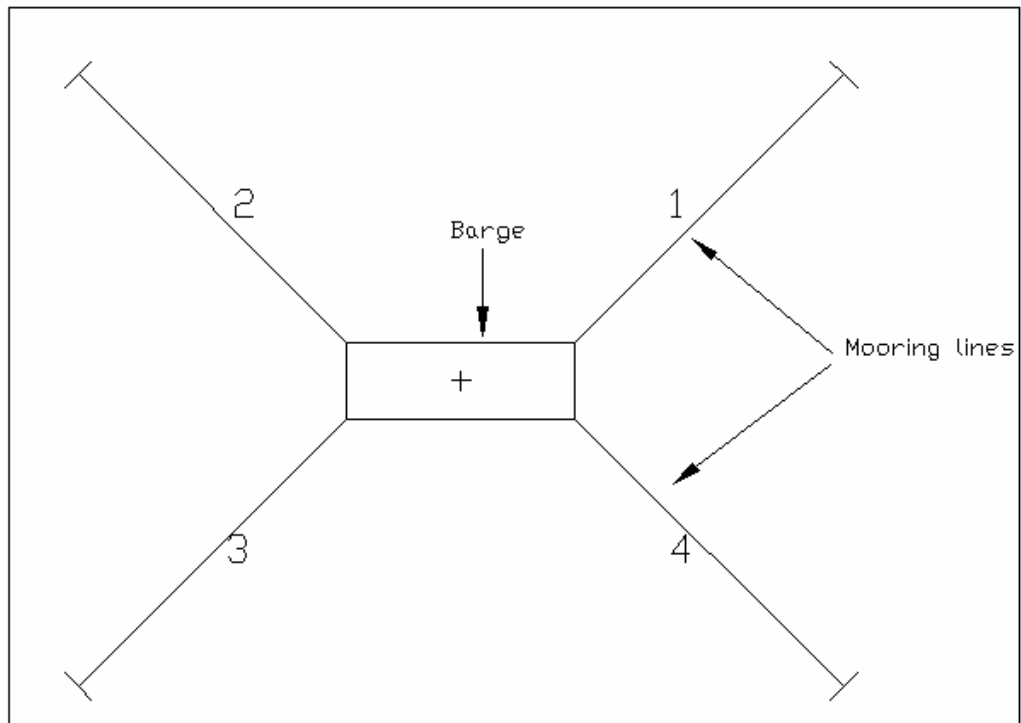
Fig. 2-1. Top view of the spread mooring system
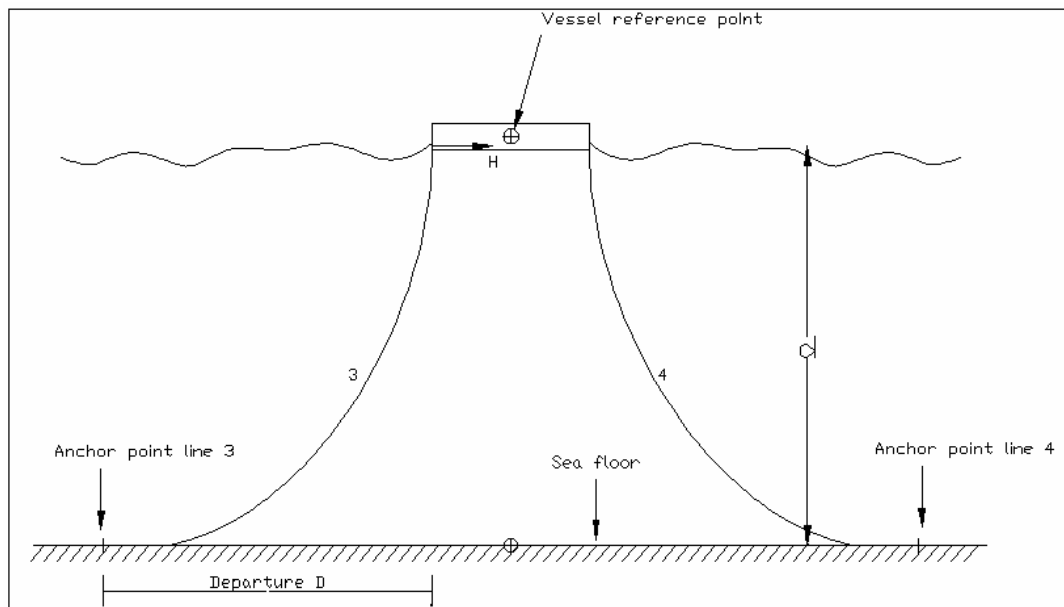
Fig. 2-2. Profile view of the mooring system
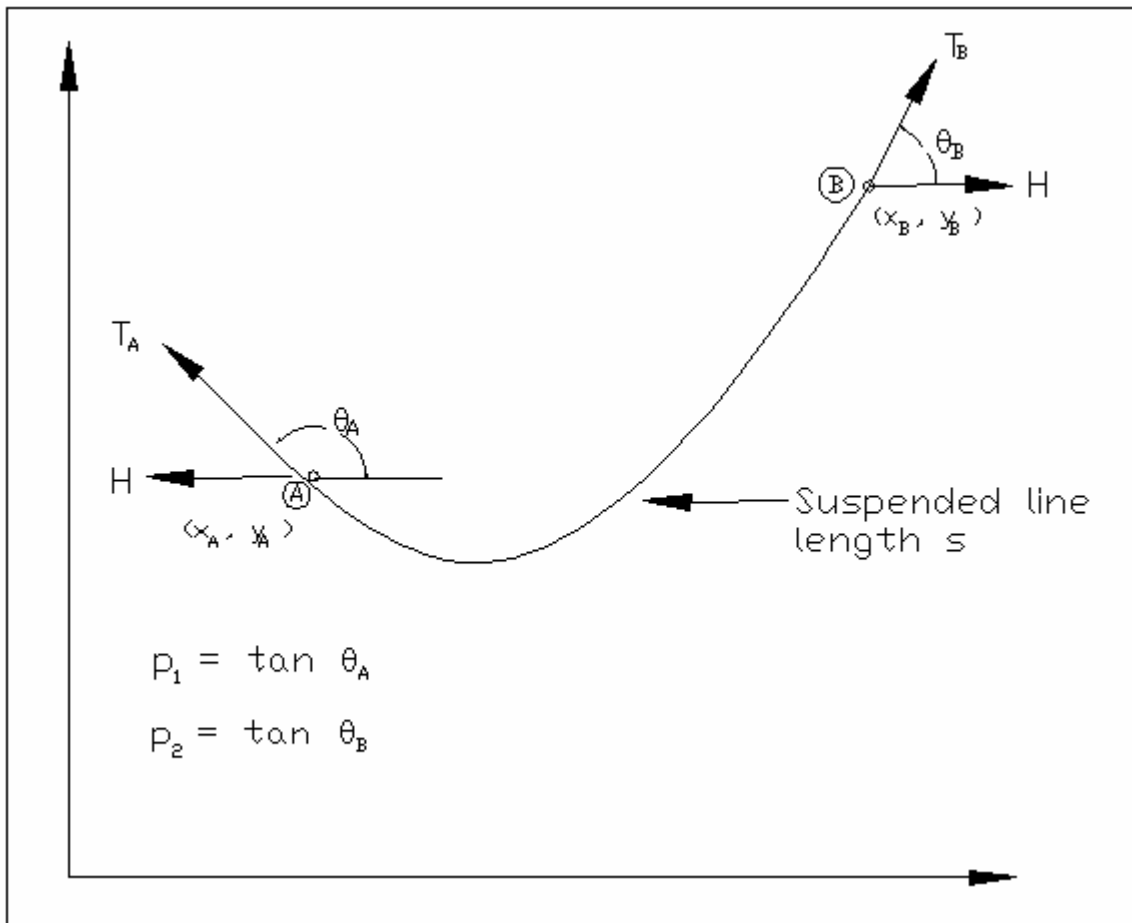
Fig. 2-3. Catenary sketch of a cable hanging between two points

Applying equilibrium conditions in the horizontal and vertical directions at points A and B, and through a series of algebraic manipulations using the catenary equation, the following three equations are derived [1-4].

$$y_B - y_A = \frac{H}{w}\left\{\sqrt{1 + p_B{}^2} - \sqrt{1 + p_A{}^2}\right\} \tag{1}$$

$$x_B - x_A = \frac{H}{w}\left\{\sinh^{-1} p_B - \sinh^{-1} p_A\right\} \tag{2}$$

$$\frac{w}{H} S = p_B - p_A \tag{3}$$

where H = horizontal restoring force as shown in Fig. 2-3

w = submerged weight of the lines per unit length

$p_A = \tan\theta_A$ and $p_A = \tan\theta_B$, θ being the angle made by line with the horizontal at points A and B respectively.

x_A, x_B, y_A, y_B are the coordinates of the points A and B with the anchor point as the origin. Solving these three equations for a given system, the parameters needed for the mooring line analysis can be obtained. The aim is to arrive at a departure versus restoring force curve which enables us to find the extent of vessel offset for different environmental loads.

Clump weights are often used at segment intersections in mooring lines to increase the restoring force and thus increase efficiency. Again resolving the free body equilibrium condition at the joint 1 in Fig. 2-4 and Fig. 2-5 where W is the clump weight, the following equation is derived:

$$p_{1B} - p_{A1} = \frac{W}{H} \tag{4}$$
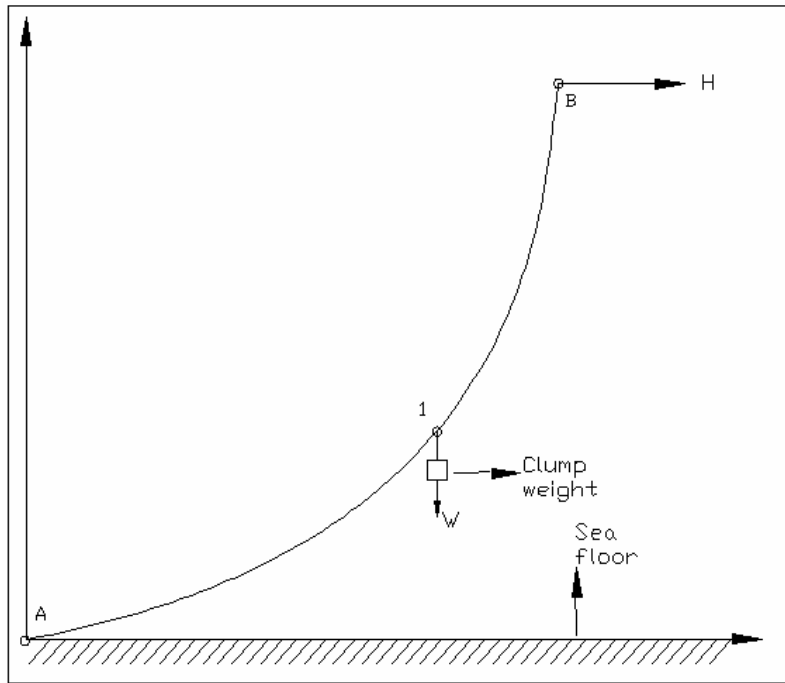
Fig. 2-4. Mooring line with clump weight
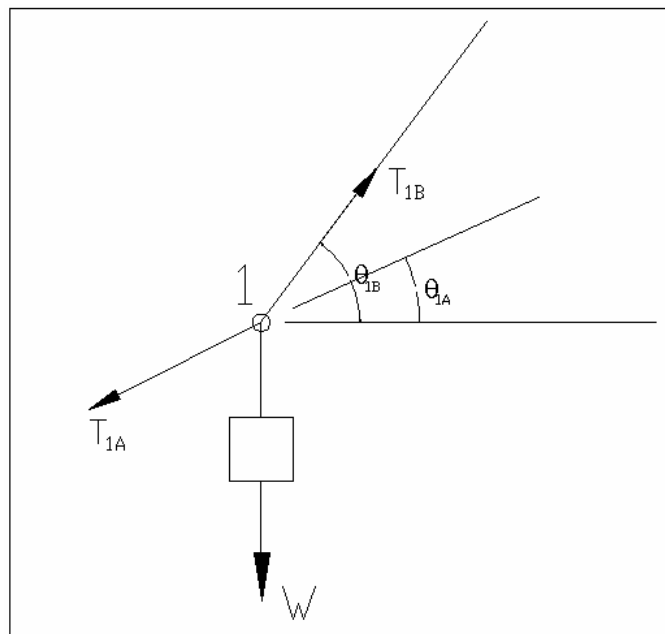
Fig. 2-5. Forces on joint 1

The clump can be partially supported by the lines and partially by the seafloor in some force configurations. If, $p_{1B} - p_{A1} = \dfrac{W}{H}$, then the clump is fully supported by the lines. If, $0 \leq p_{1B} - p_{A1} \leq \dfrac{W}{H}$, then the clump rests on the sea bottom and is partially supported by the line and partially by the seafloor.

When buoys are used between segments as shown in Fig. 2-6 and Fig. 2-7, there is a buoyant force acting due to the buoy. If D is the displacement volume of the buoy, W_{SW} is the weight of sea water and $W_{B'}$ is the weight of the buoy, then the buoyant force due to the buoy is

$$B' = (DW_{SW}) - W_{B'} \tag{5}$$

And following a similar procedure of calculation as before, the following relation is obtained:

$$p_{21} - p_{2B} = \dfrac{B'}{H} \tag{6}$$
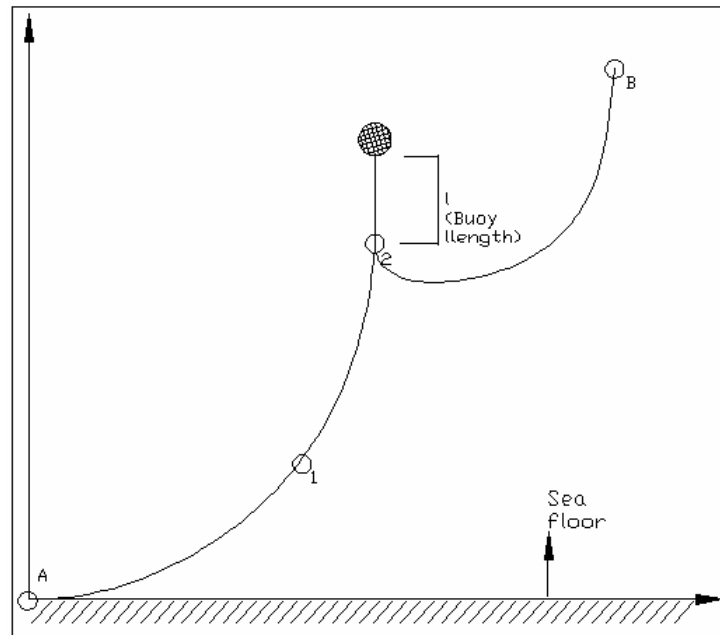
Fig. 2-6. Mooring line supported by buoy
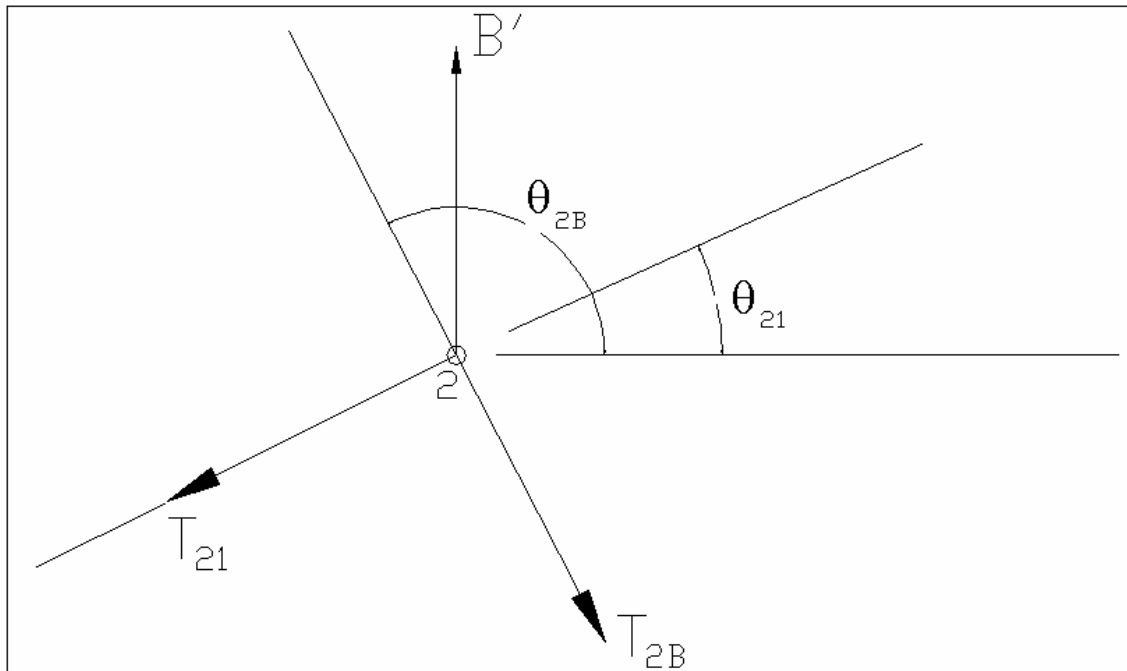
Fig. 2-7. Forces on joint 2

In most cases, mooring lines have more than one segment. Consider a multi-segmented mooring line where the environmental forces applied to the moored body due to wind, current and waves and the resultant force direction is known. The solution algorithm for this system is as follows:

1. Consider the first segment (anchor segment) to be on the floor completely and all the following segments to be fully extended. Apply equations (1), (2) and (3) subsequently on each segment to finally obtain the y coordinate of the final fairlead segment.

2. If h is the water depth and $y > h$, then follow an iterative process by laying line from the extended segments on the sea floor calculating the fairlead y coordinate at each step. Solution is obtained when $y = h$.

3. If $y < h$, then repeat the iterative process by pulling up line from segments already on floor and calculating fairlead y coordinates until $y = h$.

4. If any of the segments have clump weights or buoys, apply equations (4) and (6) to get the solution.

5. By varying the environmental force H, a chart of departure vs. H can be obtained for the line.

2.2 Static analysis of spread mooring lines

Spread mooring systems are quite common in the offshore industry. For example, deep water Spar platforms typically have 16 to 20 lines. In the static analysis of a spread mooring system, the mooring lines are analyzed individually and their resultant contributions are combined to provide the resultant restoring forces and vessel displacement. The aim is to keep this excursion under permitted limits and to ensure that all the line tensions are within the critical tension limit.

Consider a mooring system shown in Fig. 2-8 [1] with n number of lines. As seen in the previous section, the departure D versus H curve for each line is obtained. This system is in equilibrium for a force H. If there is a change in the force due to wind, wave or current, the vessel is displaced in the direction of the resultant force. Assume that the vessel is displaced by a distance X in the horizontal plane at an angle ϕ to the horizontal. If any cable is represented by j, consider any cable to be at an angle α_j to the horizontal. The departure for any cable represented by j will change from D to

$$D_j = \sqrt{D^2 + X^2 - 2DX\cos(\phi - \alpha_j)} \tag{7}$$

Also the angle α_j for the lines change to β_j which can be obtained geometrically. As an example, the angle β_1 for line 1 is shown in Fig. 2-8. To obtain the resultant restoring force acting on the ship the restoring force on each line is resolved in the direction of its application, the total resultant force being obtained as

$$F_R{}^2 = \sqrt{\left[\sum_{j=1}^{n} H_j \cos\beta_j\right]^2 + \left[\sum_{j=1}^{n} H_j \sin\beta_j\right]^2} \tag{8}$$

Using the restoring force value in the surge and sway directions the vessel displacement can be obtained from the D vs. H chart already calculated. If the vessel

displacement and line tensions are found to be outside reasonable limits, lines are suitably hauled in or payed off to maintain the vessel station. In design, one can also consider changing the characteristics of individual mooring lines, for e.g., segment lengths, chain sizes etc to keep the vessel excursions under the specified limits.
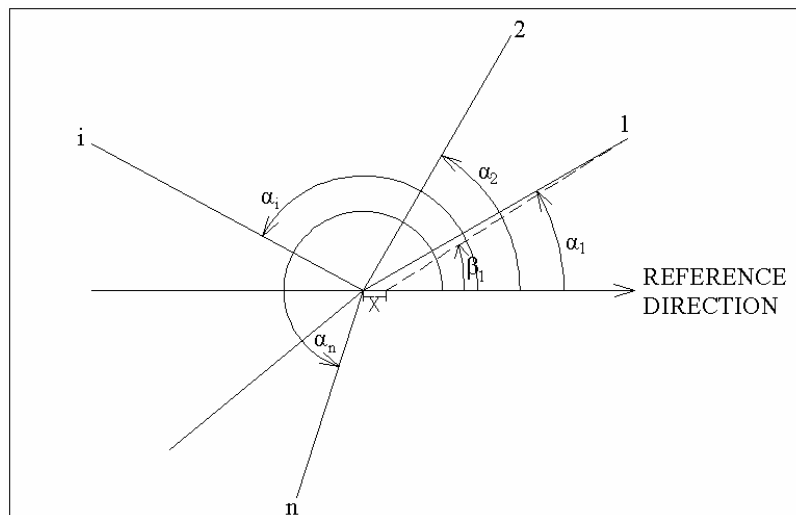
Fig. 2-8. The spread mooring system [1]

2.3   Brief review of dynamic mooring analysis

The static analysis of mooring lines provides a reasonable estimate for preliminary design. For more accurate results and final design of the mooring system, the dynamic effects of the environmental forces also have to be considered [5-7]. The non-linear platform behavior patterns and the variable drag coefficient C_D and lift coefficient C_F along the mooring lines also contribute to the dynamics. The dynamic force components are:

- Low frequency 2nd order motions: - The 2nd order wind and wave forces cause horizontal surge, sway and yaw motions at frequencies near the mooring system natural frequency.

- Wave frequency 1st order motions: - These are due to the 1st order oscillatory motions of the vessel at the wave frequency. When the inertial motions of a floating vessel dominate, these motions are generally not significantly affected by mooring stiffness.

For dynamic motion analysis, the low frequency and wave frequency vessel motions are determined using a hydrodynamic motion analysis program. The vessel motions are then translated to the fairlead and the vessel offset is calculated in accordance with the API regulations by adding the mean component already calculated through static analysis and the low and wave frequency component offsets. A time domain approach or a frequency domain approach may be used to determine the vessel offsets and line tensions. Although the time domain approach gives better and more detailed results, they are expensive and time consuming. Once the offsets are calculated, the line tensions are calculated along the same lines by adding the mean tensions to the tensions due to the low and wave frequency components.

In the case of tendon tensions for the TLP, there is an additional component at high frequency due to the higher order wave effects. These correspond to the heave, pitch and roll resonance modes of the TLP.

2.4 Fender analysis and design

2.4.1 Energy of impact

A fender is the interface between a ship and a shore facility or between two ships, and is used to absorb the energy of impact so as to protect the hull from damage. Designing the fender system involves calculation of the energy to be absorbed by the system and then designing the structure to meet this requirement.

The energy to be absorbed by the fender system can be expressed as [8]:

$$E_{fen} = \frac{1}{2}MV^2 C_e C_m C_s \qquad (9)$$

where, M is the mass displacement of the vessel and V is the approach velocity. According to [8], there are charts available based on vessel size, weight and type of impact from which a corresponding approach velocity can be chosen. For the mini-TLP

– barge experiment, both vessels are in motion and hence a relative velocity has to be considered for V in equation (9). During the experiment, accelerometers located on the barge and TLP measure the accelerations of the vessels from which the relative approach velocity can be calculated.

The vessels are not normally parallel to each other during impact. As a result the entire kinetic energy is not transferred to the fenders. This factor is represented by the eccentricity C_e. For the mini-TLP – barge experiments, C_e can be safely considered to be 1 as the vessels are coupled to each other and hence the impact is almost parallel to each other.

When the vessels move towards each other and impact, there is a certain mass of water that moves with the vessel. This is represented as the virtual mass coefficient C_m. The softness coefficient C_s is used to account for the proportion of impact energy absorbed by the fender. For soft fenders, where there is no deflection of vessel's hull, $C_s = 1.0$ as the entire energy is absorbed by the fender.

2.4.2 Fender spacing

Fender spacing is generally not more than 1/10th the length of the vessel [8]. However, for the mini-TLP – barge experiment, the fender spacing was determined by the column spacing.

For a standard ship shaped structure, the fender spacing can be determined from the vessels geometry as shown in Fig. 2-9 [8]. Note that

$$l = 2\sqrt{r^2 (r-h)^2} \tag{10}$$

where, r is the bent radius of the ships hull at the contact line and h is the compressed height of the fenders at their rated deflection.

The fender spacing can also be determined from wind and current forces. Equating them to the fender reaction forces, the following relationship can be obtained [8]:

$$N = \frac{R_a + R_c}{R} \tag{11}$$

where, N is the number of fenders required, R_a is the load due to the wind, R_c is the load due to the current and R is the fender reaction at rated deflection.
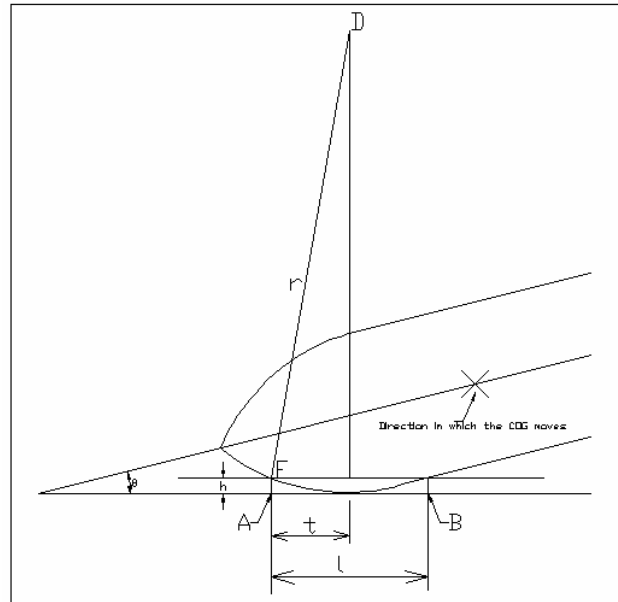
Fig. 2-9. Fender spacing [8]

2.5 Application to mini-TLP barge experiment

2.5.1 Mooring system

In the mini-TLP and barge experiment, the barge prototype had an 8-line spread mooring arrangement with 2 lines in each corner at departure angles of 30° and 60° with respect to the longitudinal axis. The TLP was outfitted with a fender system. To reduce the setup time required when changing headings of the system during the experiment, the barge 8-line mooring system was replaced with a 4-line system, each departing at 45 degrees from the barge's longitudinal axis.

The true catenary system was not reproduced, but two in-line linear springs were used to represent each of these lines. The global surge and sway static offset curves (D vs. H curves) for the original prototype mooring lines were calculated and the spring

mooring system was designed so as to match these global offset curves. Two in-line springs produce a bi-linear slope with a single point where the slope changes. Matching this model system to a non-linear prototype design requires the variation of several variables including both the spring constants, pigtail length, mooring line length and cut off length.

Such a system is represented in Fig. 2-10. Fig. 2-11 and Fig. 2-12 [9] show the superposition of the two in-line linear spring mooring design superimposed over the prototype design catenary system in surge and sway directions. From these figures, it is evident that the experimental and prototype values match quite well.
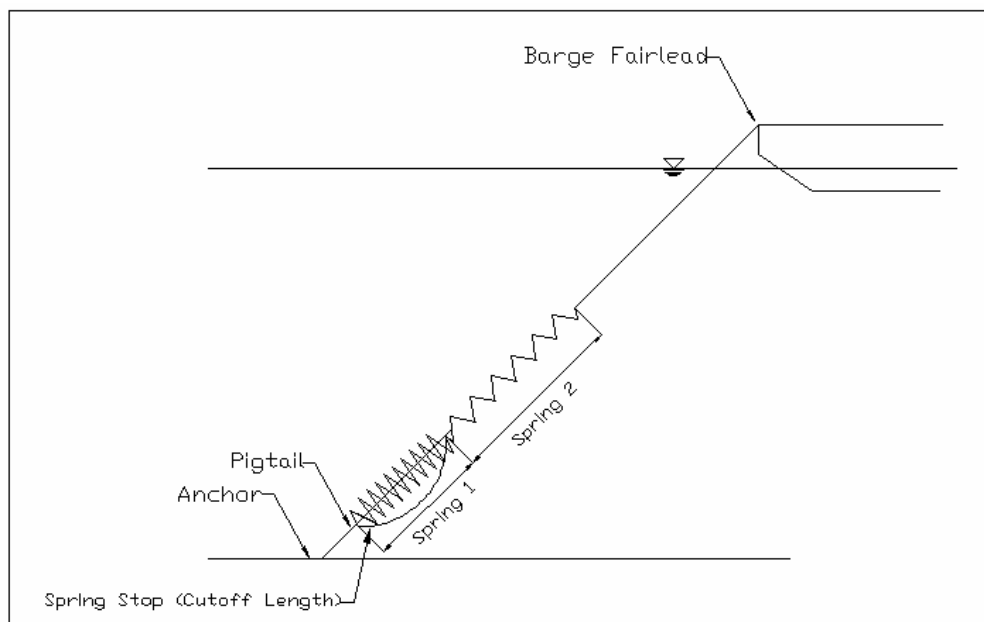
Fig. 2-10. Spring mooring system used for the experiment [9]

Surge Static Offsets
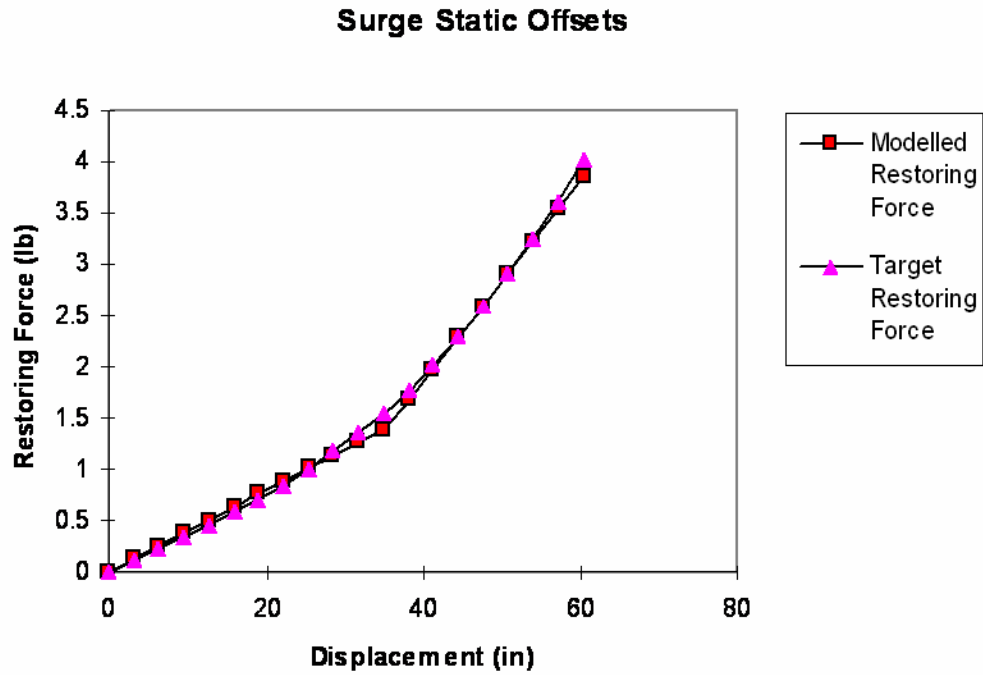
Fig. 2-11. Model vs. prototype surge restoring force comparison [9]

Sway Static Offsets
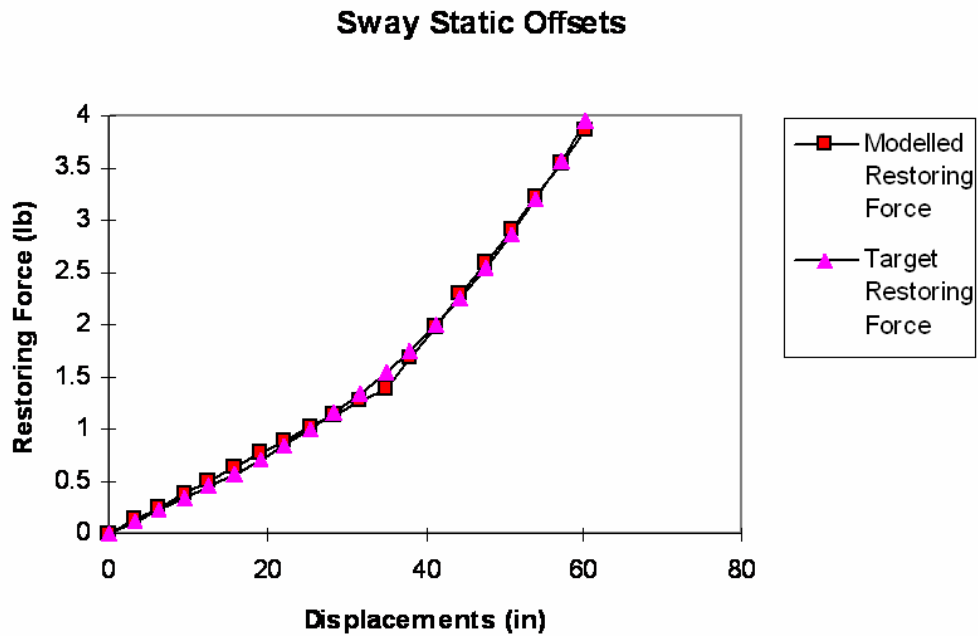
Fig. 2-12. Model vs. prototype sway restoring force comparison [9]

2.5.2 Fender and breast line system

The barge and the mini-TLP were coupled using a fender-breast line system. For the experiment, springs were used to represent the fender and the breast lines. The stiffness between the two bodies in the surge-surge, sway-sway and yaw-yaw directions were matched for the prototype and model to design the equivalent spring system. The compression spring constants for the fender system were 0.148 lb/in while the breast line spring constants were 0.194 lb/in. The compression springs were attached to a bar and a load cell was used to measure the compression force in the springs during testing. Paddles were used to act as supports for the compression springs and slide against the barge during testing so as to minimize friction. Fig. 2-13 shows the fender system installed on the mini-TLP [9].
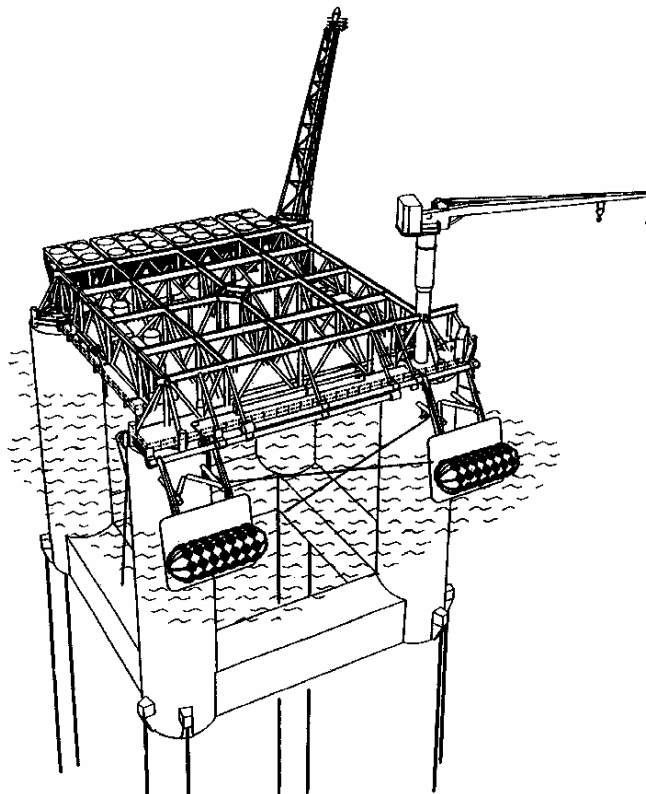
Fig. 2-13. The fender system used for the mini-TLP [9]

3. STATISTICAL ANALYSIS METHODS

Statistical analysis methods provide a common framework that enables one to interpret a variety of data sets. In the case of offshore structures, this allows the examination of variables that are central to the design of these structural systems. In particular, the non-linear response behavior for these structures is very complex and a methodical approximation is needed for design purposes. Statistical methods are integral to this design process as the parameters of interest are random processes. Through the use of statistical methods, it is possible to characterize design parameters of interest and to provide a basis for extreme value estimation.

3.1   Basic characterization of data

A data set can be characterized using some common and basic statistical formulae. These formulae define the basic attributes of time series data and the relevant equations are presented in this section. The equations presented here generally follow the form and notations used by Dr. Joseph Newton in his book 'Timeslab: A time series analysis laboratory' [10], while some of the equations follow the formulae used in MATLAB – Version 7.0.0.19920 (R14), May 06, 2004 [11].

If a random time series is defined as X consisting of n number of samples with mean $\bar{X}$, its variance σ^2 is defined as the measure of the spread of a distribution about its average value and can be expressed as

$$\sigma^2 = \sum \frac{(X - \bar{X})^2}{n}$$

(12)

The corresponding standard deviation s is a measure of how widely the measured values are dispersed from the mean value and is defined as

$$s = \sqrt{\frac{\sum (X - \bar{X})^2}{n}}$$

(13)

Skewness S is the measure of the asymmetry of the data around the sample mean and for a perfectly normal distribution, the skewness is zero. A negative skewness

indicates that the data is spread more to the left of the mean, i.e. towards lower values when compared to the mean. A positive skewness indicates that the data is spread more to the right of the mean. It is mathematically expressed in MATLAB as:

$$S = \frac{n}{(n-1)(n-2)} \sum \left(\frac{X - \bar{X}}{s} \right)^3 \tag{14}$$

The kurtosis, K indicates the crestedness or flatness of a time series distribution compared to the Normal or Gaussian distribution where for a Normal distribution, the kurtosis has a numerical value of 3. A Kurtosis greater than 3 indicates a narrowing and steeping of the distribution function while a value smaller than 3 indicates a flattening of the distribution. It is given by MATLAB as:

$$K = \left\{ \frac{n}{(n-1)(n-2)(n-3)} \sum \left(\frac{X - \bar{X}}{s} \right)^4 \right\} - \frac{3(n-1)^2}{(n-2)(n-3)} \tag{15}$$

The covariance function is used to characterize the relationship between sequential data points in a time series or between two different time series. For a single time series X, it is referred to as the autocovariance $\hat{R}_{XX}(\tau)$ and is defined in terms of a time lag τ between the data points as

$$\hat{R}_{XX}(\tau) = \frac{\sum_{t=1}^{n-\tau} \left[X(t) - \bar{X} \right] \left[X(t+|\tau|) - \bar{X} \right]}{n} \quad , |\tau| < n \tag{16}$$

The autocovariance function is always maximized at zero lag.

Similarly, for two different data sets X and Y, it is referred to as the cross covariance and is given by

$$\hat{R}_{XY}(\tau) = \frac{\sum_{t=1}^{n-\tau} \left[X(t) - \bar{X} \right] \left[Y(t+|\tau|) - \bar{Y} \right]}{n} \quad , |\tau| < n \tag{17}$$

For the times series represented by X, an autocorrelation function $\hat{\rho}_{XX}(\tau)$ can be defined for a time lag τ as

$$\hat{\rho}_{XX}(\tau) = \frac{\hat{R}_{XX}(\tau)}{\hat{R}_{XX}(0)} = \frac{\sum_{t=1}^{n-v}\left[X(t)-\bar{X}\right]\left[X(t+|\tau|)-\bar{X}\right]}{\sum_{t=1}^{n}\left[X(t)-\bar{X}\right]^2} \quad, |\tau| < n \tag{18}$$

The covariance of two sets X and Y provides an estimate of the degree of correlation between the data sets. The correlation between the two data sets defines the degree to which two quantities are linearly associated. This degree of correlation is often more conveniently expressed as the correlation coefficient $\hat{\rho}_{XY}(\tau)$. Specifically,

$$\hat{\rho}_{XY}(\tau) = \frac{\sum\left(X(t)-\bar{X}\right)(Y(t+\tau)-\bar{Y})}{\sqrt{\sum(X(t)-\bar{X})^2}\sqrt{\sum(Y(t)-\bar{Y})^2}} \tag{19}$$

The cross correlation function can also be expressed in terms of a lag τ as

$$\hat{\rho}_{XY}(\tau) = \frac{\hat{R}_{XY}(\tau)}{\sqrt{\hat{R}_{XY}(0)\hat{R}_{XY}(0)}} \tag{20}$$

Note that $\hat{\rho}_{XX}$ and $\hat{\rho}_{YY}$ are the autocorrelation functions of X and Y, while $\hat{\rho}_{XY}$ is the cross-correlation function. If $\rho_{XY}(\tau) = 0$, then the series X and Y are not cross-correlated.

This form leads to the presentation of the data in terms of a correlogram. The correlogram of a time series data set is the plot of the correlation coefficient $\hat{\rho}_{XX}(\tau)$ vs. τ for τ = 0,1,2,...,M for a maximum lag M where $-1 \le \hat{\rho}(\tau) \le 1$. If X(t+$\tau$) is perfectly linearly predictable from X(t), then $\hat{\rho}(\tau)$ is +1 and the line has positive slope. Similarly, if $\hat{\rho}(\tau)$ is -1, it indicates a perfect linear correlation between X(t) and -X(t+τ), the line having a negative slope. But if $\hat{\rho}(\tau)$ is 0, then there is no correlation between X(t) and -X(t+τ) and X(t+τ) is not perfectly linearly predictable from X(t).

We can also define cross correlograms between two different data sets represented by X and Y to see how they are related. In this case, the plot is between the cross correlation coefficient $\hat{\rho}_{XY}(\tau)$ and τ. If $\hat{\rho}_{XY}(\tau) = 0$, then the series X and Y are not cross–correlated.

3.2 Useful distribution functions

The cumulative density function (cdf) $P_X(x)$ for the series expresses the probability that a general value X of the random process is less than or equal to a threshold value x being considered. It is obtained by summing up / integrating the probabilities and is represented as

$$P_X(x) = \Pr(X \leq x) \tag{21}$$

For continuous distributions, the probability distribution function (pdf) $p_X(x)$ expresses the probability that the general value X lies between x and $(x + \Delta x)$ in the limit as $\Delta x \to 0$. It is obtained by integrating the pdf over the interval of interest and is

$$p_X(x) = \frac{dP_X(x)}{dx} = \Pr(x \leq X \leq x + \Delta x) \tag{22}$$

The necessary conditions are that $0 \leq P(x) \leq 1$ and the integral of the pdf over its entire range is equal to 1.

Every time series data set follows a certain distribution pattern. Some of the time series patterns observed for engineering results can be quite complex. There are some standard distribution functions that are well known [12-13] and if the data can be shown to follow any of these patterns, the analysis of the data may become straightforward. The most common is the Normal or Gaussian distribution pattern. A time series X, with mean $\bar{X}$ and variance σ^2, is said to be normally distributed if its pdf is given by

$$p(x) = \frac{1}{\sigma\sqrt{2\pi}} e^{\left[\frac{-(x-\bar{X})^2}{2\sigma^2}\right]} \tag{23}$$

The Gaussian pdf is illustrated in Fig. 3-1.
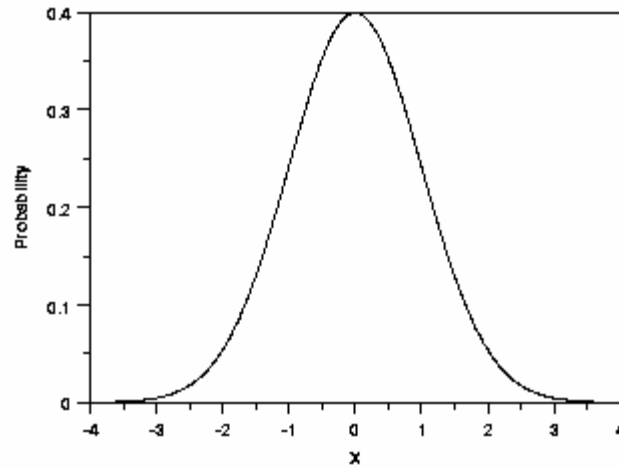
Fig. 3-1. Example of Gaussian pdf

For a normal distribution, the pdf is a symmetrical, bell shaped curve centered at its mean $\overline{X}$. For a standard normal distribution, $\overline{X} = 0$ and $\sigma^2 = 1$. Prior to analysis, all data is corrected to have a zero mean. The bandwidth ε for a process is represented as:

$$\varepsilon = 1 - \frac{m_2^{\,2}}{m_0\, m_4}, \quad 0 \le \varepsilon \le 1 \tag{24}$$

where m_0, m_2 and m_4 represent the zeroth, second and fourth moments of the spectra [14]. For a completely broad banded process, ε -> 1. Generally, the extreme values of a wide-banded Gaussian process are normally distributed.

The extremes of a narrow banded Gaussian process with a narrow banded spectrum (ε -> 0) generally follows the Rayleigh probability distribution. A typical Rayleigh pdf is shown in Fig. 3-2 and is given as:

$$p(x) = \frac{x}{\sqrt{m_0}} e^{\left[\frac{-x^2}{2m_0}\right]}, \qquad 0 < x < \infty \tag{25}$$
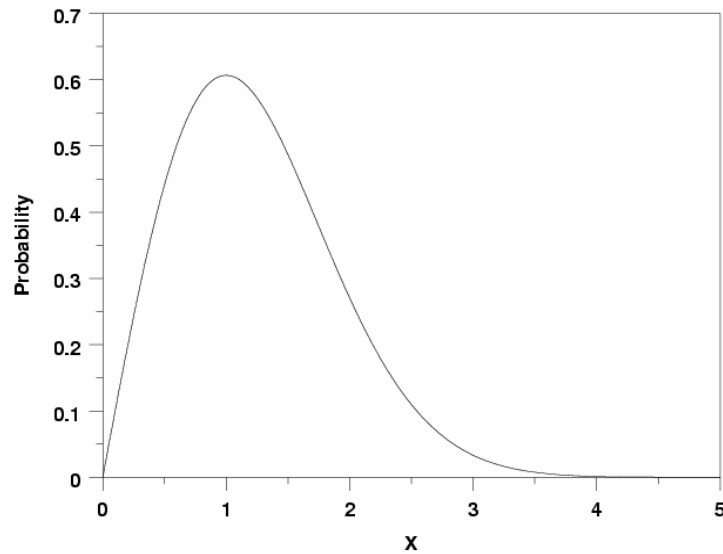
Fig. 3-2. Example of Rayleigh pdf

The standard Weibull distribution is represented by a 3-parameter pdf as [12]

$$p(x) = \frac{\beta}{\eta}\left(\frac{x-\gamma}{\eta}\right)^{\beta-1} e^{-\left(\frac{x-\gamma}{\eta}\right)^{\beta}} \quad where, \ p(x) \geq 0; \ x \geq 0 \ or \ \gamma, \beta > 0; \eta > 0; \ -\infty < \gamma < \infty \quad (26)$$

and β is called the shape parameter or Weibull slope. It refers to the slope of the line in the Weibull probability plot. Many probability distributions are not single distribution but are a family of distributions. This is due to the distribution having one or more shape parameters. Generally η is held constant for changes in β. η is called the scale parameter. The effect of an increase in η with constant β is to stretch out the pdf to the right and reduce the peak or height while a decrease in η with constant β shrinks the pdf to the left and increases the peak. γ is called the location parameter. It translates the pdf, i.e. the pdf simply shifts left or right on the horizontal axis. Often, the location parameter is not used and is set to zero to obtain a two parameter Weibull distribution.

If the process of interest is broad banded, several maxima and minima can occur during a cycle defined by zero crossings. For a process defined by X(t), the positive maxima are defined by $\left\{X(t) > 0, \dot{X}(t) = 0, \ddot{X}(t) < 0\right\}$ and the negative minima by

$\left\{ X(t) < 0, \dot{X}(t) = 0, \ddot{X}(t) > 0 \right\}$. Often for these extreme value predictions, the Weibull probability distribution gives a more accurate picture than the Gaussian or Rayleigh distributions.

3.3 Spectrum and cross spectral analysis

3.3.1 The concept of phase difference

Time series data usually has cycles, i.e. the data has crests and troughs. Two data sets are said to be 'in phase' with each other if the crests and troughs of the two series are almost respectively aligned with each other. They are said to be 'out of phase' if a crest in one series is almost aligned with a trough in the other or if a trough in one series is almost aligned with a crest in the other. So when two series represented by X and Y are in phase, a crest or trough in X is accompanied in a few time units by a similar crest or trough in Y. But when they are out of phase, the crest or trough in Y occurs within a few time units of a respective trough or crest in X.

3.3.2 Spectral density and coherence function

The Fourier transform of the autocorrelation function is equal to the power spectral density of the random process X (t) and can be expressed as

$$S_{XX}(\omega) = \frac{1}{2\pi} \int_{-\infty}^{\infty} R_{XX}(\tau) e^{-2\pi i \omega \tau} d\tau \qquad (27)$$

This equation yields the auto spectral density function $S_{XX}(\omega)$ of the process. The inverse of the spectrum recovers the correlation function as shown below.

$$R_{XX}(\tau) = \int_{-\infty}^{\infty} S_{XX}(\omega) e^{2\pi i \omega \tau} d\omega \qquad (28)$$

The cross spectral density is a complex valued function and can be expressed as

$$S_{XY}(\omega) = c_{XY}(\omega) - i q_{XY}(\omega) \qquad (29)$$

where, $c_{XY}(\omega)$ is the real part called the co-spectral density and $q_{XY}(\omega)$ is the imaginary part called the quadrature - spectral density.

The cross spectral density is also expressed in terms of its amplitude and phase as

$$S_{XY}(\omega) = A_{XY}(\omega).e^{i\phi_{XY}(\omega)}$$

where, $A_{XY}(\omega) = |S_{XY}(\omega)|$ represents the amplitude spectrum and

$$\phi_{XY}(w) = \tan^{-1}\left[\frac{-q_{XY}(w)}{c_{XY}(w)}\right]$$ represents the phase spectrum.

In the frequency domain, the response of a system to a unit force spectrum can be described by a transfer function. It is a normalized function of wave frequency and connects the input force spectral density to the spectral density of the response. It is expressed as

$$S_{RR}(f) = [H(f)]^2.S_{FF}(f) \tag{30}$$

3.3.3 Coherence spectrum

A complex coherency function can be defined from the cross spectral density as

$$w_{XY}(\omega) = \frac{S_{XY}(\omega)}{\sqrt{S_{XX}(\omega)S_{YY}(\omega)}} \tag{31}$$

and the Coherency function can be defined as [10]

$$W_{XY}(\omega) = |w_{XY}(\omega)| = \frac{A_{XY}(\omega)}{\sqrt{S_{XX}(\omega)S_{YY}(\omega)}} \tag{32}$$

The coherency spectrum is a normalized version of the amplitude spectrum and $w_{XY}^2(\omega)$ represents the squared coherency spectrum which measures the correlation between the two processes at each frequency. If both the auto spectral densities are positive, then the coherency function and thus the squared coherency function are between zero and one for all frequencies.

4. MINI-TLP – BARGE EXPERIMENTS

4.1   The experimental setup

The experiment involved a mini-TLP and a barge coupled to each other with breast lines. Tests were carried out on scale models of this two-body system in the OTRC model basin at a scale ratio of 1:62 for a target water depth of 1000 meters. The main particulars of the barge for the prototype and the scale model are given in Table 4-1 [9], while details of the mini-TLP are given in Table 4-2 [13]. The vessels are supposed to operate in the Gulf of Guinea, off the coast of Nigeria and the basic environmental patterns for the test are shown in Table 4-4 [13].

The natural periods of the TLP motion were compared with the actual available measured prototype results. Table 4-3 shows a comparison between the TLP heave, surge, pitch and yaw natural periods for the prototype and the model. As can be seen, the values are practically similar although the TLP surge and yaw values are slightly different for the experiment results.

Table 4-1. Main particulars of the barge for the prototype and scale model

Parameter	Prototype	1:62 scale
Weight	8533 MT	76.95 lb
Overall Length	91.5 m	58.1 in
Length at water surface	89.4 m	56.77 in
Width	27.5 m	17.46 in
Operating draft	3.7 m	2.35 in
Length of the flat portion of the barge bottom	72.9 m	46.29 in
COG (X)	0 m	0 in
COG (Y)	0 m	0 in
COG (Z)	6.8 m	4.32 in
Roll radius of gyration	7.77 m	4.93 in
Pitch radius of gyration	31.51 m	20.01 in
Yaw radius of gyration	31.91 m	20.26 in
Separation distance between TLP and barge	10 m	6.35 in

Table 4-2. Main particulars of the mini-TLP prototype

Parameter	Prototype Value
Draught (m)	28.50
Column diameter (m)	8.75
Column separation distance (m)	28.50
Pontoon height (m)	6.25
Pontoon width (m)	6.25
Deck clearance (m)	10.00
Mass (including topside and outfitting) (t)	5180
Displacement (t)	10320
Number of tethers	8
Number of risers (excluding catenaries)	12
Natural period surge / sway (s)	133
Natural period yaw (s)	121

Table 4-3. Comparison of natural periods for TLP motion

	Prototype values	Model results
TLP heave (sec)	2.6	2.6
TLP surge (sec)	133	140
TLP pitch (sec)	4.9	4.9
TLP yaw (sec)	121	101

Table 4-4. Basic environmental parameters

Parameter	Value
Significant wave height - H_s (m)	4.0
Peak period - T_p (s)	16.0
Peakedness factor – γ	2.0
Current velocity - V_c (m/s)	0.95
Wind velocity at $z_0 = 10$ m (m/s)	25.65
Wind velocity at platform reference height $z_r = 17.2$ m (m/s)	27.41

The riser and mooring line alignment and the TLP and barge positions for the 0 deg and -90 deg headings are as shown in Fig. 4-1. Fig. 4-2 represents the actual mini-TLP – barge system while Fig. 4-3 and Fig. 4-4 are pictures of the actual model tests conducted at OTRC. The complex instrumentation and the coupling system between the bodies can be clearly seen.
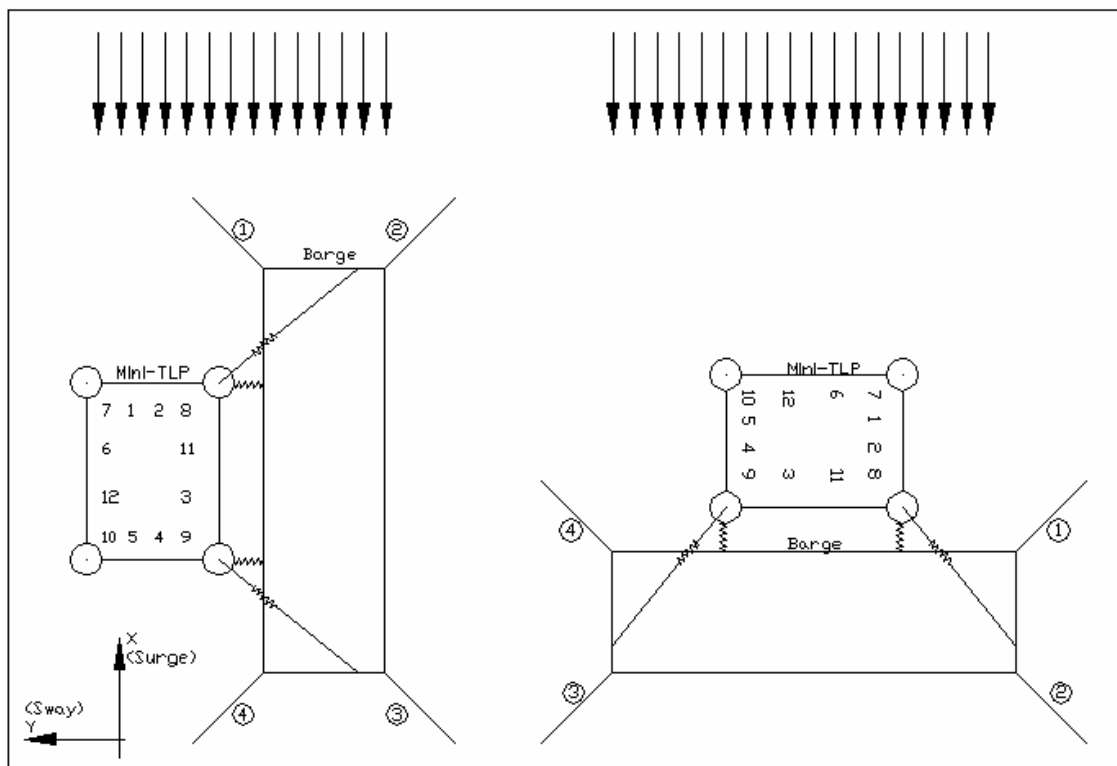

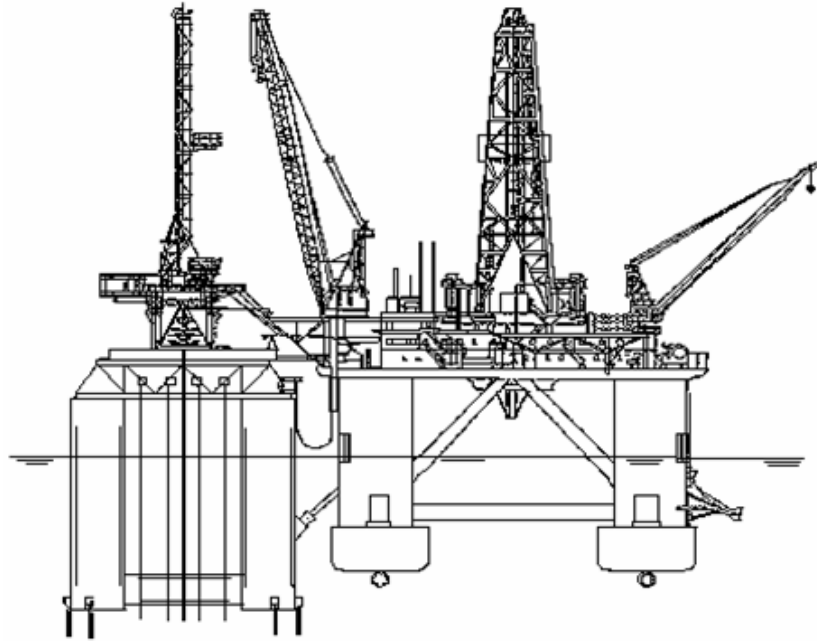Fig. 4-1. Mini-TLP and barge experimental setup

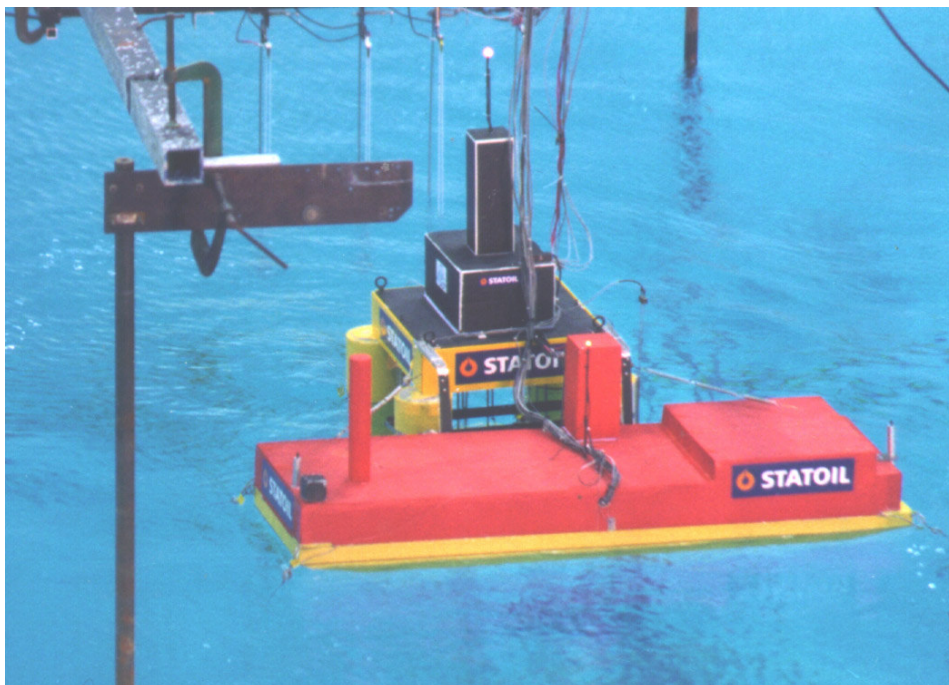Fig. 4-2. Actual representation of the mini-TLP and barge

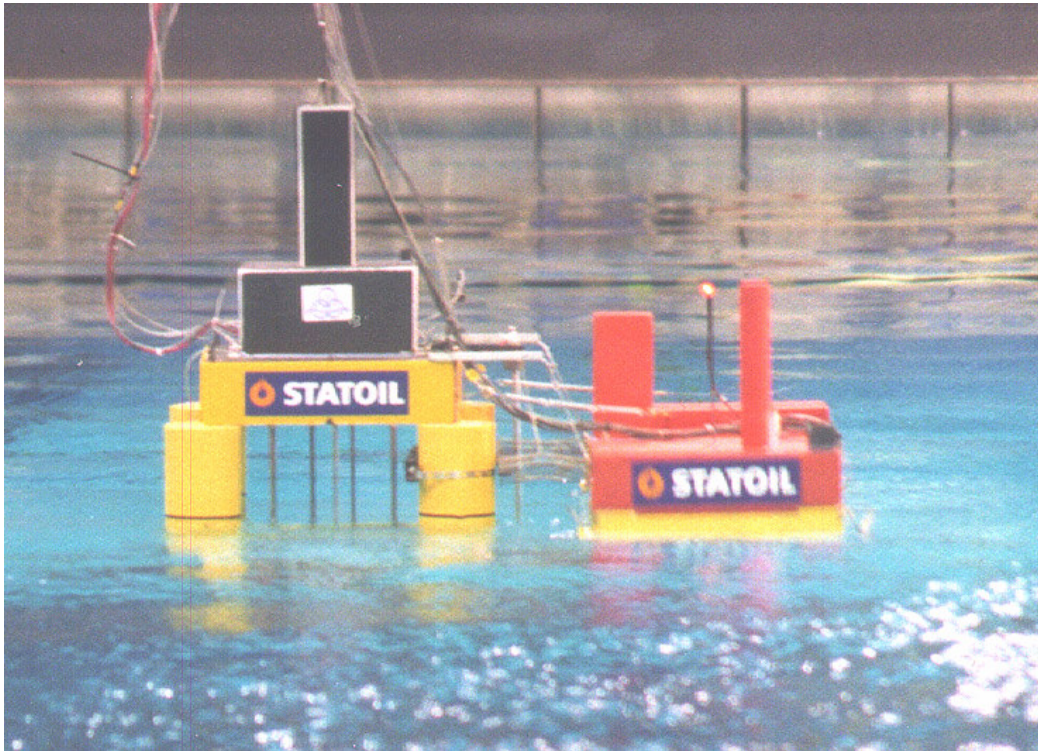Fig. 4-3. Profile view of the mini-TLP and barge experiment at OTRC

Fig. 4-4. Transom view of the mini-TLP and barge experiment at OTRC

4.2   Mooring and fender system

Each vessel had a separate mooring system. The mini-TLP originally had 8 tethers (2 in each corner) in addition to 12 risers. A spread mooring system of 8 mooring lines (2 in each corner with departure angles of 30 and 60 degrees from longitudinal axis) was used for the prototype barge in the original design. The barge mooring line details are given in Table 4-5 [9]. An equivalent spring system was used to represent the barge system and the fender-breast line system. The specifics of this system have been explained in Section 2.5.

Table 4-5. Prototype barge mooring properties

Number of mooring lines	8
Number of segments / line	3
Total line length	2750 m
Line departure angles	30 & 60 deg
Upper segment length	250 m
Upper segment diameter	2 in double cable
Mid segment length	2000 m
Mid segment diameter	3 in cable
Lower segment length	500 m
Lower segment diameter	4 in chain
Buoy between 1st and 2nd segments	Approx. 5m dia

4.3   The experiment

During the testing of the coupled system, the center of the mini-TLP was aligned with the center of the model basin's deep pit and when the system was rotated for measurements at different headings, the barge was rotated around the mini-TLP. The system was tested both under individual wind, wave and current forces and also in a complete, combined environment (wind + wave + current). The tests included the coupled and uncoupled cases for different environment headings. Studies were done for both West Africa and Gulf of Mexico environments. The TLP with its deep and slender columns is more sensitive to current than to waves while the barge with a shallower draft and large water plane area is more sensitive to waves. The measurements for each wave heading included –

- The waveheights, fender wave, current and wind data.
- Surge, sway and heave for the TLP and motion in all six DOF for the barge.
- The line tensions in the 4 mooring lines in the barge measured at the fairleads.
- Tensions in all risers measured at the sea floor and
- The compression force between the two bodies, i.e. the fender forces.

5. ANALYSIS OF COUPLED BODY MOORING AND FENDER SYSTEM

The next step involves analyzing the results from the experiments conducted on the floating two body system involving the mini-TLP and the tender barge. The process involves statistical analysis of mooring line and tendon tensions and the fender forces in the system, and determination of how they are related to each other and with the incident environment (wind, current and waves) for two different environment headings of zero and -90 deg. MATLAB – Version 7.0.0.19920 (R14) is used as a programming tool to read the data files containing the experiment results and analyze them. The distribution pattern of the data is first analyzed and their conformance to a Gaussian distribution is checked. Then the extreme values are determined and they are compared to an ideal Weibull distribution pattern. The final stage involves the spectral and cross-spectral analysis.

Table 5-1 lists the different cases that were analyzed and the associated file names from the experiment. A few cases such as the -90 deg heading wind only case did not have any available data and hence were not analyzed. Fig. 5-1 shows the time series plots for waveheight, current velocity and wind velocity while Fig. 5-2 shows the time series plots for mooring line and tendon tensions and fender forces. These results are for the 0 degree coupled wind + wave + current case.

Table 5-1. Test cases analyzed

| Condition	Description	Heading	
		0 deg	*-90 deg*
Current only	Coupled - all mooring	c1c0_001	c1c_90_001
Wind only	Coupled - all mooring	c1w0_001	No data
Waves only	Coupled - all mooring	c1v0_001(WA)	c1v_90_002 (WA)
Wind + Waves + Current	Coupled - all mooring	c1a0r1_001	c1a_90r1_004
Current only	Uncoupled – no soft mooring	uc1c0_001	uc1c_90_001
Wind only	Uncoupled – no soft mooring	No data	No data
Waves only	Uncoupled – no soft mooring	No data	uc1v_90_001 (WA)
Wind + Waves + Current	Uncoupled – no soft mooring	uc1a0r1_001	uc1a_90r1_004
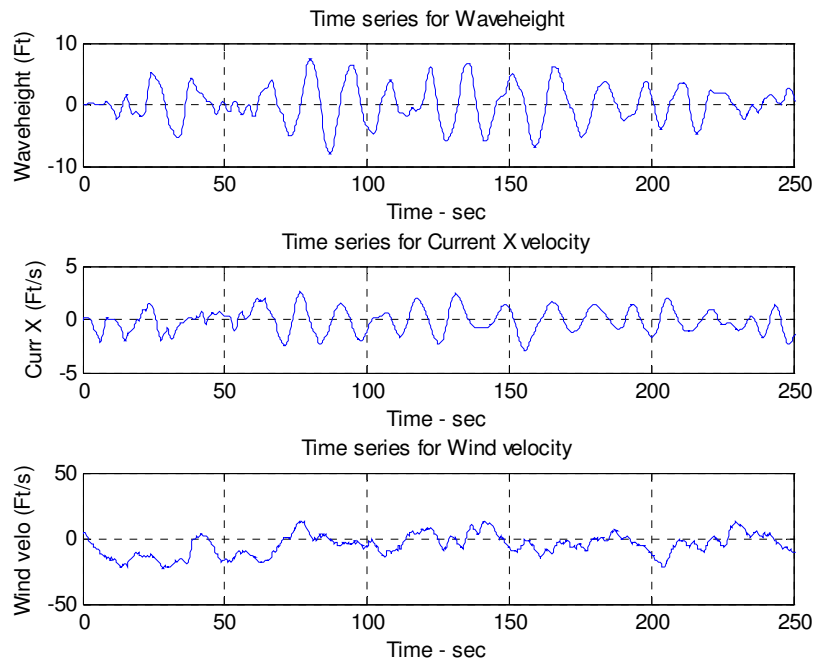
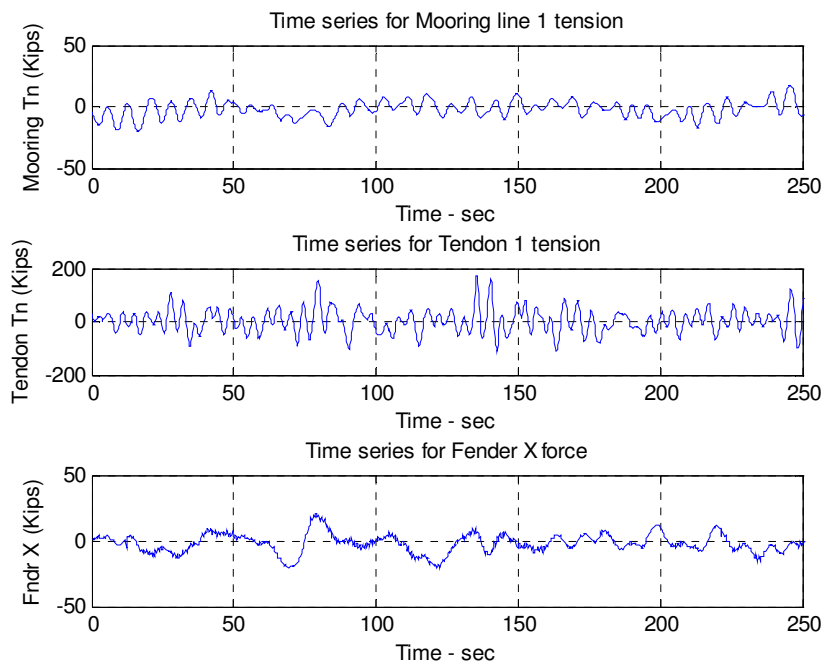Fig. 5-1. Time series plots for wave, current and wind

Fig. 5-2. Time series plots for mooring and tendon tensions and fender forces

5.1 Statistical parameters

The basic statistical parameters are calculated for the data sets for the different cases. The parameters calculated are the maximum value, minimum value, mean, variance, standard deviation, skewness, kurtosis and the process bandwidths. These are good initial indicators as to how the data is distributed and they give a fair idea as to how the analysis has to proceed. The volume of data output from the experiment is enormous and it is not practical to show all the results here. Only the most important observations and results are represented.

Table 5-2 lists the statistical parameters for the 0 degree current only coupled case while Table 5-3 lists the results for the -90 degree current only coupled case. As is evident, the difference between the maxima and minima for the current velocity and the resulting mooring line and tendon tensions and fender forces is very small. The variance from the mean for these parameters is also very small. This indicates that for practical purposes, the current force can be assumed to be a steady force at the mean value and the resulting forces and tensions can also be assumed to be steady.

The individual wind only and wave only cases are not covered here and instead, the combined wind + wave + current case is analyzed in detail. Table 5-4 shows the 0 degree combined environment coupled case results Table 5-5 shows the -90 degree combined environment coupled case results. As can be seen from these, the skewness values for most parameters are close to 0 and the kurtosis values are close to 3 indicating that the data is very close to a Gaussian distribution. However, there are some exceptions that are marked in gray. Another point of interest is the process bandwidth. As can be seen, the bandwidths are very close to 1 in most cases indicating that the processes are broad banded. Again there are a few exceptions that are marked in gray. From the general trend of the results, it can be safely assumed that in most cases the data is represented as a broad banded Gaussian process. The few exceptions could possibly be attributed to experimental anomalies or interference effects between the two bodies acting in such close proximity.

Table 5-2. Statistical parameters for 0 degree heading for the current only coupled case

Data	CurrentX	CurrentY	Waveht	Mooring Tension Line1	Mooring Tension Line2	Mooring Tension Line3	Mooring Tension Line4	FenderX	Tendon 1 Tension	Tendon 2 Tension	Tendon 3 Tension	Tendon 4 Tension	Spring 1 Force	Spring 2 Force
	Ft/sec	*Ft/sec*	*Ft*	*Kips*	*Kips*	*Kips*	*Kips*	*Kips*	*Kips*	*Kips*	*Kips*	*Kips*	*Kips*	*Kips*
Max data	3.68	2.00	0.32	316.21	302.50	270.70	277.62	277.99	580.98	612.54	560.03	530.32	234.31	185.71
Min data	1.53	-3.63	-0.29	298.26	283.57	252.42	260.98	240.29	513.91	552.61	503.75	464.48	206.91	157.89
Mean	3.68	-0.01	0.00	307.48	293.54	261.87	269.45	258.02	547.50	579.42	531.33	496.75	221.33	172.49
Variance	0.29	0.12	0.00	7.86	10.94	9.84	7.24	16.98	89.75	59.84	68.30	38.26	8.43	12.63
Std Dev	0.54	0.35	0.03	2.80	3.31	3.14	2.69	4.12	9.47	7.74	8.26	6.19	2.90	3.55
Skewness	-0.29	-0.05	0.14	0.06	-0.14	0.02	-0.06	0.28	0.01	0.26	-0.02	-0.29	0.20	-0.23
Kurtosis	3.31	4.60	13.29	3.16	2.65	2.81	2.69	4.08	2.47	2.84	2.61	3.29	4.28	3.44
Bandwidth	1.00	0.99	0.72	1.00	1.00	1.00	1.00	0.99	0.99	0.98	0.98	0.97	0.99	1.00

Table 5-3. Statistical parameters for -90 degree heading for the current only coupled case

Data	CurrentX	CurrentY	Waveht	Mooring Tension Line1	Mooring Tension Line2	Mooring Tension Line3	Mooring Tension Line4	FenderX	Tendon 1 Tension	Tendon 2 Tension	Tendon 3 Tension	Tendon 4 Tension	Spring 1 Force	Spring 2 Force
	Ft/sec	*Ft/sec*	*Ft*	*Kips*	*Kips*	*Kips*	*Kips*	*Kips*	*Kips*	*Kips*	*Kips*	*Kips*	*Kips*	*Kips*
Max data	5.08	2.41	0.56	321.97	245.35	307.93	261.09	158.94	675.83	565.21	470.48	524.11	176.35	196.37
Min data	*1.53*	-0.78	-0.13	293.67	223.11	284.07	232.74	133.26	627.93	509.57	423.93	472.30	160.41	172.92
Mean	3.25	0.41	0.22	306.54	233.14	297.45	247.89	145.02	650.48	537.63	446.71	499.56	167.22	186.44
Variance	0.27	0.14	0.00	19.78	11.80	13.08	14.05	8.68	33.45	54.41	21.23	36.50	4.23	7.80
Std Dev	0.52	0.37	0.05	4.45	3.43	3.62	3.75	2.95	5.78	7.38	4.61	6.04	2.06	2.79
Skewness	0.11	0.17	-0.23	0.34	0.22	-0.27	-0.41	-0.10	-0.11	0.05	0.07	-0.17	0.48	-0.46
Kurtosis	2.96	3.52	3.64	3.26	3.16	3.20	3.92	3.24	3.11	2.77	2.98	2.82	3.38	3.95
Bandwidth	1.00	1.00	0.91	1.00	1.00	1.00	1.00	0.97	0.97	0.98	0.96	0.98	0.99	0.99

Table 5-4. Statistical parameters for 0 degree heading for the wind + wave + current coupled case

Data	CurrentX	CurrentY	Wind	Waveht	Mooring Tension Line1	Mooring Tension Line2	Mooring Tension Line3	Mooring Tension Line4	FenderX	Tendon 1 Tension	Tendon 2 Tension	Tendon 3 Tension	Tendon 4 Tension	Spring 1 Force	Spring 2 Force
	Ft/sec	*Ft/sec*	*Ft/sec*	*Ft*	*Kips*	*Kips*	*Kips*	*Kips*	*Kips*	*Kips*	*Kips*	*Kips*	*Kips*	*Kips*	*Kips*
Max data	7.93	3.24	139.12	13.76	370.52	374.21	248.19	260.20	286.76	804.56	828.69	750.54	760.22	274.41	200.56
Min data	-0.76	-4.07	70.29	-12.61	313.22	295.87	204.70	217.54	221.75	381.90	308.64	266.70	241.05	192.59	131.95
Mean	3.78	0.01	104.10	-0.09	339.79	328.94	228.68	240.07	256.26	560.71	558.79	502.32	503.75	233.41	162.92
Variance	1.30	0.28	91.53	9.11	50.71	76.29	32.72	29.70	72.41	2038.3	3547.8	2038.1	3330.90	118.75	65.81
Std Dev	1.14	0.53	9.57	3.02	7.12	8.73	5.72	5.45	8.51	45.15	59.56	45.15	57.71	10.90	8.11
Skewness	-0.09	-0.08	-0.12	0.12	0.00	-0.06	0.03	0.01	0.00	0.15	-0.01	-0.04	0.02	0.09	0.14
Kurtosis	2.86	4.87	2.83	3.28	3.18	3.16	3.22	2.97	3.12	3.80	3.04	3.88	3.22	3.25	3.38
Bandwidth	0.90	0.94	0.99	0.89	0.93	0.93	0.97	0.97	0.99	0.80	0.92	0.88	0.83	0.99	0.99

Table 5-5. Statistical parameters for -90 degree heading for the wind + wave + current coupled case

Data	CurrX	CurrY	Wind	Waveht	Mooring Tension Line1	Mooring Tension Line2	Mooring Tension Line3	Mooring Tension Line4	FenderX	Tendon 1 Tension	Tendon 2 Tension	Tendon 3 Tension	Tendon 4 Tension	Spring 1 Force	Spring 2 Force
	Ft/sec	*Ft/sec*	*Ft/sec*	*Ft*	*Kips*	*Kips*	*Kips*	*Kips*	*Kips*	*Kips*	*Kips*	*Kips*	*Kips*	*Kips*	*Kips*
Max data	7.85	1.88	136.54	13.68	410.57	233.52	380.66	229.88	611.42	830.21	758.89	945.66	872.73	288.43	291.55
Min data	-0.45	-1.09	72.56	-11.38	318.29	169.39	295.23	179.42	109.45	81.76	54.79	281.05	279.10	141.48	110.18
Mean	3.77	0.28	104.23	0.05	359.10	204.36	332.08	207.07	290.66	492.71	447.70	568.86	538.12	205.87	193.66
Variance	1.31	0.17	76.68	9.16	96.99	53.28	87.39	44.54	1931.80	6137.08	5371.33	4442.19	3690.73	375.50	442.36
Std Dev	1.14	0.41	8.76	3.03	9.85	7.30	9.35	6.67	43.95	78.34	73.29	66.65	60.75	19.38	21.03
Skewness	-0.16	0.04	-0.01	-0.13	0.06	-0.06	0.06	-0.15	0.31	-0.12	-0.11	0.28	0.28	0.21	0.16
Kurtosis	3.02	3.03	2.87	3.46	3.33	3.19	3.24	3.07	4.40	3.38	3.31	3.69	3.63	3.40	3.33
Bandwidth	0.88	0.98	0.99	0.95	0.84	0.93	0.78	0.97	0.97	0.79	0.91	0.86	0.80	0.97	0.97

The remaining cases (wind only, wave only, current only and wind + wave + current) for the 0 degree heading and -90 degree headings for the coupled and uncoupled cases show similar trends and are hence not shown here. These tables provide some initial guidelines for the detailed data analysis to follow and hence are covered only briefly. The data distribution patterns and spectral densities are analyzed in detail in the following sections.

5.2   Data distribution

The statistical parameters for the data sets indicate that the data is mostly normally distributed as the skewness values are close to 0 and the kurtosis values tend to 3. The next step is to investigate in detail the distribution pattern followed by each data set. The histogram for the data set is first plotted. This is followed by the normal probability plot for the data which fits the series to a linear normal distribution fit. If the outcome is a linear plot, it indicates a normal distribution. Deviations from this linear trend are most obvious for cases marked in grey in Table 5-2, Table 5-4, Table 5-3 and Table 5-5. Next is the plot of the probability density function. MATLAB uses a function called 'normpdf' to compute the normal pdf at each value of the data set using the corresponding parameters in mean and standard deviation. It plots an ideal pdf for a normal distribution. Then the actual pdf for the data in question is plotted and is superimposed on the ideal pdf and it is then compared to see if the distribution is normal.

Next, the cumulative distribution function is plotted for the data and is compared with the ideal case for normal distribution. The 'normcdf' function in MATLAB computes the normal cdf at each value of the data set using the corresponding parameters in mean and standard deviation. As before, the ideal cdf for the normal distribution is plotted. Then actual cdf is calculated as the cumulative of the pdf and is superimposed on the ideal cdf.

Although the data itself generally follows a normal distribution pattern, the extreme values do not necessarily follow normal distribution. Hence it is attempted to fit the extreme values for each series to the Weibull distribution pattern. The extreme values

including the positive maxima, positive minima, negative maxima and the negative minima are identified from the time series using the zero-crossing analysis. Table 5-6 shows the scale parameters η and the shape parameters β for the extreme values for the 0 degree coupled case for the combined environment.

Table 5-6. Extreme value Weibull parameters for the 0 degree heading coupled case for wind + wave + current

	Positive maxima		Positive minima		Negative maxima		Negative minima	
	η	β	η	β	η	β	η	β
Current X	1.30	1.54	0.81	1.25	0.70	1.09	1.26	1.38
Current Y	0.51	1.26	0.35	1.19	0.35	1.13	0.53	1.23
Mrng Tn 1	7.14	1.36	4.94	1.20	5.09	1.24	7.32	1.37
Mrng Tn 2	9.02	1.44	5.97	1.19	6.89	1.36	9.42	1.46
Mrng Tn 3	5.85	1.32	4.94	1.19	3.73	1.19	5.34	1.31
Mrng Tn 4	5.33	1.34	4.28	1.22	4.18	1.29	5.38	1.41
Fender X	7.76	1.29	6.68	1.22	6.64	1.20	7.72	1.28
Tendon 1	47.29	1.26	22.03	1.12	27.46	1.33	48.93	1.44
Tendon 2	61.33	1.34	39.47	1.16	39.10	1.20	61.43	1.37
Tendon 3	46.12	1.33	27.02	1.18	25.14	1.15	44.96	1.30
Tendon 4	64.79	1.45	32.44	1.14	32.22	1.17	63.54	1.42

The 'wblplot' function is used to plot the Weibull probability plot and to estimate if the extreme values follow the Weibull distribution. A linear plot indicates Weibull distribution. The 'wblfit' function is used to derive the parameters of the Weibull distribution and these parameters are in turn used as input for the 'wblpdf' function to plot the ideal pdf distribution for the extreme values. The actual pdf is also plotted in the same figure to enable a comparison and determine how closely the extreme values follow the Weibull pdf pattern. The 'wblcdf' function is then used to plot the ideal Weibull cdf for the extreme values and the actual cdf is then plotted in the same figure.

Table 5-7 and Table 5-8 show the skewness and kurtosis values for mooring line tensions in line 1 for all the cases considered in the experiment. As can be seen, for most cases, the skewness tends to 0 and kurtosis tends to 3. Any deviation is marked in grey.

These are cases that are observed to have maximum deviation from the linear Gaussian fit.

Table 5-7. Skewness and kurtosis for coupled case mooring line tensions

	Coupled case							
	0 degree heading				-90 degree heading			
	Current	Wind	Wave	Combination	Current	Wind	Wave	Combination
Skewness	0.06	0.19	0.07	-0.004	0.34	-	0.03	0.006
Kurtosis	3.16	3.57	3.05	3.18	3.26	-	2.82	3.33

Table 5-8. Skewness and kurtosis for uncoupled case mooring line tensions

	Uncoupled case							
	0 degree heading				-90 degree heading			
	Current	Wind	Wave	Combination	Current	Wind	Wave	Combination
Skewness	0.08	-	-	0.05	0.50	-	0.05	0.13
Kurtosis	3.23	-	-	2.94	3.36	-	2.79	3.38

The Gaussian distribution and extreme Weibull distribution patterns are analyzed here for the 0 degree coupled case mooring line tension (line 1) and tendon 1 tension for the combined environment. Fig. 5-3 shows the distribution pattern for the mooring line tension for line 1. The figure shows that the mooring line tensions are a close fit to an ideal Gaussian distribution with 0 skewness. The pdf has a slight peak when compared to the ideal Gaussian distribution which indicates a slightly higher kurtosis value. This is substantiated by the numbers in Table 5-7 which shows a skewness of 0 and kurtosis of 3.18 for mooring tension for line 1. But for practical purposes the data can be safely assumed to be normally distributed. Fig. 5-4 shows the local maxima and minima for the mooring tension for line 1 while Fig. 5-5 shows the Weibull fit for the positive maxima.
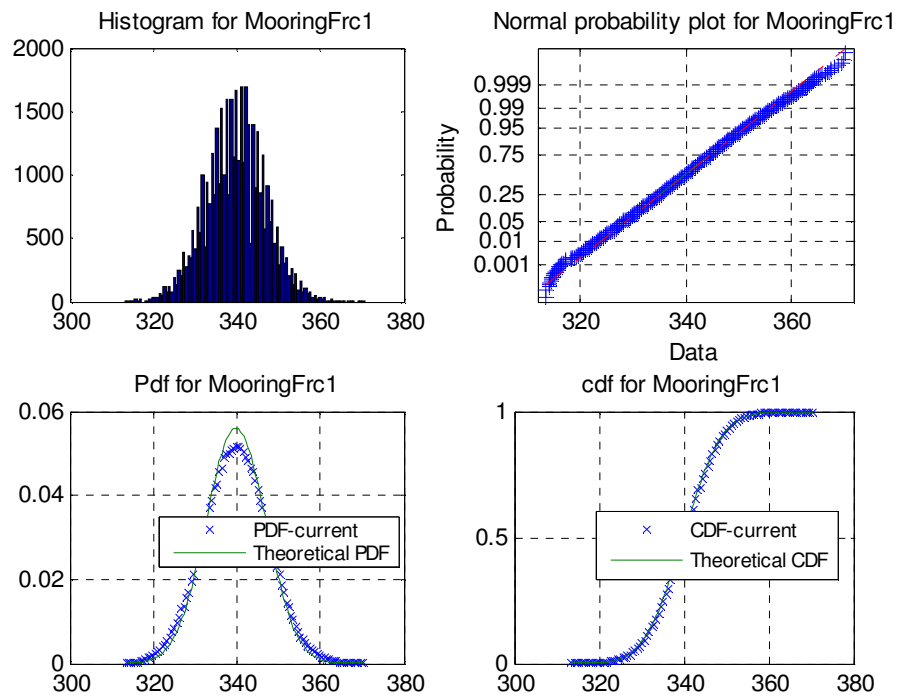
Fig. 5-3. Gaussian distribution fit for mooring line tension in line 1
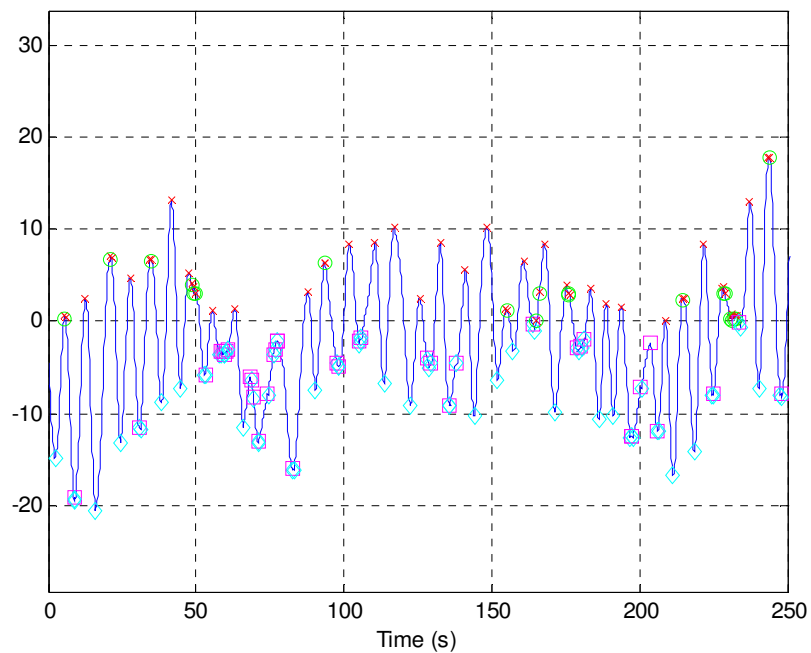
Fig. 5-4. Local maxima and minima for mooring line tension in line 1
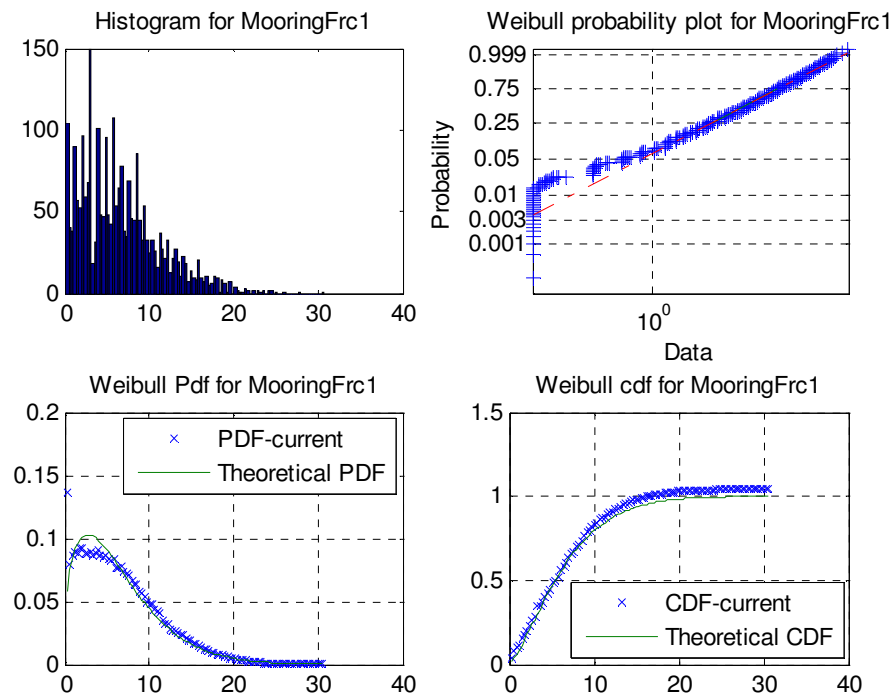
Fig. 5-5. Weibull distribution fit for positive maxima for mooring line tension in line 1

The data points towards the tail of the extreme value distribution are more significant as the point of focus here is the extreme values. A probability of exceedance curve is used to compare the ideal Weibull curve with the curve for the experimental results [15]. The plot represents the probability of the measured peaks exceeding a particular value 'a'. The most probable maximum (MPM) gives a theoretical estimate of the expected maximum value for a specified condition. The 3 hour MPM value is generally considered in the design of floating structures. To determine the 3-hour MPM, the data is divided into 1 minute intervals and the peak maxima in each time interval are collected. The assumption made here is that the maxima for each 1 minute interval are independent of each other. The cdf for this 1 minute maxima distribution is raised by 180 (for 3 hours) and its pdf is plotted. The 3 hour MPM is calculated as the peak value from this pdf and is marked in the probability of exceedance plot. The distribution values and

the MPM are normalized by the standard deviation of the distribution. The results were re-plotted by increasing the time intervals to 3 minutes (and raising the cdf values to a power of 60) and the MPM values were found to be very similar to the 1 minute interval values indicating the selection of time interval did not change the MPM value significantly.

The time series data measured from the experiment is for a 3 hour distribution. The normalized probability of exceedance for the tendon tension (0 degree coupled case for wave only environment) is plotted for the maxima in the first one hour of data in Fig. 5-6. Fig. 5-7 shows the exceedance plot for the first 2 hours of data while Fig. 5-8 shows the plot for the entire 3 hour duration with the MPM value. A comparison of the Weibull parameters for the three time durations is shown in Table 5-9. The aim here is to see if the time series is statistically stationary which is proved by the fact that these parameters do not show a significant variation with increasing time duration.

As can be seen from these figures, the ideal Weibull characterizes the measured maxima quite well for the low and moderate responses. However, for the extreme values near the tail, the Weibull fit overestimates the values. The 3 hour normalized MPM (with a 1 minute interval) for the tendon tension for the 3 hour data sample is 6.27. Similar results are observed for mooring line tensions (MPM = 5.93 for 0 degree wave only case) and fender forces (MPM = 6.35 for 0 degree wave only case) with the Weibull showing a good fit to the low and moderate values, but overestimating the largest values. A comparison of the MPM values for tendon tensions calculated with a 1 minute and 3 minute interval for different time durations is shown in Table 5-9. The values do not show a significant variation with a change in the time interval. Also, an MPM value greater than 3.86 is indicative of the degree of non-linearity involved in the system. The MPM values calculated here for mooring line tensions, tendon tensions and fender forces show highly non-linear characteristics.

Table 5-9. Comparison of Weibull parameters and MPM for tendon tensions

	η	β	*3 hr MPM – 1 min interval*	*3 hr MPM – 3 min interval*
1 hour	58.5	1.63	7.04	7.22
2 hour	64.93	1.64	6.36	6.52
3 hour	65.13	1.62	6.27	6.42
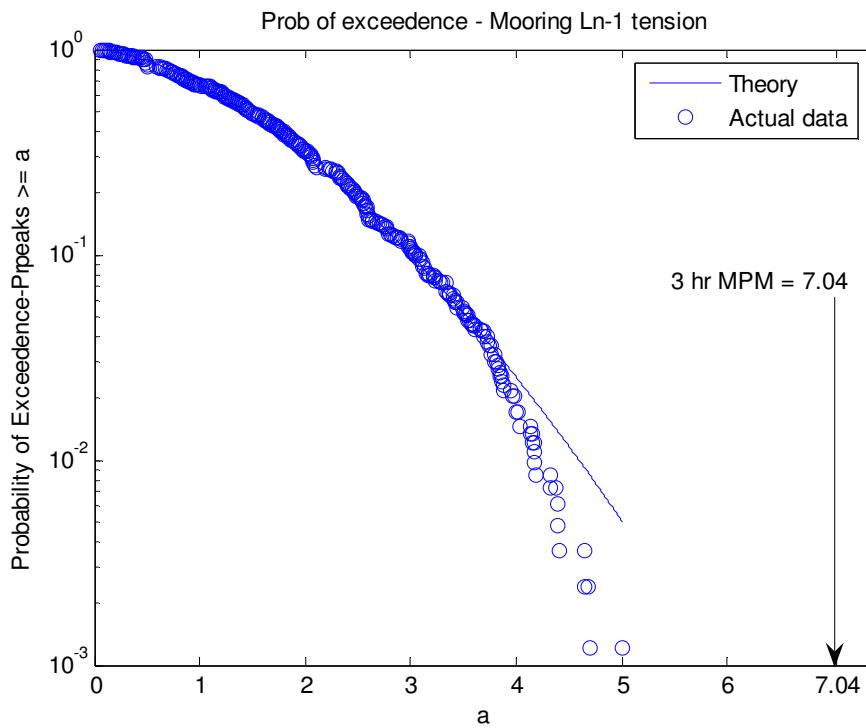
Fig. 5-6. Probability of exceedance for 1 hour duration
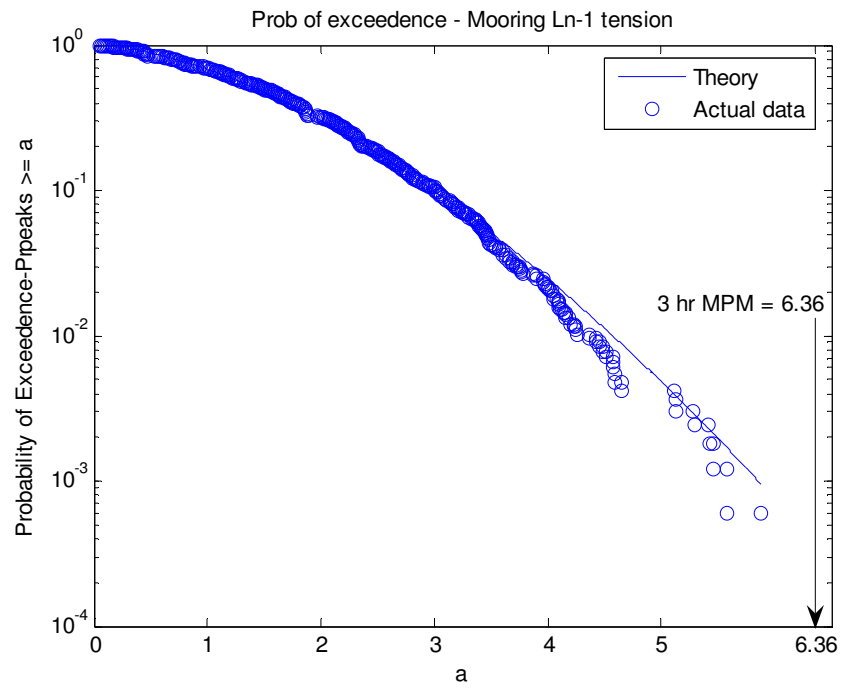
Fig. 5-7. Probability of exceedance for 2 hour duration
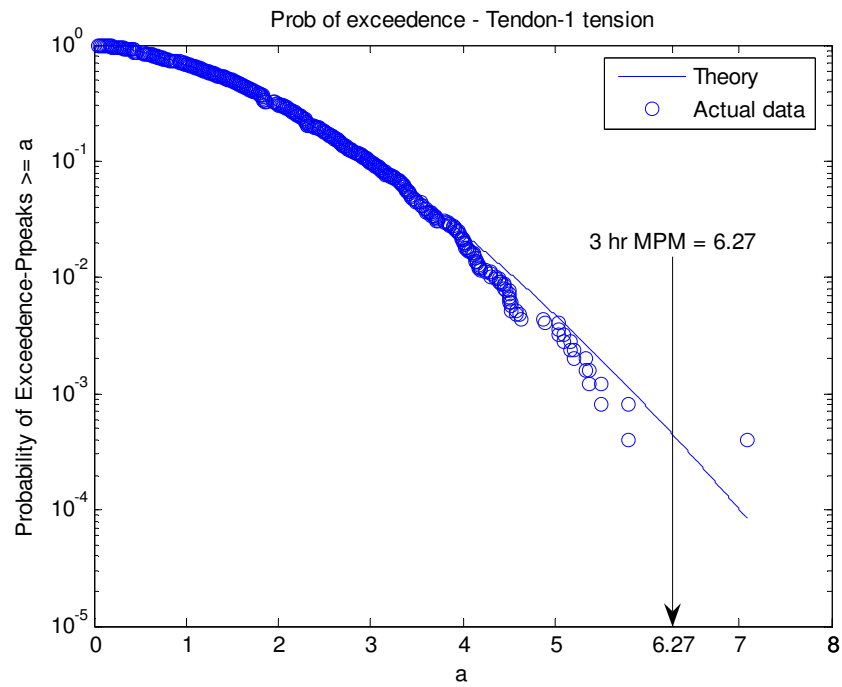
Fig. 5-8. Probability of exceedance and MPM for 3 hour duration

The Gaussian distribution patterns for tendon tensions and fender forces also show results similar to those of mooring line tensions. Table 5-10 and Table 5-11 show the skewness and kurtosis values for all the cases considered in the experiment for tendon tensions while Table 5-12 shows the results for fender forces. Any deviations from normal behavior are marked in gray. Observing the data distribution trends for mooring line tensions, tendon tensions and fender forces shown, it is evident that they are more or less normally distributed. In most cases, the kurtosis values tend to 3 while the skewness values are very close to 0. So it can be safely assumed that the mooring line and tendon tensions and fender forces follow a Gaussian distribution. However, the extreme values are not normally distributed and hence are fitted on to a Weibull distribution. As has been seen, the extreme values are overestimated by an ideal Weibull distribution and are hence not a very good fit.

Table 5-10. Skewness and kurtosis for coupled case tendon tensions

	Coupled case							
	0 degree heading				-90 degree heading			
	Current	Wind	Wave	Combination	Current	Wind	Wave	Combination
Skewness	0.01	0.14	0.08	0.15	-0.11	-	0.00	-0.12
Kurtosis	2.47	2.87	3.12	3.80	3.11	-	3.10	3.38

Table 5-11. Skewness and kurtosis for uncoupled case tendon tensions

	Uncoupled case							
	0 degree heading				-90 degree heading			
	Current	Wind	Wave	Combination	Current	Wind	Wave	Combination
Skewness	0.73	-	-	-0.02	0.12	-	-0.06	0.40
Kurtosis	9.24	-	-	3.03	2.82	-	3.03	6.28

Table 5-12. Skewness and kurtosis for fender forces

	Coupled case							
	0 degree heading				-90 degree heading			
	Current	Wind	Wave	Combination	Current	Wind	Wave	Combination
Skewness	0.28	-0.04	0.17	-0.01	-0.1	-	0.08	0.31
Kurtosis	4.08	3.12	3.17	3.12	3.24	-	3.28	4.40

5.3 Spectral analysis and transfer functions

The spectral density distribution for each data set is next plotted. Fig. 5-9 shows the spectral density plot for waveheights for 0 degree coupled combined environment case. The figure shows a comparison between a 512 point Fourier transform, 2048 point Fourier transform and 4096 point transform. The spectral plot becomes more complex as the number of points increases and the peak goes up. The 512 point fast Fourier transform is seen to give a clearer peak.

Fig. 5-10 shows a similar spectral density plot for mooring line 1 tension. As is evident, the 512 point Fourier transform does not resolve the low frequency component of tension very well, although the wave frequency component is well represented. However, for this analysis, the data trends are more important rather than the actual values and hence the 512 Fourier transform is used through out as this gives simpler plots and hence facilitates comparisons between the different cases.

Also, the 512 point Fourier transform is seen to fit the JONSWAP spectrum the best. Fig. 5-11 shows the fit of the 512 point spectral plot of the waveheight to a JONSWAP spectrum with $\gamma = 2$ (which was used for the experiment).

The frequency transfer functions for the cases corresponding to the spectral density plots are also calculated. All cases analyzed here are for the wind + wave + current combined environmental case unless otherwise stated.
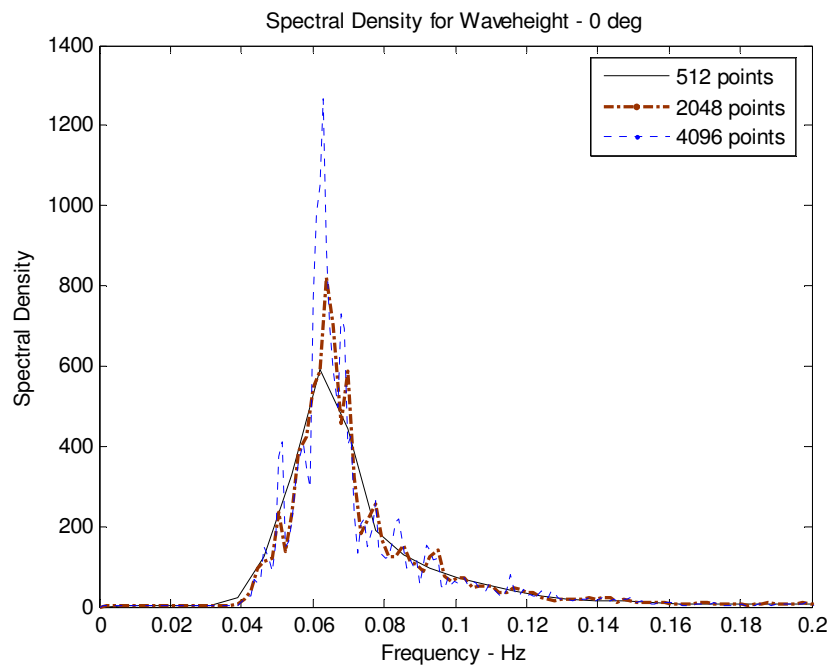
Fig. 5-9. Waveheight Spectral density for 0 degree coupled case
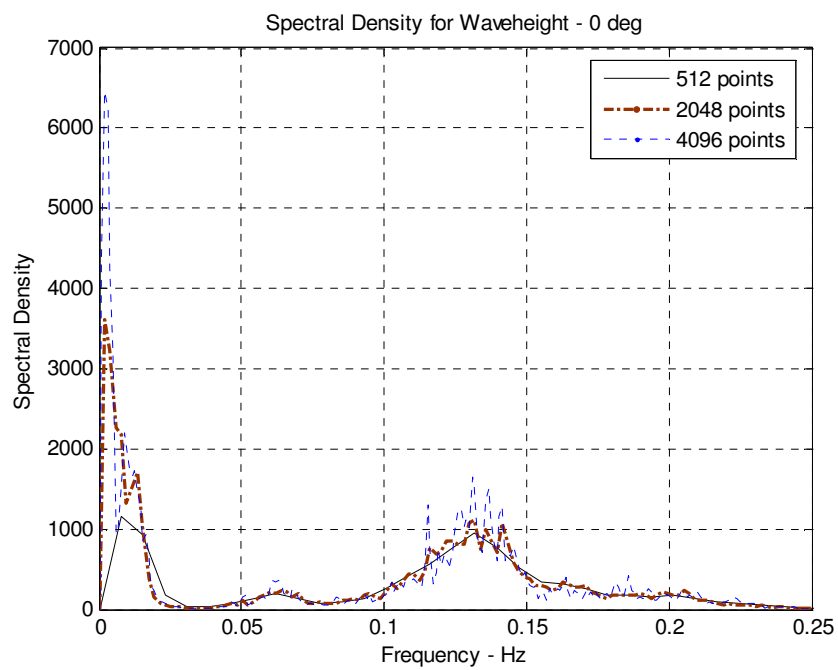
Fig. 5-10. Mooring line 1 tension spectral density for 0 degree coupled case
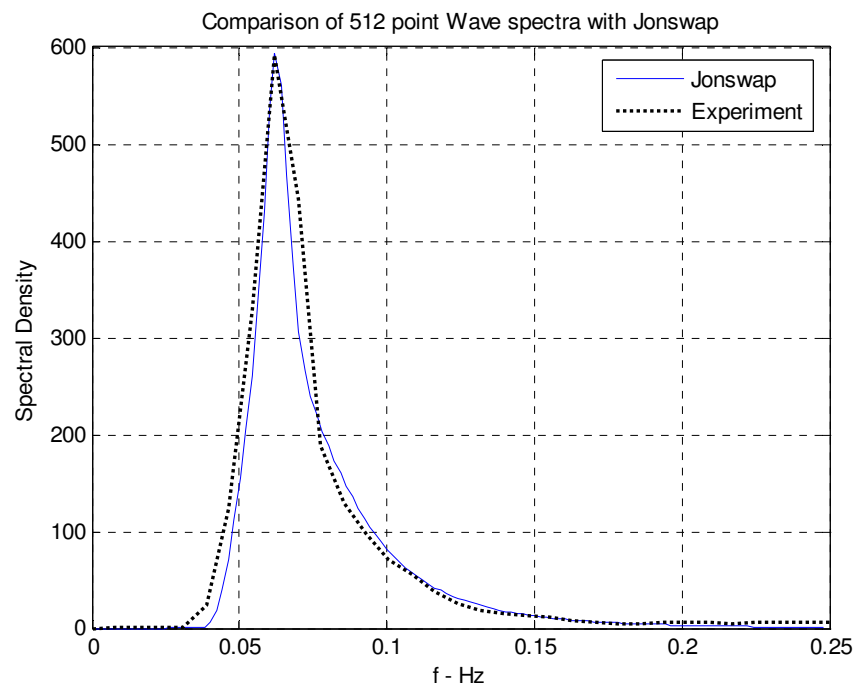
Fig. 5-11. Comparison of wave elevation spectrum with JONSWAP

An inspection of the spectral density and transfer function plots for the surge, sway and heave motions for the mini-TLP and barge give varied results. Fig. 5-12 and Fig. 5-13 show the spectral densities for the 0 degree uncoupled barge surge and sway motions respectively with an 8192 point Fourier transform. Both plots show a peak at approximately 0.008 Hz. This peak is preceded by other smaller peaks. The idea of the exercise is to prove that the 512 points spectra shown in the later plots do not correspond to the definition of a red spectrum and the peaks that correspond to the lowest frequencies (0.008 Hz for TLP surge, barge surge, barge sway etc) are not a result of the red spectrum effect. In a red spectrum for a 0 mean process, the value is zero at zero frequency and the peak is at the largest value at the lowest frequency in the spectra.
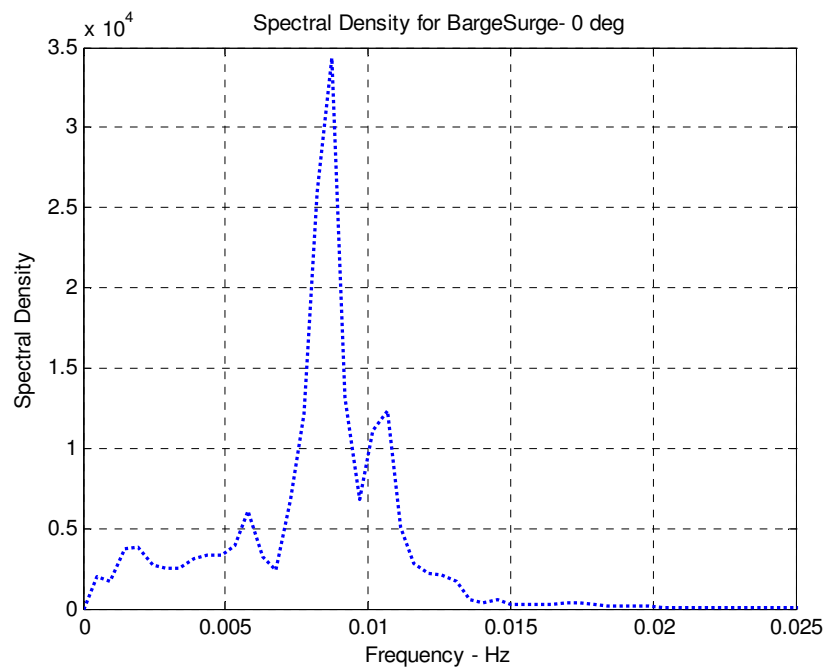
Fig. 5-12. Barge surge 8192 point spectral density for 0 degree heading
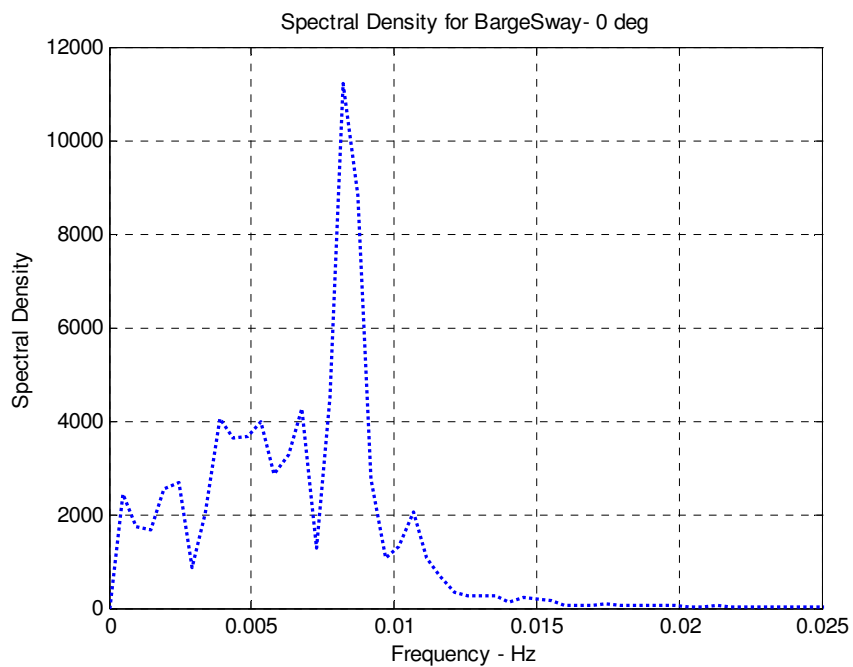
Fig. 5-13. Barge sway 8192 point spectral density for 0 degree heading

The spectral density plots shown henceforth follow the 512 point Fourier transform. The coupled and uncoupled cases are compared for the 0 degree and -90 degree environmental headings. The TLP motions are not significantly different for the coupled and uncoupled case. This is because the TLP is relatively stiff due to the tendon pull and hence coupling effects are minimal for the TLP motion. The spectra are very similar for both cases and so are the RAOs. This is evident from Fig. 5-14 which shows the 0 degree heading spectral density comparison for TLP surge for coupled and uncoupled cases. TLP surge is primarily a low frequency motion (period $\approx$ 125 sec). But here, the wave frequency motions (indicated by the second peak at 0.062 Hz) are equally significant.
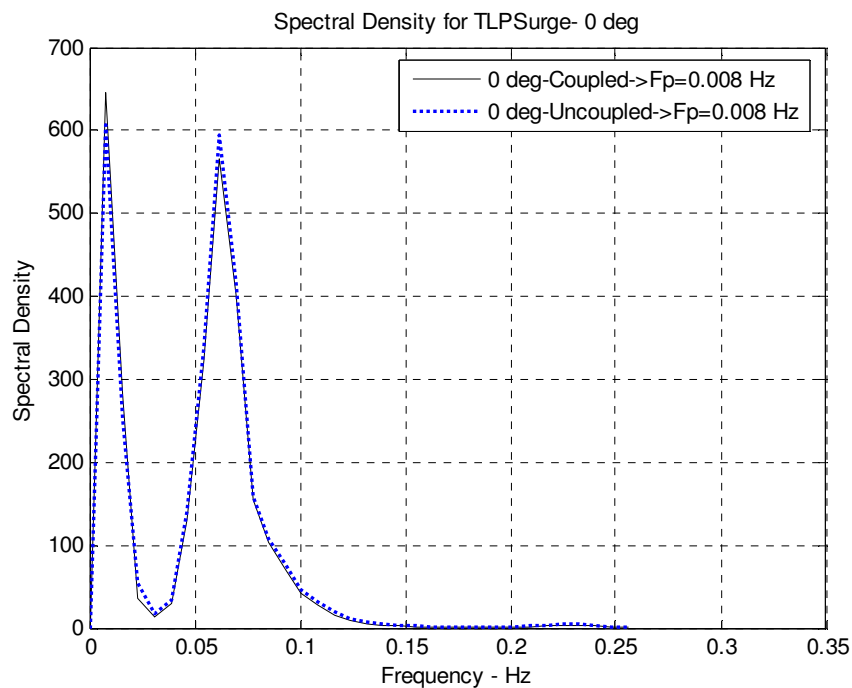
Fig. 5-14. TLP surge spectral density for 0 degree heading

Transfer Function for TLPSurge - 0 deg
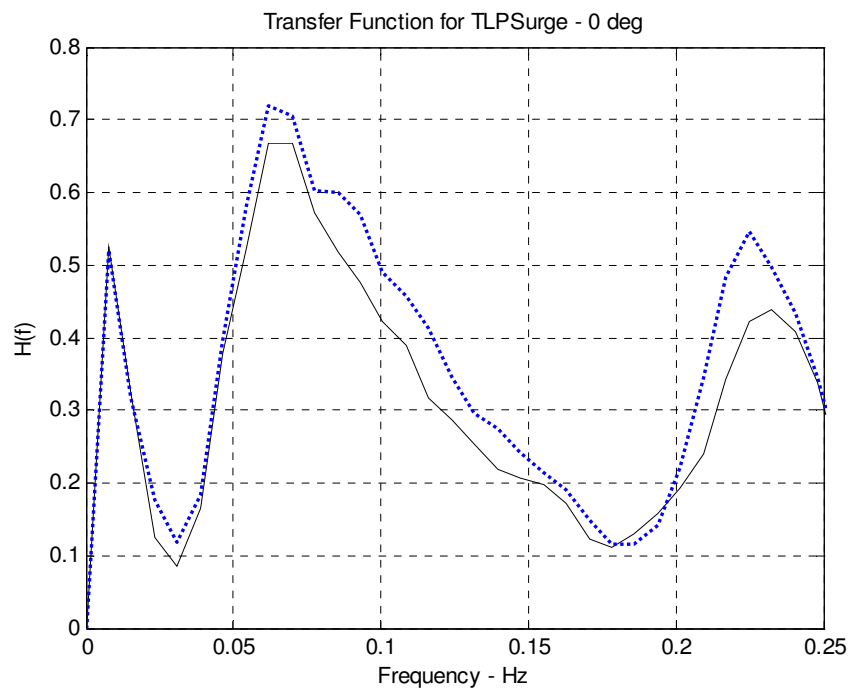
Fig. 5-15. TLP surge transfer function for 0 degree heading

Similar results are observed for all TLP motions. The TLP sway and heave motions show a pattern similar to the surge motion and are hardly influenced by the coupling between the bodies. TLP heave is seen to be a high frequency motion with periods of around 3 seconds. These in turn contribute to the high frequency tension components in tendon tension. The TLP roll, pitch and yaw data are unavailable for analysis.

However, the barge motions are significantly reduced when the vessels are coupled. The barge is a moored structure and hence is not very stiff in motion. When coupled to the mini-TLP, the fenders and springs take a significant portion of the load and hence the surge and sway motions are reduced significantly. Fig. 5-16 shows the 0 degree spectral density comparison for barge surge motion. Barge surge motion shows a significant reduction when the bodies are coupled. In the uncoupled case, both barge surge and sway are dominated by high period motions with periods of approximately 125 seconds.
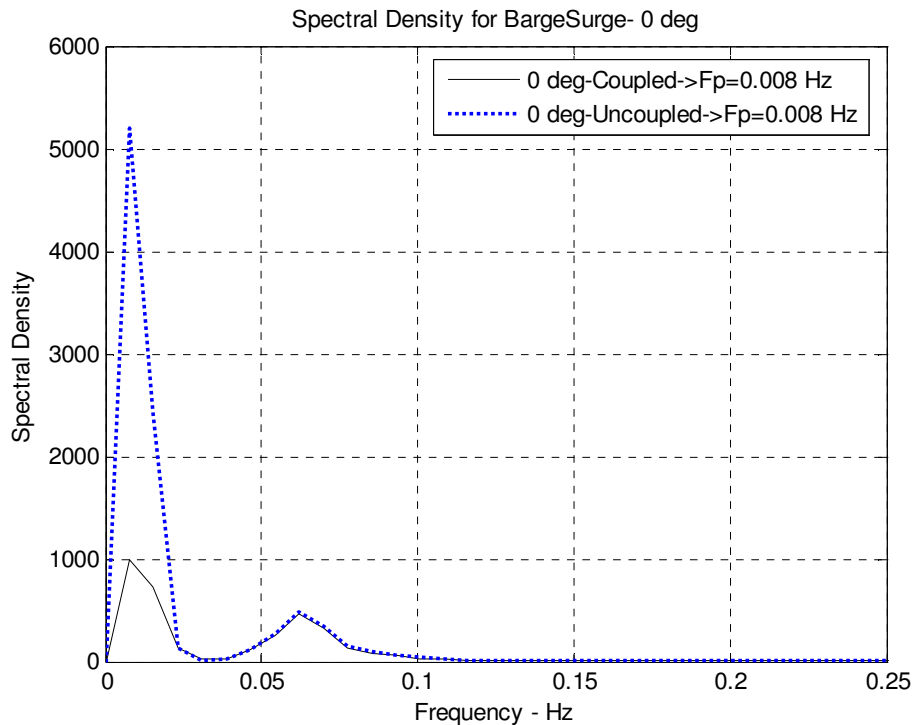
Fig. 5-16. Barge surge spectral density for 0 degree heading

The barge sway response also shows an identical behavior pattern. But for the -90 degree heading, the barge sway motions remain unchanged in both coupled and uncoupled cases. The barge is masked to a large extent by the mini-TLP for the -90 degree environment heading. This reduces the overall magnitude of the barge motion in all degrees of freedom. Further, for the -90 degree heading the barge sway motion, which is transverse to the direction of the environment, is hardly big enough to engage the coupling system. Hence, both coupled and uncoupled cases show very similar results. Fig. 5-17 shows the spectral density plots for the barge sway motion in 0 degree heading while Fig. 5-18 shows the corresponding plot for the -90 degree heading.

Similar to the TLP heave, Barge heave also does not show a significant response to the coupling between the bodies. Hence it can be concluded that the coupling between the

bodies provides stiffness only in the horizontal plane and hence the vertical motions are relatively unchanged.

The barge pitch motion is seen to be largely unaffected by the coupling between the two bodies. However, coupling effects reduce barge roll motion. Fig. 5-19 shows the spectral density plot for barge roll for the 0 degree combined environment. This is expected since the barge roll motion will be countered by a restoring force from the breast line system holding the two vessels thus reducing the roll motion for coupled case.

In the case of barge yaw motion for the 0 degree heading, the coupled case exhibits more yaw than the uncoupled case. This is because here the system takes on the incident environment from the bow and the barge is influenced significantly in yaw by the breast lines and fenders, giving it a yaw couple. However for the -90 degree heading, the environment is incident from the beam side and hence the yaw motion is more in the uncoupled case and the fender and breast line effects disappear. Fig. 5-20 shows the spectral density for the barge yaw motion for the 0 degree case and Fig. 5-21 shows the yaw spectrum for the -90 degree case.
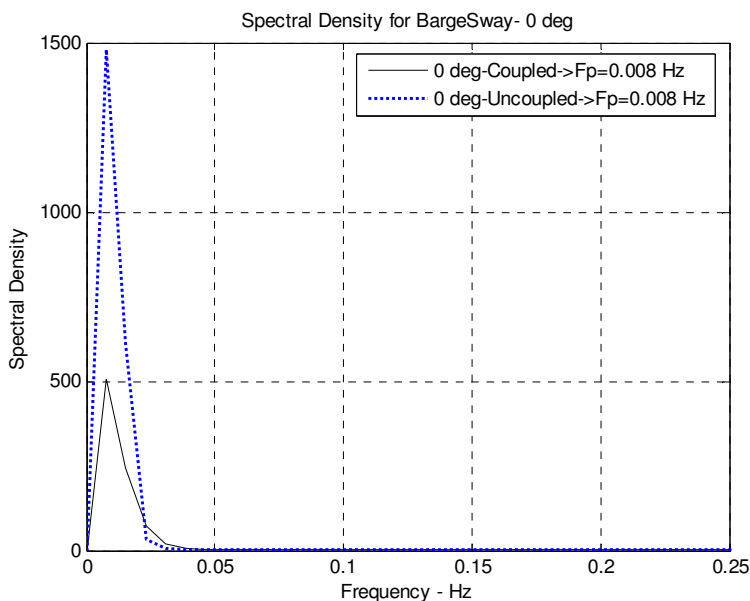
Fig. 5-17. Barge sway spectral density for 0 degree heading
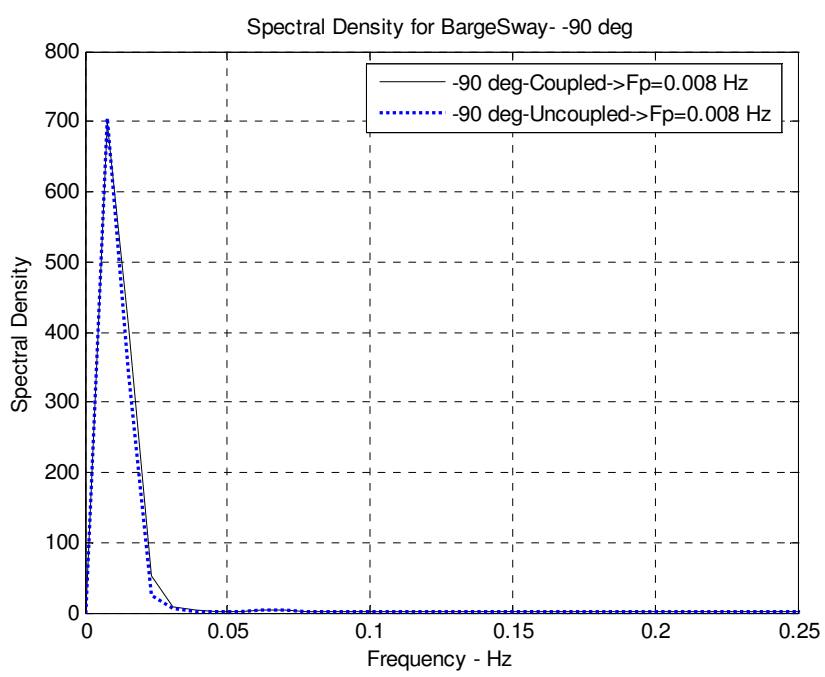
Fig. 5-18. Barge sway spectral density for -90 degree heading
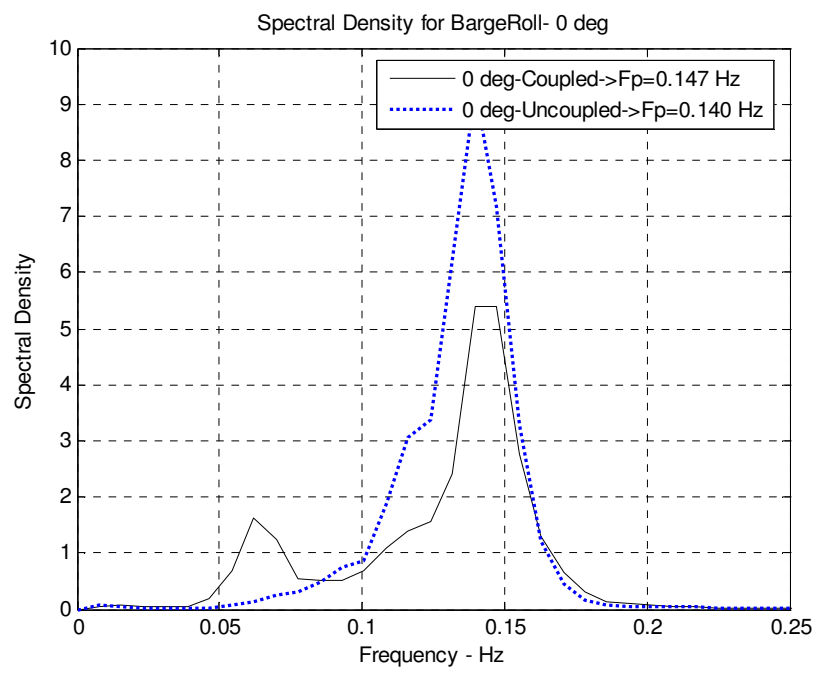
Fig. 5-19. Barge roll spectral density for 0 degree heading
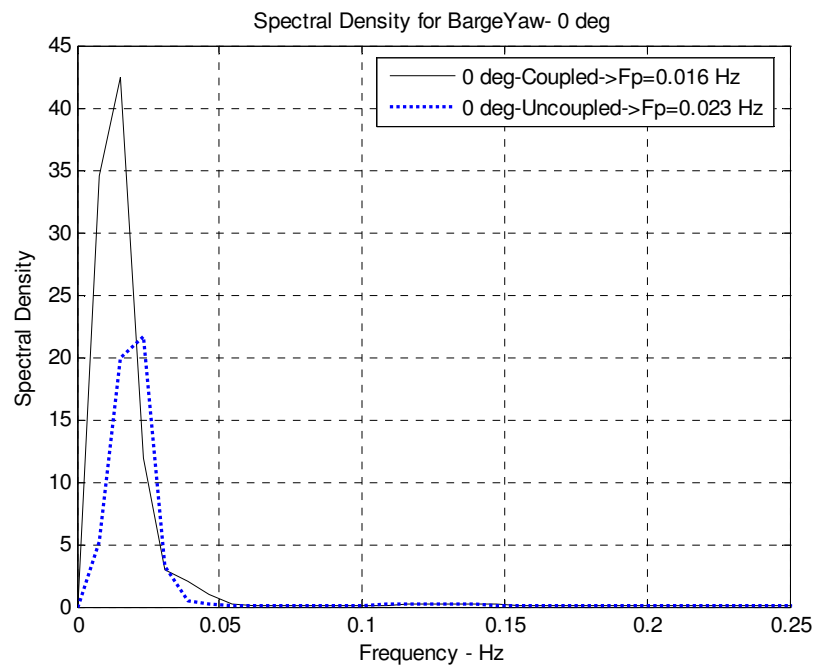
Fig. 5-20. Barge yaw spectral density for 0 degree heading
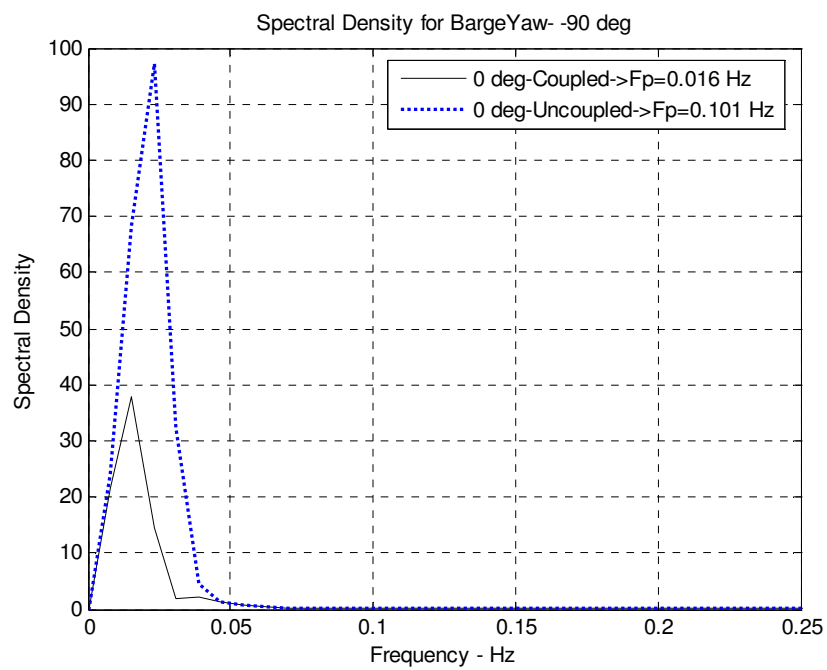
Fig. 5-21. Barge yaw spectral density for -90 degree heading

Fig. 5-22 and Fig. 5-23 show the spectral densities for the mooring line tensions for the 0 degree and -90 degree headings respectively. Fig. 5-24 shows the corresponding transfer function for the 0 degree case. The low frequency resonance effects and the wave frequency effects can be clearly identified. For e.g. the spectral density for mooring line 1 tension shows a peak at 0.008 Hz. This corresponds to the resonant low frequency response and is in the correspondence with the barge surge and sway spectral densities. However, the mooring line tension also shows another peak at 0.133 Hz. Observing the transfer functions for the mooring line 1 tension from Fig. 5-24 and the spectral density peaks for the waveheight, its is obvious that this peak at 0.133 Hz represents the wave frequency effects. A similar relation is established for the low frequency peaks at 0.008 Hz by studying the mooring line tension transfer function with the barge surge and sway spectral densities.

It is evident from the mooring tension spectra and transfer functions that when the 2 bodies are coupled, the mooring lines have much lower mooring line tensions than when they are uncoupled. The fenders and breast lines share a portion of the mooring line loads when the bodies are coupled thus significantly reducing the tensions in the lines. Another interesting observation is that the coupling reduces the mooring tensions only at the resonant lower frequency range. In the wave frequency region, the tensions are relatively unchanged for the coupled and uncoupled cases. The wave spectrum does not change for the coupled and uncoupled case. At the wave frequency, the tensions are influenced only by the sum frequency effects of the wave. As the wave itself does not change significantly, the tensions at these frequencies are not influenced by the coupling effects.

Also, for the 0 degree heading, the resonant low frequency effects are dominant while for the -90 degree case, the wave frequency effects are dominant (except for line 4). An inspection of the barge surge RAOs show that for the -90 degree heading, the barge surge RAOs reduce by a significant amount (as the environment is beam side) when compared to the 0 degree (as the environment is from the bow side) while the

wave remains unchanged for both cases. This further proves the effect of the barge surge motion on the mooring tension low frequency range.
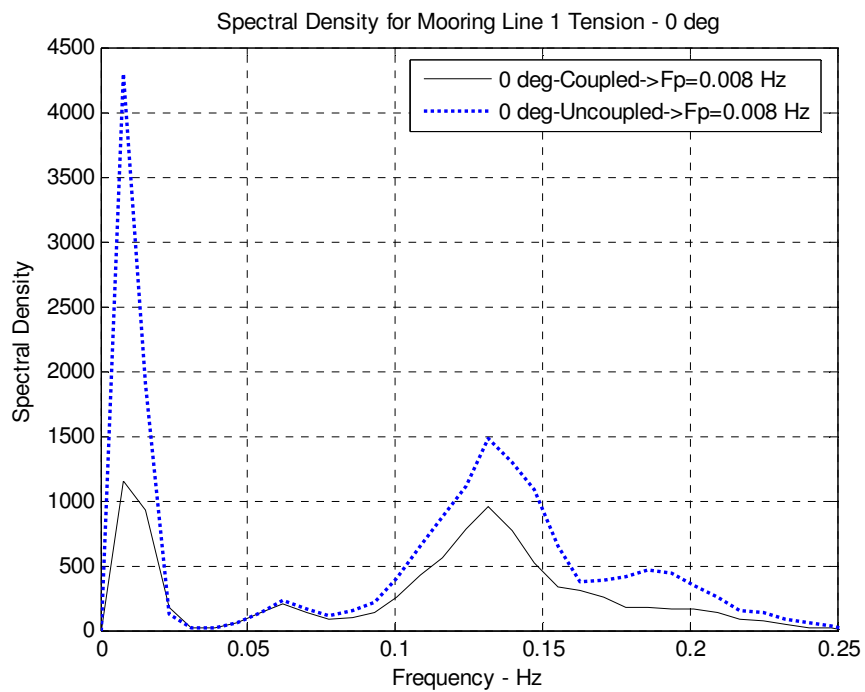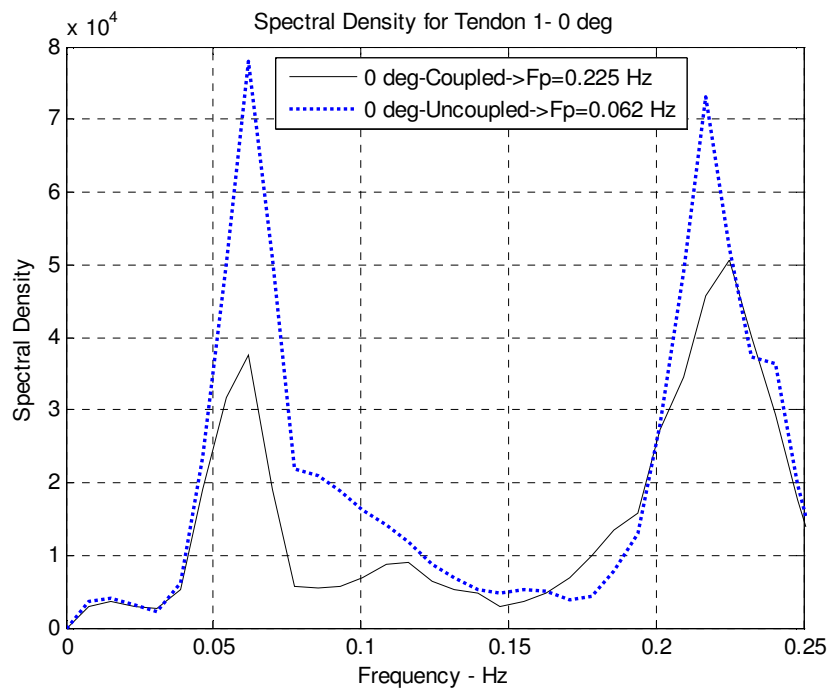

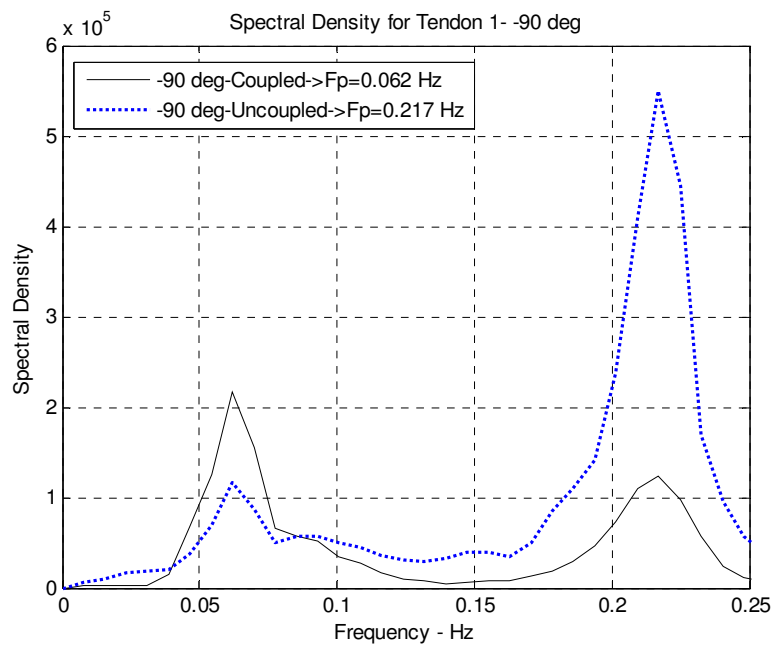Fig. 5-22. Mooring line 1 tension spectral density for 0 degree heading
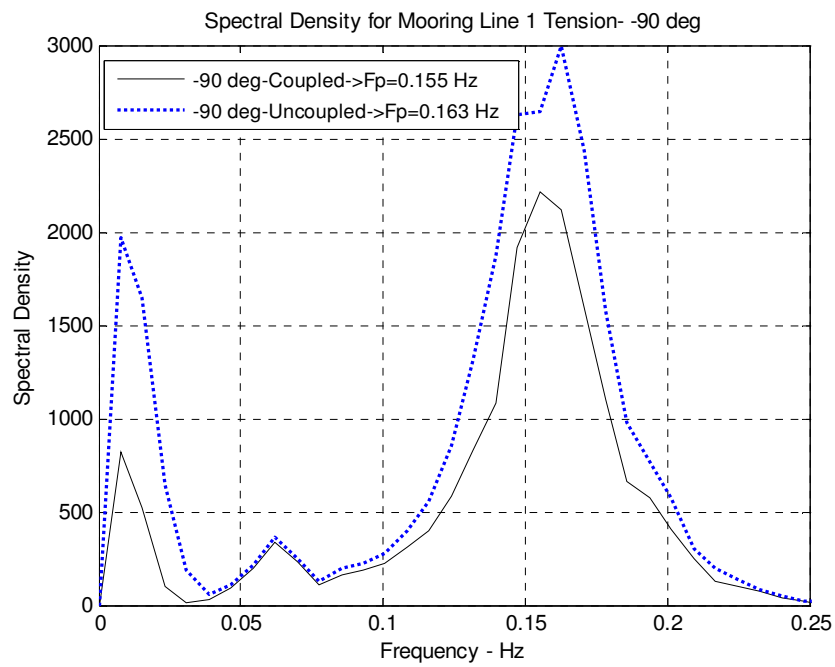
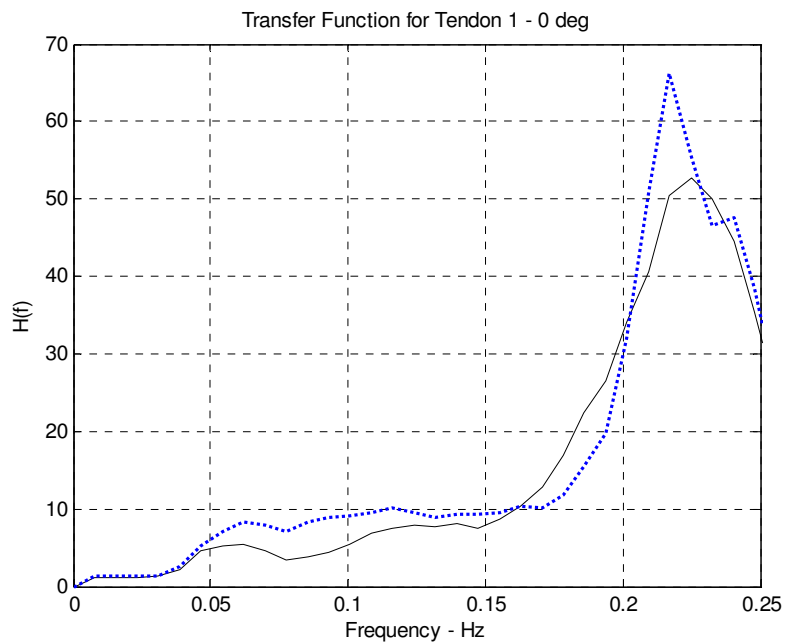Fig. 5-23. Mooring line 1 tension spectral density for -90 degree heading
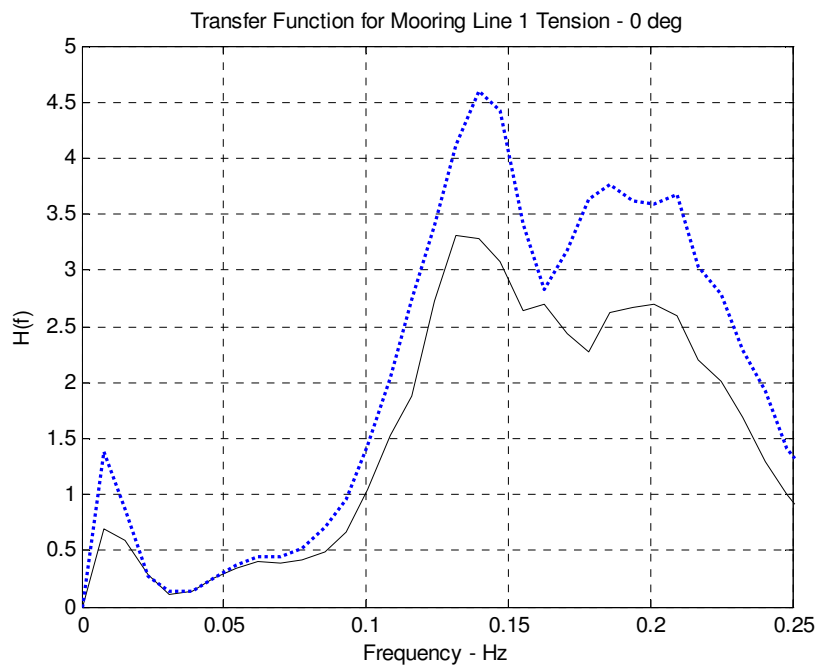
Fig. 5-24. Mooring line 1 tension transfer function for 0 degree heading

Fig. 5-25 shows the spectral densities for the tendon tensions for the 0 degree heading while Fig. 5-26 shows the corresponding tendon tension spectra for the -90 degree heading. The transfer function corresponding to the 0 degree heading is represented in Fig. 5-27. In addition to the low frequency resonance component and the wave frequency component, an additional high frequency peak can be observed for the tendon tensions. These correspond to the sum frequency effects and are in the higher frequency ranges of TLP heave, roll and pitch. For e.g. the uncoupled tendon 1 tension has an identifiable peak at 0.008 Hz which corresponds with the TLP surge and sway peaks at this frequency. These are the low frequency resonance components of the tension. A second peak at 0.062 Hz is the wave frequency component. In addition to these, a third peak is observed at approximately 0.225 Hz. These are the high frequency components and are attributed to the non-linear sum frequency wave effects.

As Fig. 5-25 indicates, the coupled case tendon tensions are much lower than the uncoupled case. But the difference in tensions for the coupled and uncoupled cases are not as pronounced as that for mooring tension as the tendons are already very taut. For the -90 degree case, the coupled and uncoupled cases show a significant difference in the high frequency tension component. The uncoupled case shows a much more dominant high frequency effect. These could be due to damping effects on TLP heave, pitch or roll motions in coupled case. But it is not possible to verify this as TLP pitch or roll data is unavailable while TLP heave remains unchanged for the 2 cases.

Also, the difference between the wave frequency and high frequency effects are much more pronounced in the -90 degree case with the uncoupled case having a very significant peak at high frequency. So for the -90 degree coupled case, the wave frequency component dominates while for the uncoupled case, the sum frequency component dominates. The wave remains unchanged for the 2 cases, hence it can be assumed that coupling significantly reduces TLP pitch and roll motions causing a reduced high frequency component.

The behavior patterns of the mooring lines and tendons are very different. The low frequency component changes significantly for the coupled and uncoupled cases in

mooring tension as the surge and sway motions of the barge reduce with coupling. However, the TLP surge and sway motions do not change much with coupling. The additional high frequency effects in tendon tensions are due to the sum frequency wave effects and can be attributed to the low period TLP heave, pitch and roll motions. This component is absent for the mooring line tensions as the line is a catenary and not a taut system like the TLP tendon.

Fig. 5-25. Tendon 1 tension spectral density for 0 degree heading

Fig. 5-26. Tendon 1 tension spectral density for -90 degree heading

Fig. 5-27. Tendon 1 tension transfer function for 0 degree heading

Fig. 5-28 shows the spectral densities for the fender X force for the 0 degree case while Fig. 5-29 shows the corresponding spectral density for the -90 degree case. The forces in the springs representing the corresponding breast line forces are shown in Fig. 5-30 for the coupled -90 degree case. The -90 degree case shows a clear peak for the fender force and the spring forces as the environment acts on the beam of the vessels and the relationship between the environmental forces and the fender / spring forces is more linear. As expected, the magnitudes of the forces are also much larger for the -90 degree case. The fender force shows a clear peak which corresponds to the wave forcing as does the spring forces for the -90 degree case. For the 0 degree case, the spring force spectra is spread over a wide band of frequencies which is indicative of the non-linear interactions between the incident environment from the bow and the vessel motions.
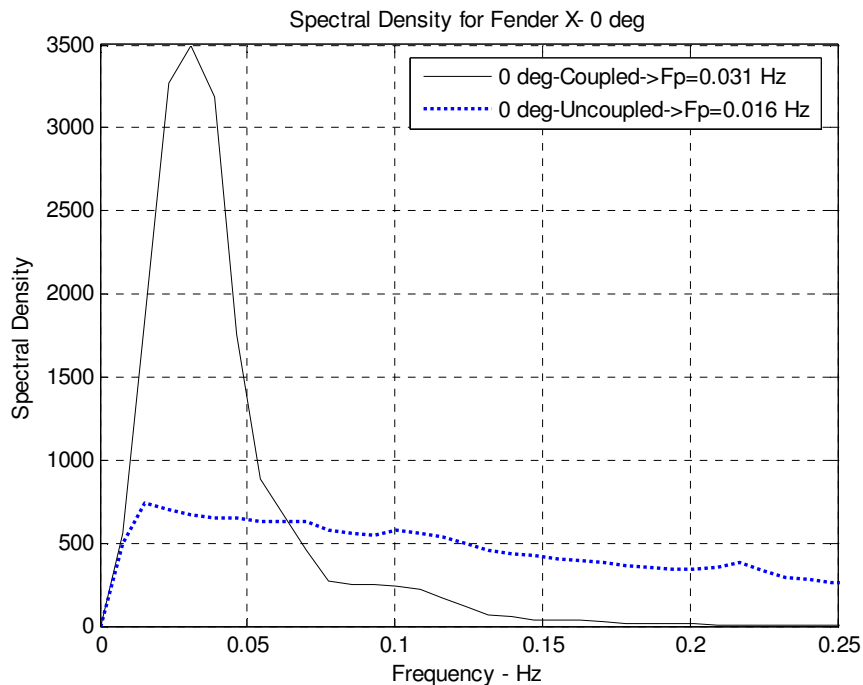
Fig. 5-28. Fender X spectral density for 0 degree heading
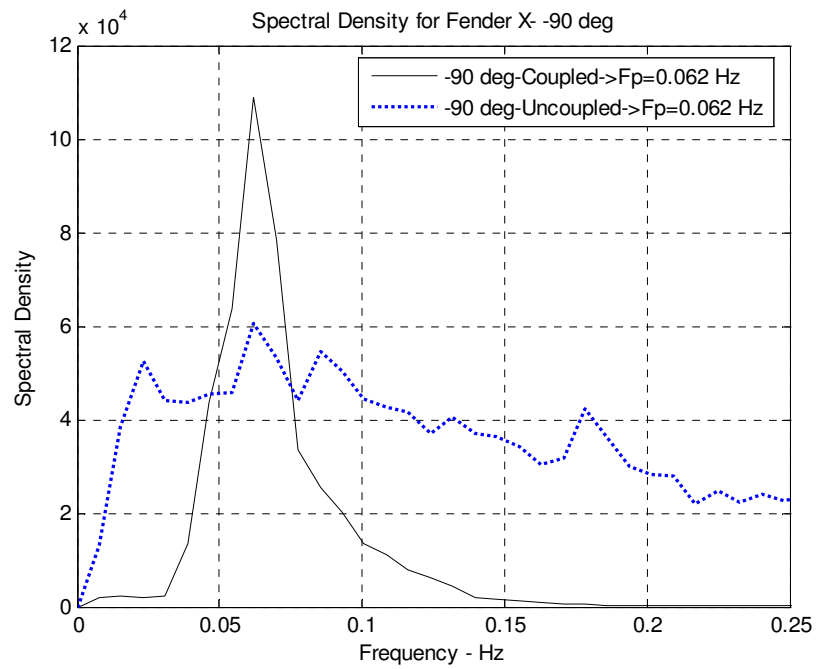
Fig. 5-29. Fender X spectral density for -90 degree heading
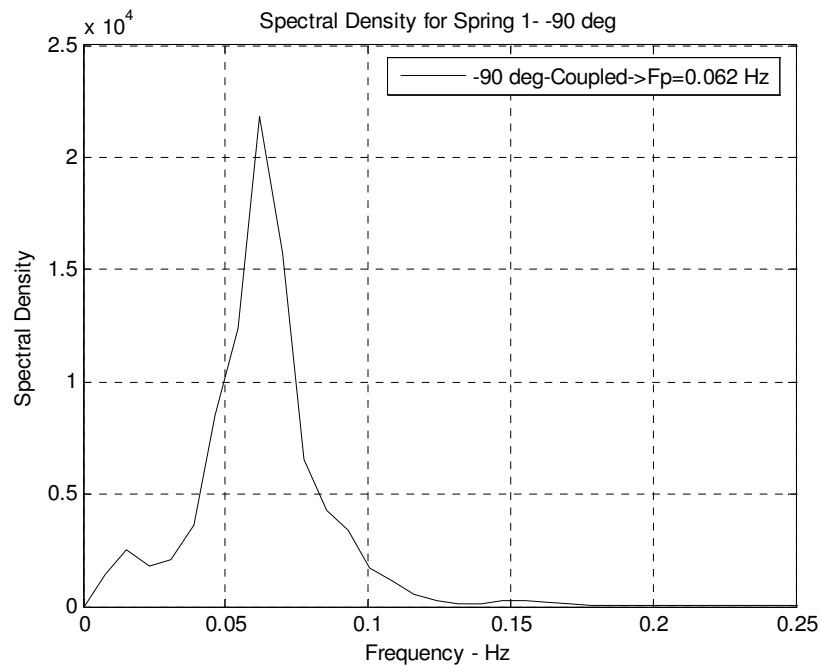
Fig. 5-30. Spring force spectral density for -90 degree heading

5.4   Cross spectral analysis

The cross spectral analysis is used to interpret the relationship between the different parameters measured during the experiment. A thorough investigation of all the results for the different cases is not feasible, hence only the results for the wind + wave + current case are considered here. This condition involves all the forcing components and hence should give a good indication of the correlation results which can then be applied for all the other cases as well. The mooring tension in line 1 has been considered for correlations involving mooring line tensions. Similarly, tendon tensions for tendon 1 and spring forces for spring 1 have been used.

Fig. 5-31 shows the coherence spectrum and cross correlogram between TLP surge and mooring tension in line 1 for the coupled and uncoupled cases for 0 degree environmental heading. It is evident that between the frequencies of 0.05 Hz and 0.15 Hz, the 2 parameters are very much predictable from one another as the linear coherence values in this range are close to 1. Also, for coupled case, TLP surge and mooring line 1 tension show a much higher correlation as can be seen from the cross correlogram. Similar results are observed for the -90 degree heading as well.

Fig. 5-32 analyses the cross correlation between TLP surge and the fender X forces for the 0 degree case while Fig. 5-33 shows the corresponding cross correlation for the incident -90 degree case. As can be seen from the linear coherence spectrum, the 2 parameters are more or less independent of each other for the 0 degree heading. However, as expected, for the -90 heading, the linear correlation between the 2 parameters is quite strong over the entire band of frequencies as the environment acts from the beam and in the direction of surge motion. Fig. 5-34 shows the relation between the TLP surge and the forces in spring 1 for the 0 degree heading while Fig. 5-35 shows the corresponding cross correlation for the -90 degree heading. The linear coherence function shows a very strong linear correlation between the 2 quantities for the majority of the frequencies for both 0 and -90 degree headings. The correlogram also shows a high correlation value indicating the 2 parameters are closely related to each other.
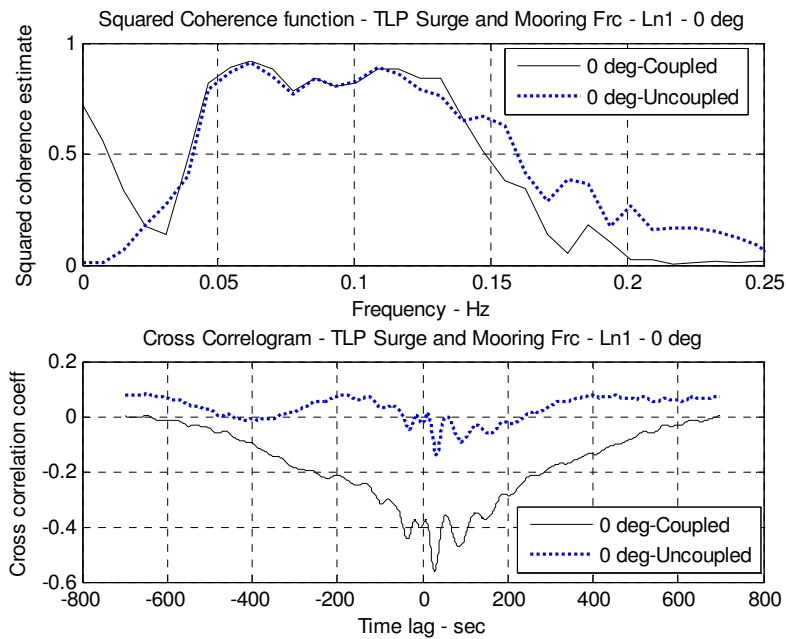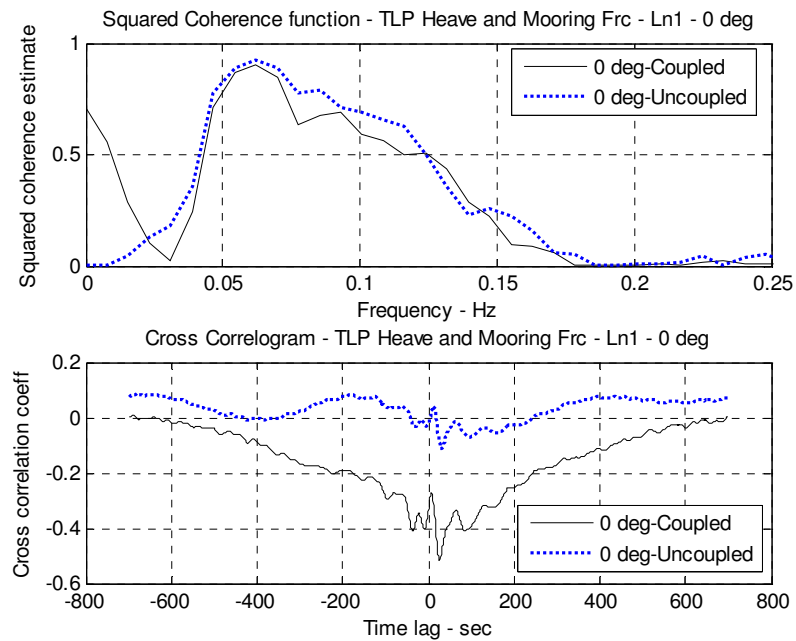
Fig. 5-31. Cross correlation: TLP surge and mooring line 1 tension for 0 degree heading
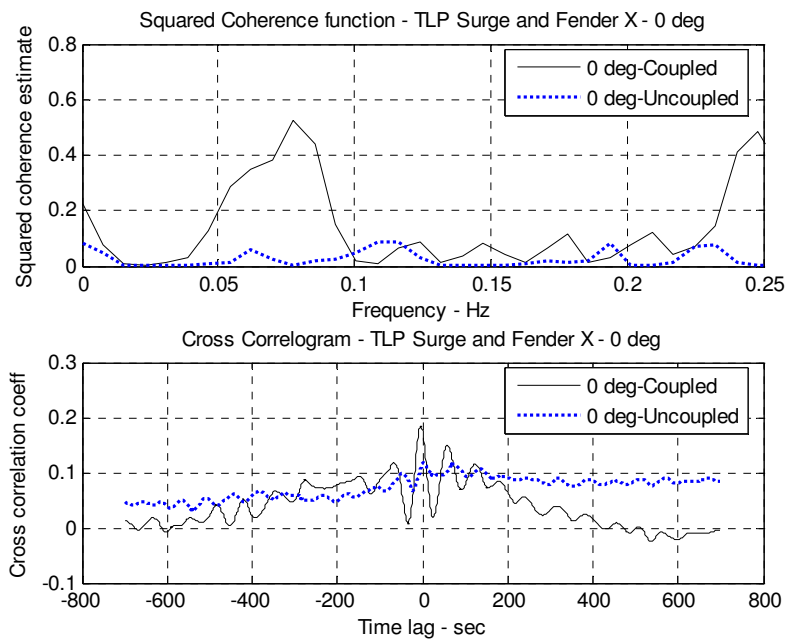
Fig. 5-32. Cross correlation: TLP surge and fender X for 0 degree heading
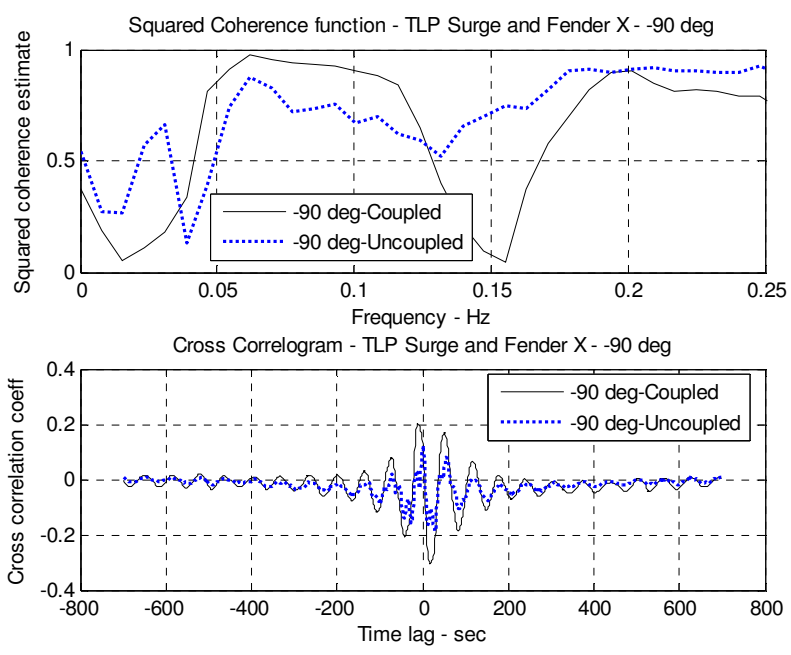
Fig. 5-33. Cross correlation: TLP surge and fender X for -90 degree heading
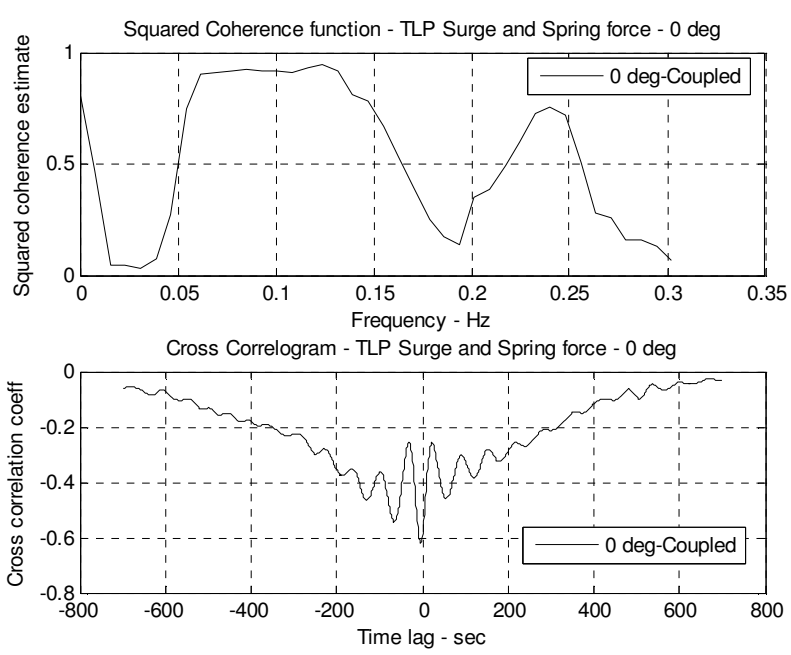
Fig. 5-34. Cross correlation: TLP surge and spring force for 0 degree heading
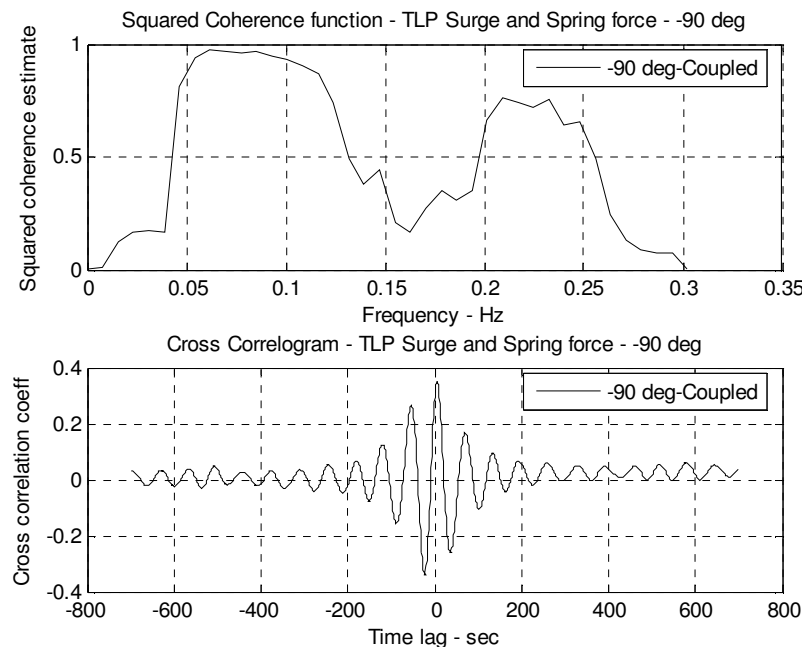
Fig. 5-35. Cross correlation: TLP surge and spring force for -90 degree heading

Fig. 5-36 and Fig. 5-37 show the coherence spectrum between barge surge and tension in tendon 1 for the 0 degree heading and -90 degree heading respectively. The coherence function shows a strong linear correlation between 0.05 Hz and 0.1 Hz. Surprisingly, the correlation is higher for the uncoupled case when compared to the coupled case for the 0 degree heading. The barge surge value shows a sharp decrease when the vessels are coupled. An inspection of the spectral density for the barge surge shows that the coupled case surge values are significantly lower than the uncoupled case surge for the 0 degree heading. This difference is relatively less pronounced for the -90 degree heading. This is one of the reasons for the barge surge in the uncoupled case to have a slightly higher degree of linear correlation with the tendon tension for 0 degree heading.

The cross relation between barge surge and fender X force is exactly the same as for the TLP surge – fender X case with almost no correlation for the 0 degree case and a very strong linear relationship for all the frequencies in -90 degree heading.
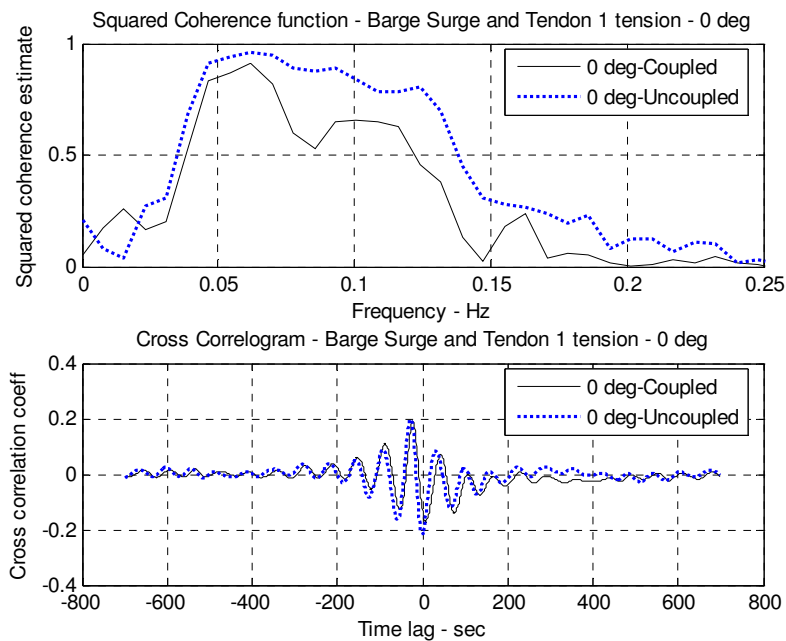
Fig. 5-36. Cross correlation: barge surge and tendon 1 tension for 0 degree heading
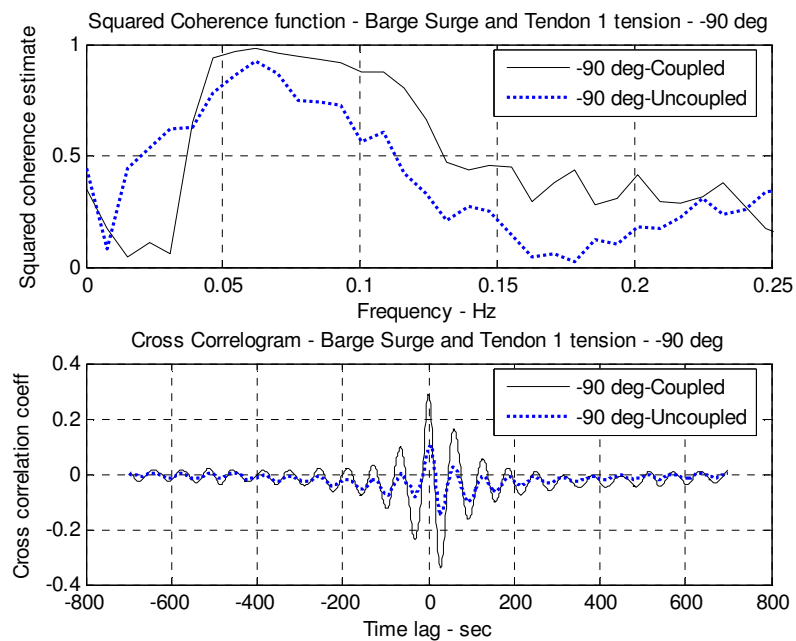
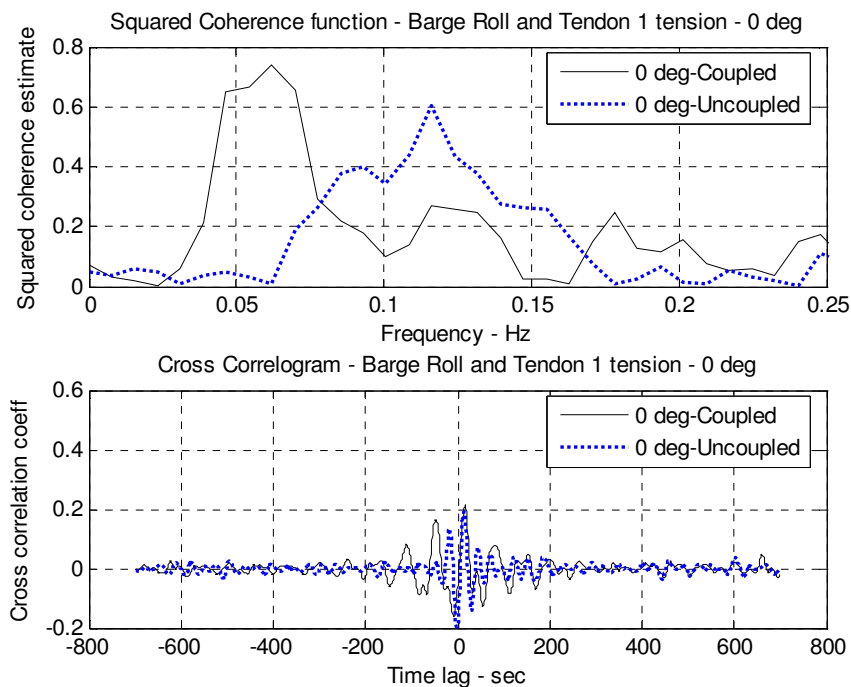

Fig. 5-37. Cross correlation: barge surge and tendon 1 tension for -90 degree heading

Fig. 5-38 shows the relation between barge sway and tendon 1 tension for the 0 degree heading while Fig. 5-39 shows the corresponding coherence for the -90 degree case. The results show that there is almost no linear coherence between the two quantities for either heading. Similar results are observed for all the cross correlations involving TLP and barge sway. Thus it is evident that neither TLP sway nor barge sway are significantly related to any of the mooring/ tendon/ spring tensions or fender forces and sway is a relatively independent quantity.
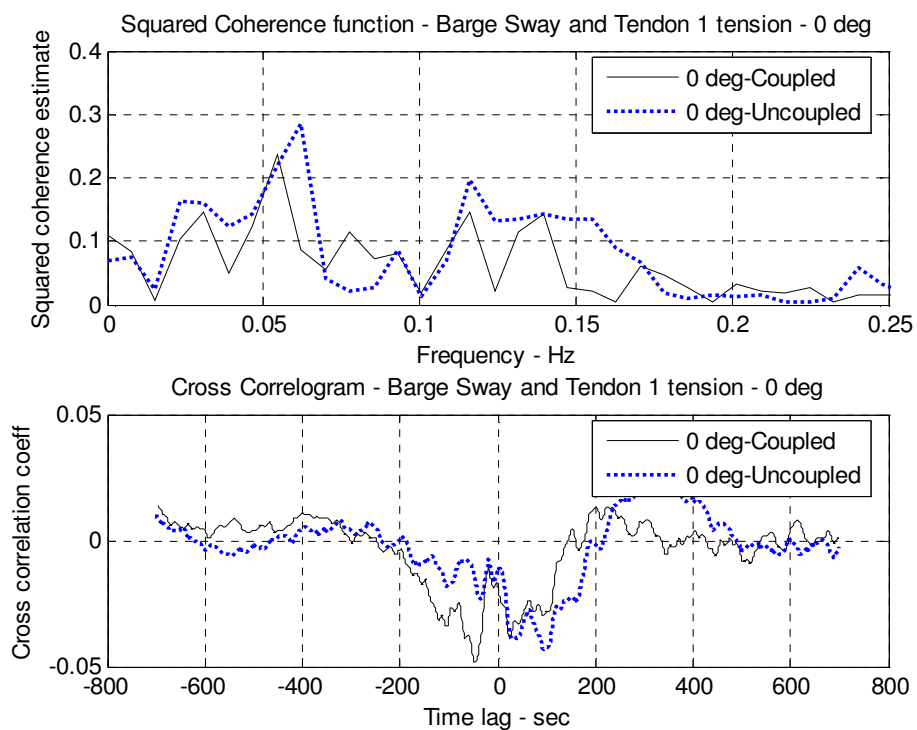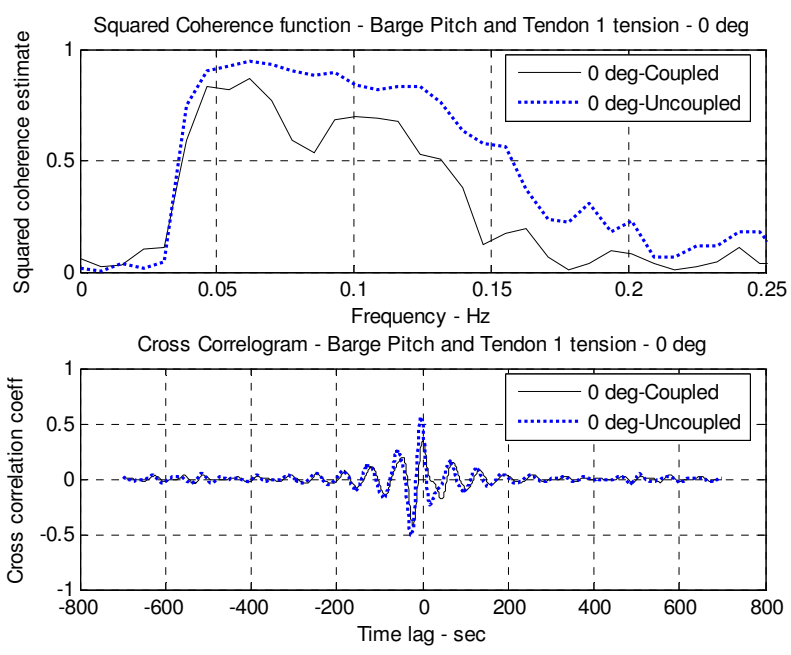

Fig. 5-38. Cross correlation: barge sway and tendon 1 tension for 0 degree heading
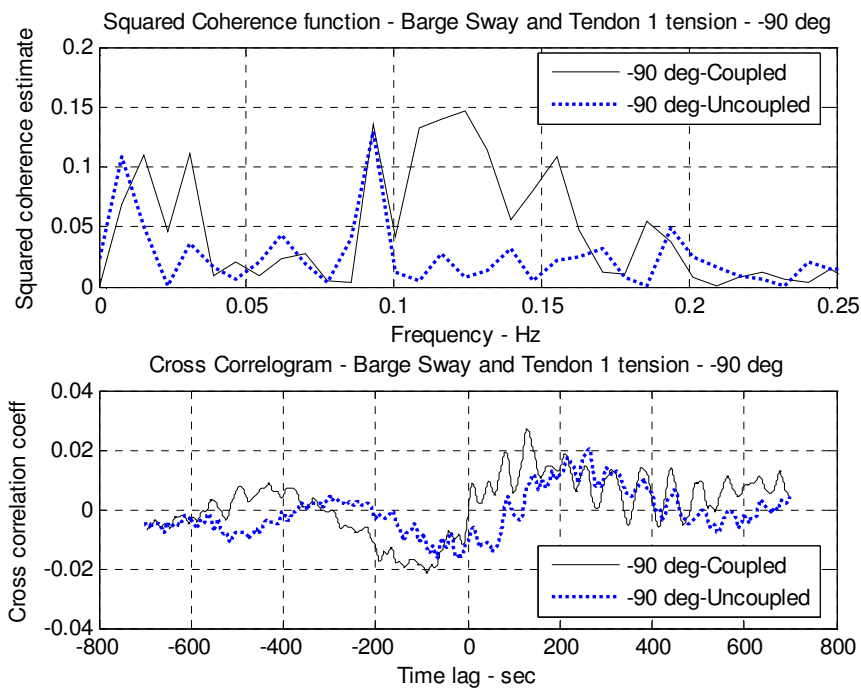
Fig. 5-39. Cross correlation: barge sway and tendon 1 tension for -90 degree heading

Fig. 5-40 shows the cross spectral analysis between TLP heave and the mooring line tension for the 0 degree heading. There is a strong linear correlation between the two for a frequency band of 0.05 Hz to 0.13 Hz. The -90 degree heading also shows very similar results. Fig. 5-41 shows the results for TLP heave – fender X analysis for the 0 degree heading. For the 0 degree heading case, there is almost no correlation between the 2 except in the frequency band between 0.05 Hz and 0.1 Hz (only for coupled case). The -90 degree heading case shows a similar trend for coherence. The cross analysis results between TLP heave and the spring force and the results are again exactly the same as those for the heave correlation with mooring line tension. Hence it is obvious that TLP heave only influences the mooring and fender forces in this small frequency range.

Fig. 5-40. Cross correlation: TLP heave and mooring line 1 tension for 0 degree heading
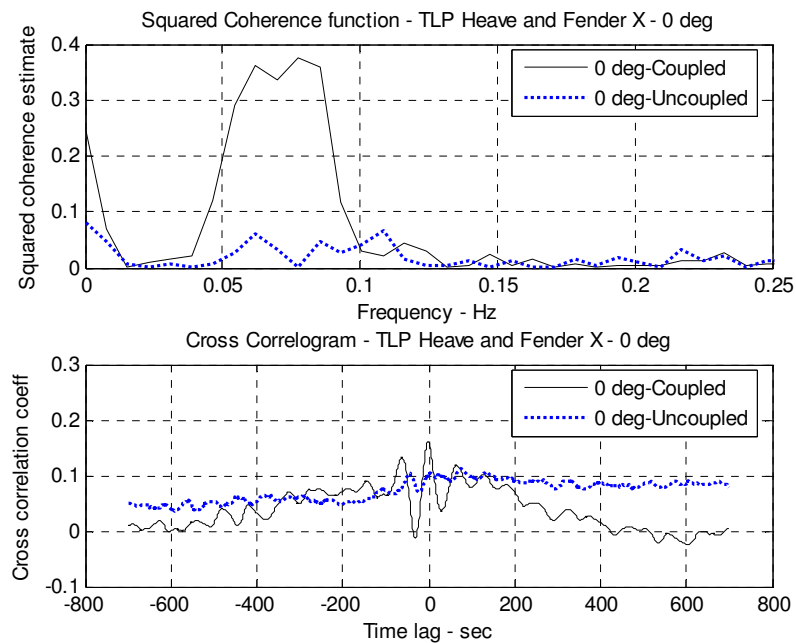
Fig. 5-41. Cross correlation: TLP heave and fender X for 0 degree heading

Fig. 5-42 shows the results for cross analysis between barge heave and tendon 1 tension for the 0 degree heading with similar results being observed for the -90 degree heading also. Again, the coherence is strong between a frequency range of 0.05 Hz to 0.15 Hz and falls off after that. However for the 0 degree heading, the uncoupled case shows a much stronger correlation than the coupled case.

The interaction effects between barge heave and the fender force for the -90 degree are similar to the corresponding TLP heave – fender X -90 degree case. A very strong linear relation is observed between the two parameters between 0.05 Hz and 0.15 Hz. However, for the 0 degree heading a poor correlation is seen for all the frequencies. So for the -90 degree case, both TLP and barge heave influence the fender forces significantly. The coherence analysis between barge heave and spring forces show results that are similar to the TLP heave – spring force analysis. The 0 degree case shows a strong correlation between 0.05 Hz and 0.15 Hz. But the -90 degree case shows a high coherence value for a much larger band of frequencies (0.05 to 0.2 Hz).
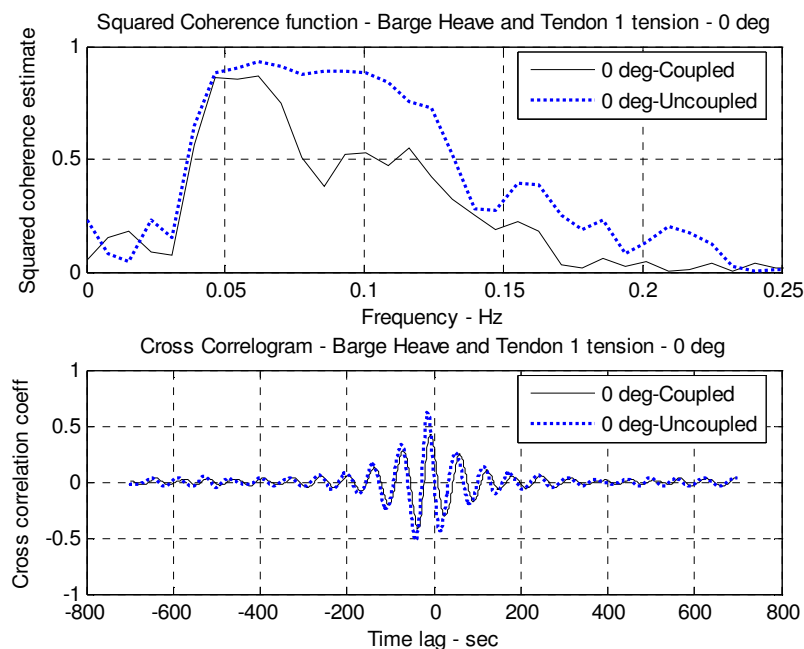
Fig. 5-42. Cross correlation: barge heave and tendon 1 tension for 0 degree heading

Fig. 5-43 and Fig. 5-44 show the results of the cross spectral analysis between barge roll and tendon tension. For the 0 degree heading, the coherence between the two is very low except for a small frequency band. However for the -90 degree case, there is a strong liner relationship between barge roll and tendon tension between 0.05 Hz and 0.15 Hz. This is expected since the -90 degree case has the incident environment acting on the system from beam side. The coupled case shows a better coherence as coupling reduces barge roll motion. The cross spectral analysis results between barge roll motion and fender X force and between barge roll motion and spring force yield results similar to the previous trends. The correlation is poor for 0 degree heading in both cases. However for the -90 degree case, there is a high degree of coherence and the quantities show a linear correlation for a wide band of frequencies.

Fig. 5-43. Cross correlation: barge roll and tendon 1 tension for 0 degree heading
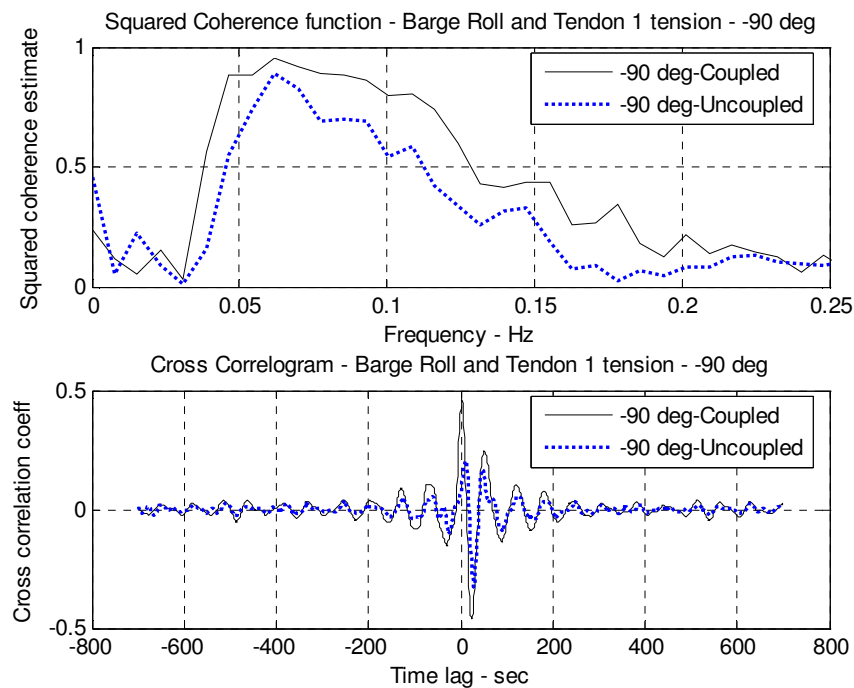
Fig. 5-44. Cross correlation: barge roll and tendon 1 tension for -90 degree heading

Fig. 5-45 shows the results from the cross spectral analysis between barge pitch and tendon tension for the 0 degree heading. An interesting observation here is that the two quantities show a strong linear coherence for the 0 degree heading (for both coupled and uncoupled cases). But for the -90 heading, the coherence values are very low. A poor correlation is observed between the barge pitch forces and fender forces for both 0 and - 90 degree headings. The results for the -90 degree case are shown in Fig. 5-46. The results for correlation between barge pitch and spring forces are very similar to those between barge pitch and tendon tension. The 0 degree heading results show very strong linear correlations while the -90 degree heading results show almost no correlation. Thus, the barge pitch motion influences the tendon and spring forces only in the 0 degree heading when the environment is incident from the bow. It has no interaction with the fender forces for either of the headings.

Fig. 5-45. Cross correlation: barge pitch and tendon 1 tension for 0 degree heading
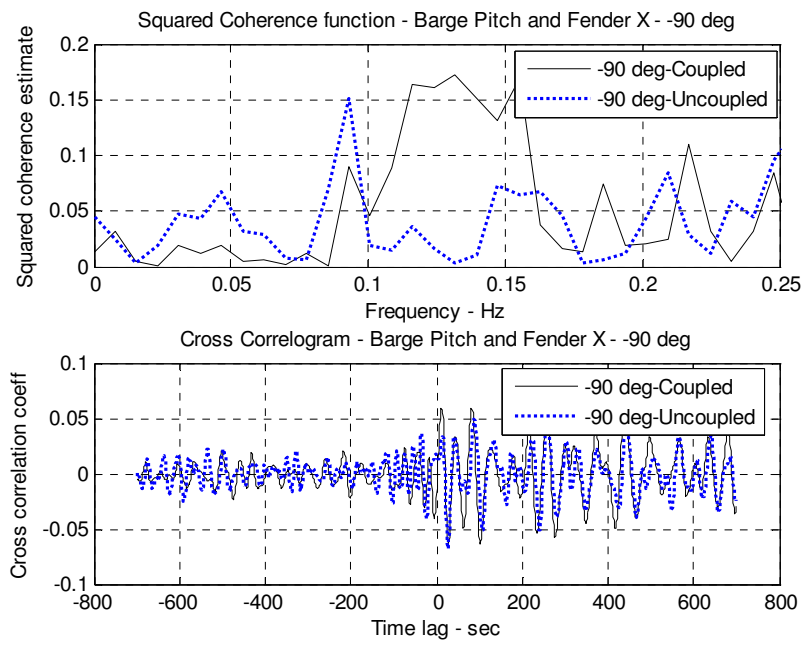
Fig. 5-46. Cross correlation: barge pitch and fender X for -90 degree heading

Fig. 5-47 analyses the interaction results between barge yaw and tendon tension for the 0 degree case while Fig. 5-48 analyses the corresponding cross correlation for the -90 degree heading. The relationship between the two is not very strong as the linear coherence plot shows a coherence value of around 0.7 at frequencies between 0.06 Hz and 0.15 Hz. However, for the -90 degree heading, the uncoupled case shows almost no correlation between the two parameters. Fig. 5-49 shows the cross spectral results between barge yaw and fender forces for the -90 degree heading. For the 0 degree heading, there is no linear correlation between the two. But as expected, there is a certain degree of linear relationship between the two for the -90 degree heading. Again, the coherence is close to 0.6 for a small range of frequencies. For the coherence analysis between barge yaw and the spring forces, both 0 degree and -90 degree cases show a certain degree of interaction effect between the two parameters. The coherence value is around 0.7 for a wide band of frequencies. So it can be interpreted that barge yaw does have a certain degree of influence on tendon and spring forces for both 0 and -90 degree headings.
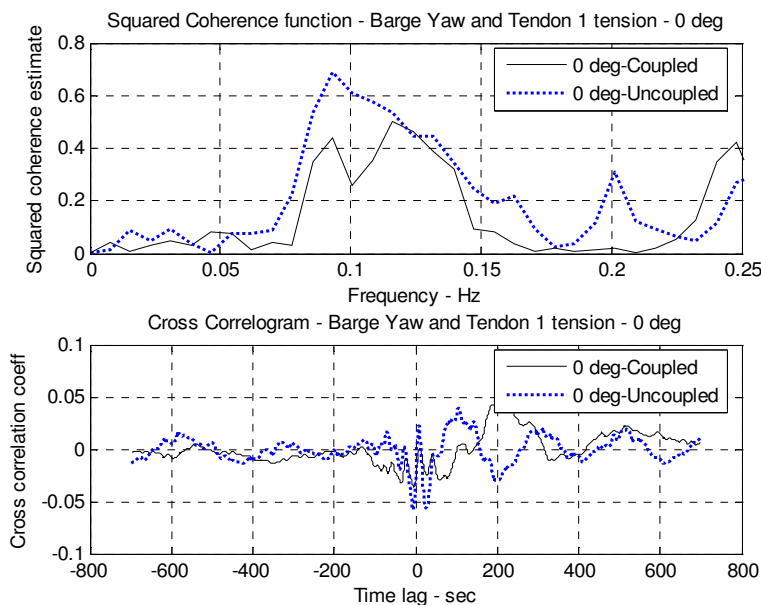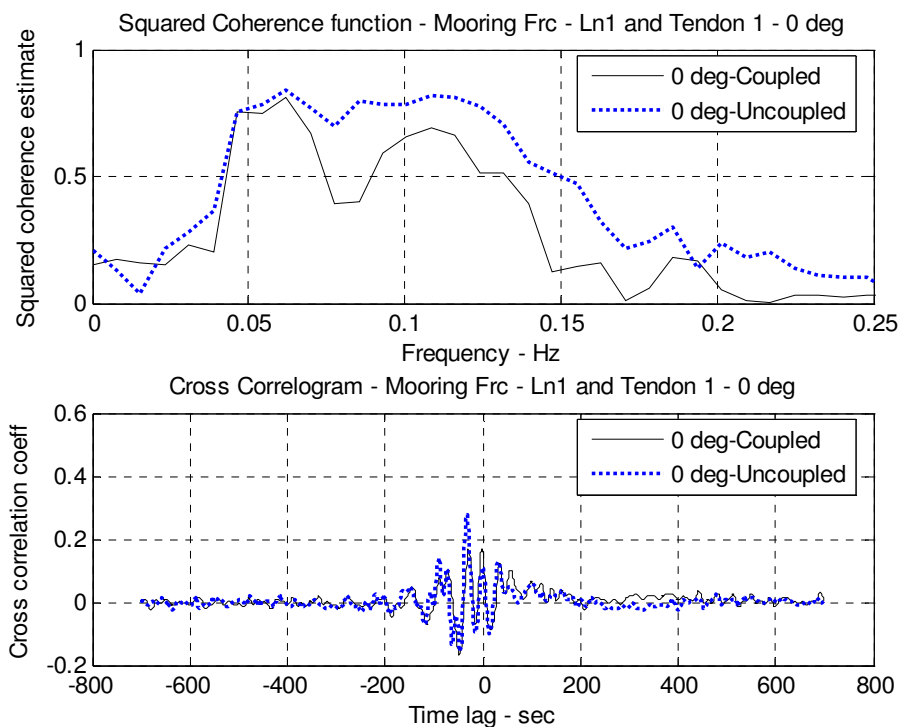

Fig. 5-47. Cross correlation: barge yaw and tendon 1 tension for 0 degree heading
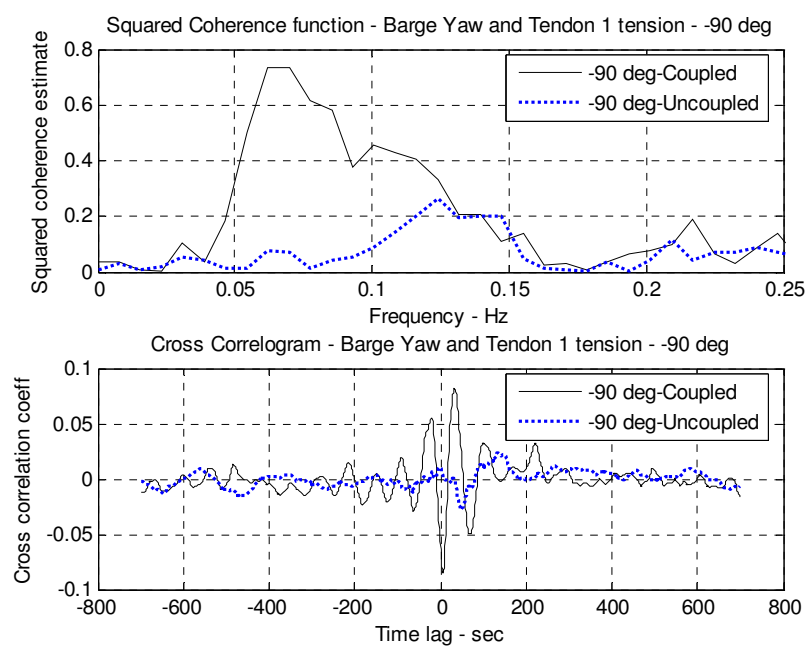
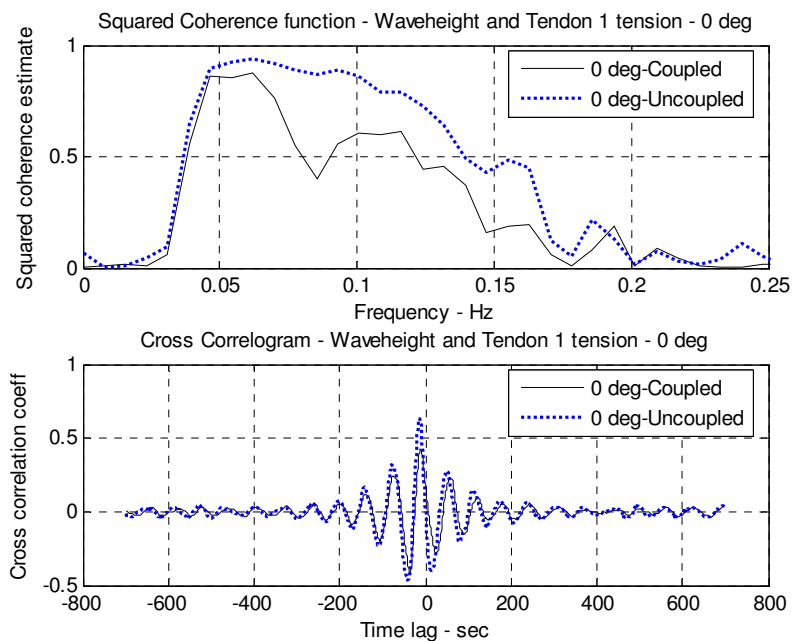Fig. 5-48. Cross correlation: barge yaw and tendon 1 tension for -90 degree heading
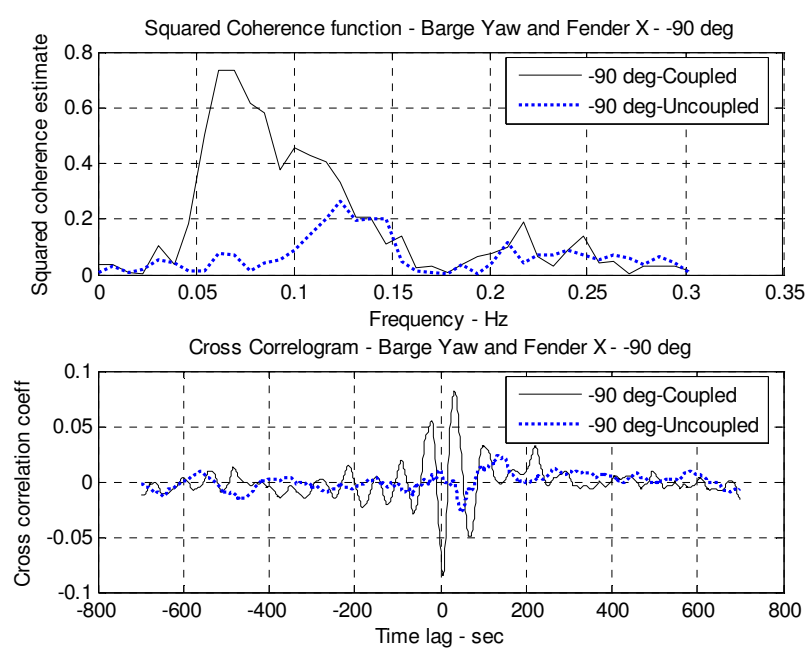
Fig. 5-49. Cross correlation: barge yaw and fender X for -90 degree heading

Fig. 5-50 and Fig. 5-51 show the results from cross spectral analysis between mooring line tension in line 1 and fender X forces for the 0 degree and -90 degree headings respectively. As before, the 0 degree heading case shows almost no correlation between the two quantities. But, when the incident environment is from the beam (-90 degree heading), the two quantities show a very strong linear correlation for a wide band of frequencies. A very similar interaction effect is observed for the cross analysis between tendon tension and fender forces as well.
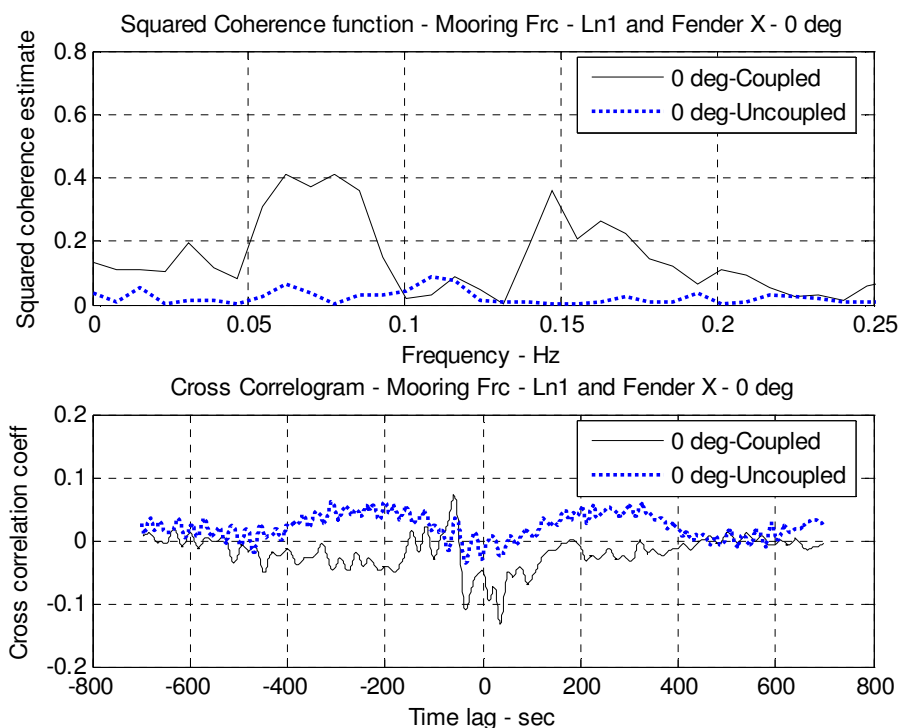
Fig. 5-50. Cross correlation: mooring line 1 tension and fender X for 0 degree heading
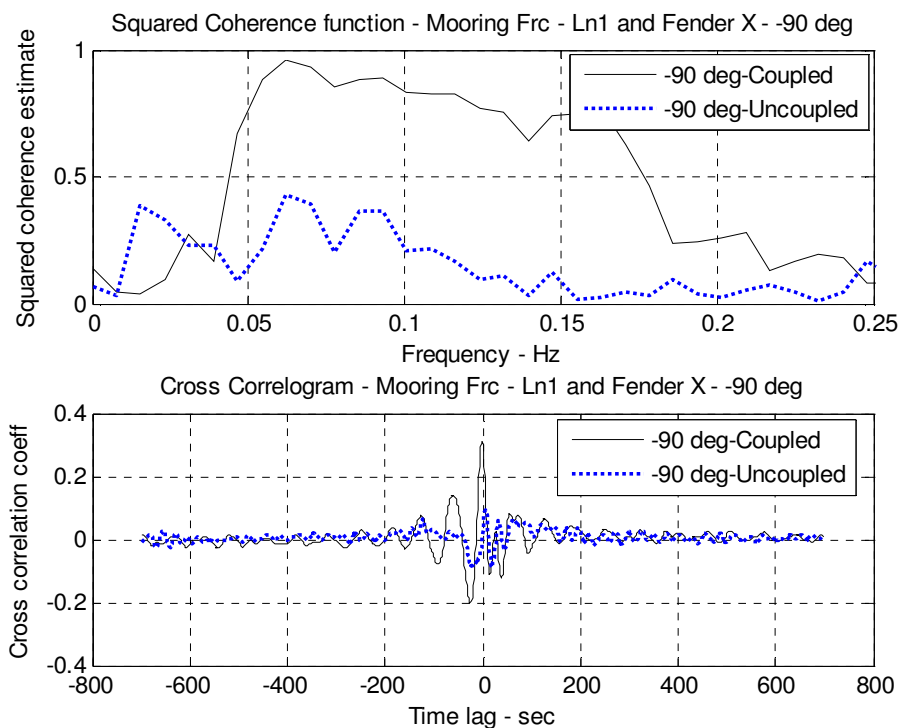
Fig. 5-51. Cross correlation: mooring line 1 tension and fender X for -90 degree heading

Fig. 5-52 and Fig. 5-53 show the analysis results for correlation between mooring line tension and spring forces for 0 degree heading and -90 degree heading respectively. Again, there is a strong linear correlation between the two parameters for both 0 degree and -90 degree cases although as expected, the -90 degree case shows a strong coherence value over a much wider band of frequencies. The relationship between tendon tensions and spring forces and between fender forces and spring forces is similar in nature. The fenders and the springs (representing the breast lines) together form the coupling system between the bodies and it is to be expected that they will linearly influence each other for any environment heading. So it is obvious that the fenders, mooring lines and the tendons have a strong influence on the spring forces.
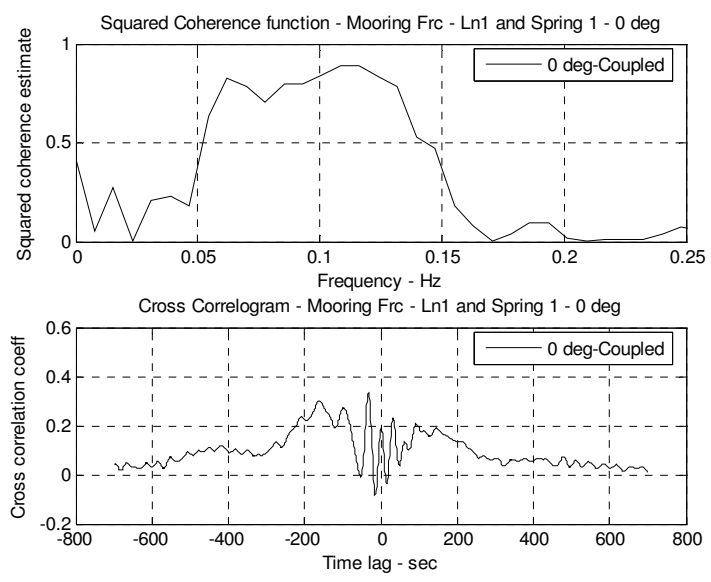
Fig. 5-52. Cross correlation: mooring line 1 tension and spring 1 force for 0 degree
heading
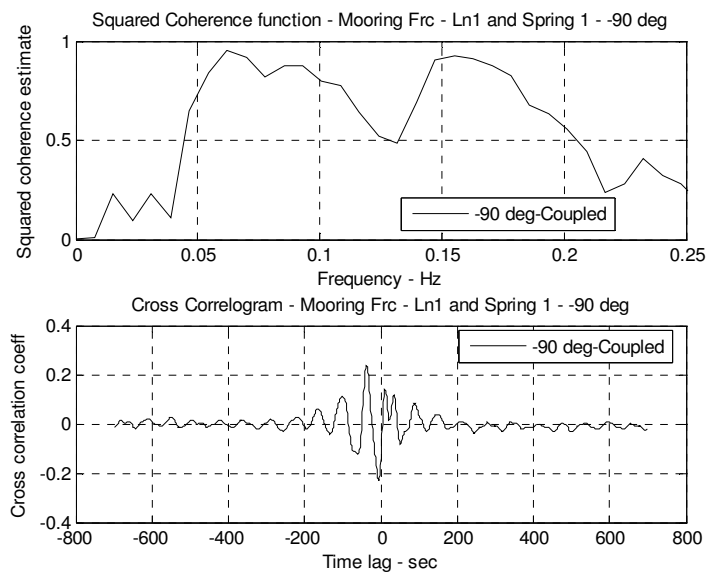
Fig. 5-53. Cross correlation: mooring line 1 tension and spring 1 force for -90 degree
heading

Fig. 5-54 shows the cross analysis results for mooring line tension and tendon tension for the 0 degree heading and Fig. 5-55 shows the corresponding results for the -90 degree heading. Both show a very strong linear correlation for both coupled and uncoupled cases. Hence, there are interaction effects between mooring line and tendon tensions to a certain degree irrespective of the environment heading and irrespective of whether the vessels are connected to each other or not.

Fig. 5-54. Cross correlation: mooring line 1 and tendon 1 tension for 0 degree heading
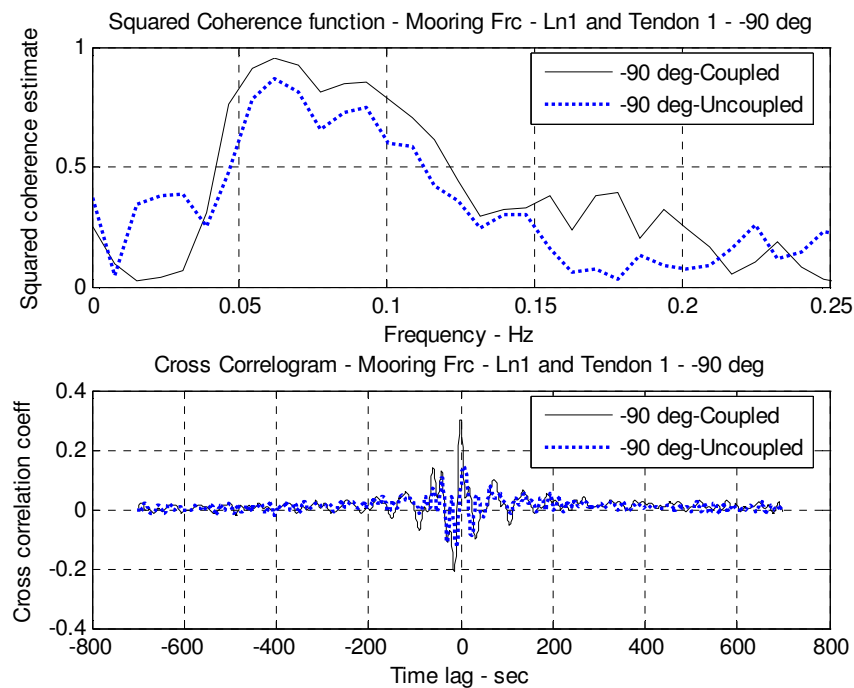
Fig. 5-55. Cross correlation: mooring line 1 and tendon 1 tension for -90 degree heading

Fig. 5-56 and Fig. 5-57 show the cross spectral analysis results for the waveheight and mooring line tension for 0 degree and -90 degree respectively. The coherence spectrum shows a very good correlation between the 2 parameters for both 0 degree and -90 degree cases for the band of frequencies between 0.05 Hz and 0.15 Hz. Both coupled and uncoupled cases show very similar results implying that coupling effects are not very important for the waveheight – mooring line tension interactions. Fig. 5-58 and Fig. 5-59 show the cross spectral results for analysis between waveheight and tendon tensions for 0 and -90 degree headings. Again, there is a good degree of coherence for the frequency band between 0.05 Hz and 0.15 Hz for both 0 degree and -90 degree cases. However, the uncoupled case shows a higher correlation for the 0 degree case. The parameter that is important here is the tendon tension as the waveheight remains unchanged for both coupled and uncoupled cases. The tendon tension reduces slightly with coupling effects.
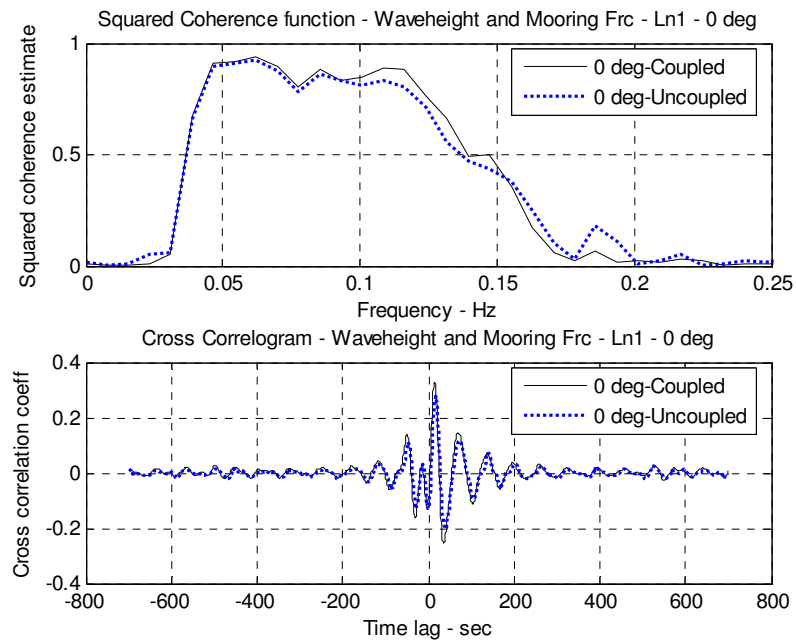
Fig. 5-56. Waveheight and mooring line 1 tension for 0 degree heading
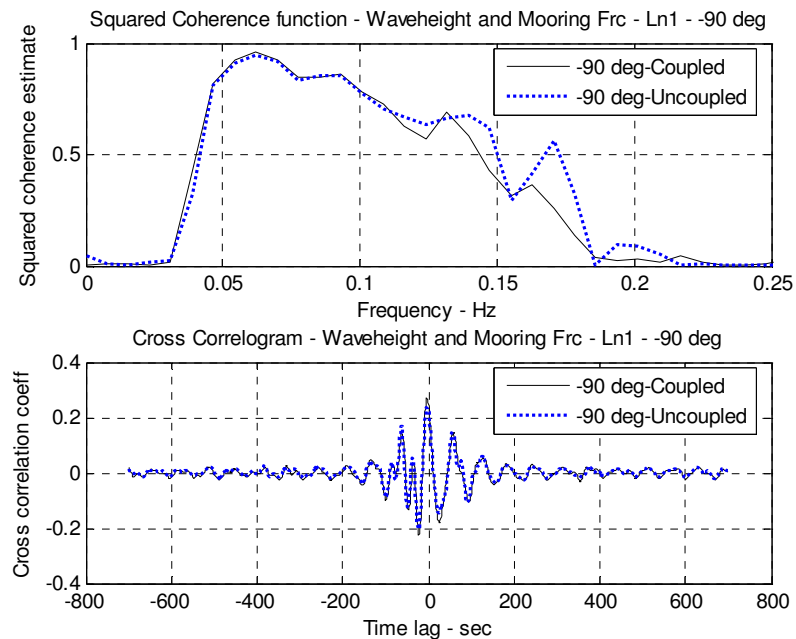
Fig. 5-57. Cross correlation: waveheight and mooring line 1 tension for -90 degree heading

Fig. 5-58. Cross correlation: waveheight and tendon 1 tension for 0 degree heading
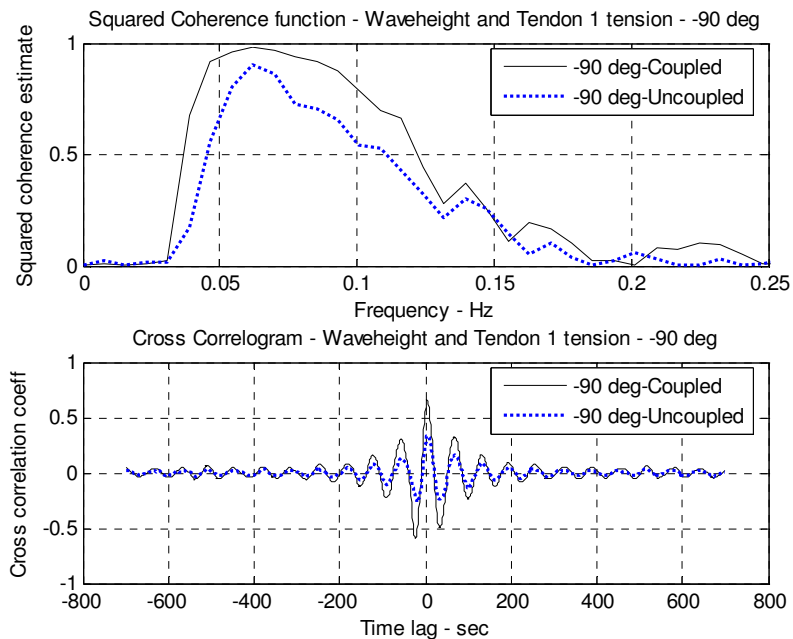
Fig. 5-59. Cross correlation: waveheight and tendon 1 tension for -90 degree heading

Fig. 5-60 shows the cross spectral analysis between waveheight and fender forces for the 0 degree heading while Fig. 5-61 shows the corresponding results for the -90 degree heading. As expected, the -90 degree heading case shows very high linear correlation between the two parameters for a wide band of frequencies. The waves hit the coupled system from the beam side for the -90 degree case pushing the TLP against the barge and hence a linear correlation between the waves and fender forces is expected. The 0 degree case has the waves hitting the system from the bow and hence the relation between waveheight and fender forces cannot be a linear one. Fig. 5-62 and Fig. 5-63 show the results for the waveheight – spring force cross analysis for the 0 degree and -90 degree headings respectively. Both 0 degree and -90 degree cases show a very strong linear relationship over a wide band of frequencies implying that the waves directly influence the tension in the breast lines connecting the TLP and barge.
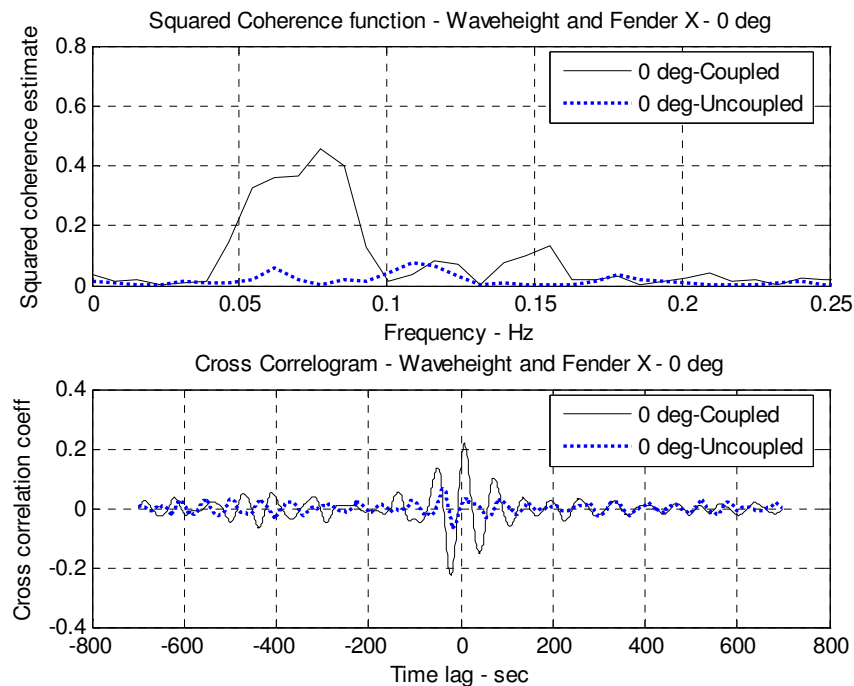
Fig. 5-60. Cross correlation: waveheight and fender X for 0 degree heading
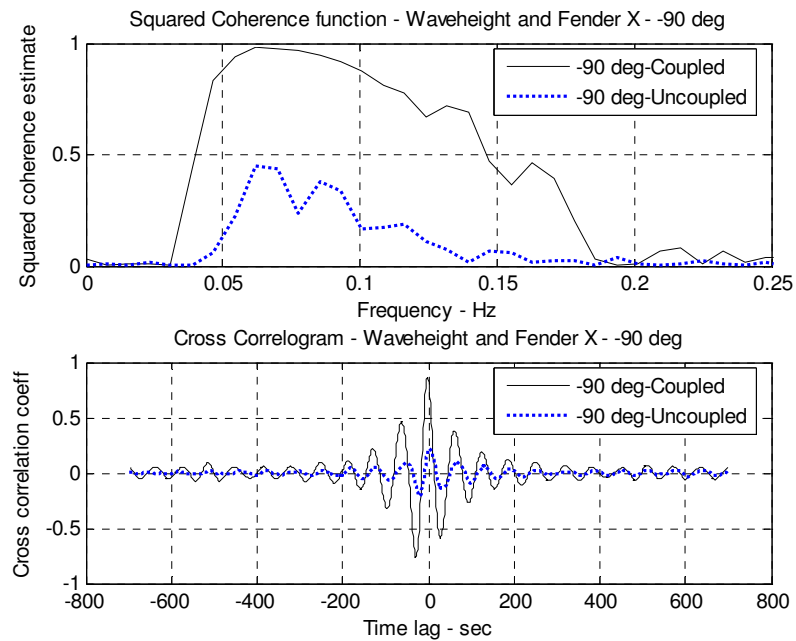
Fig. 5-61. Cross correlation: waveheight and fender X for -90 degree heading
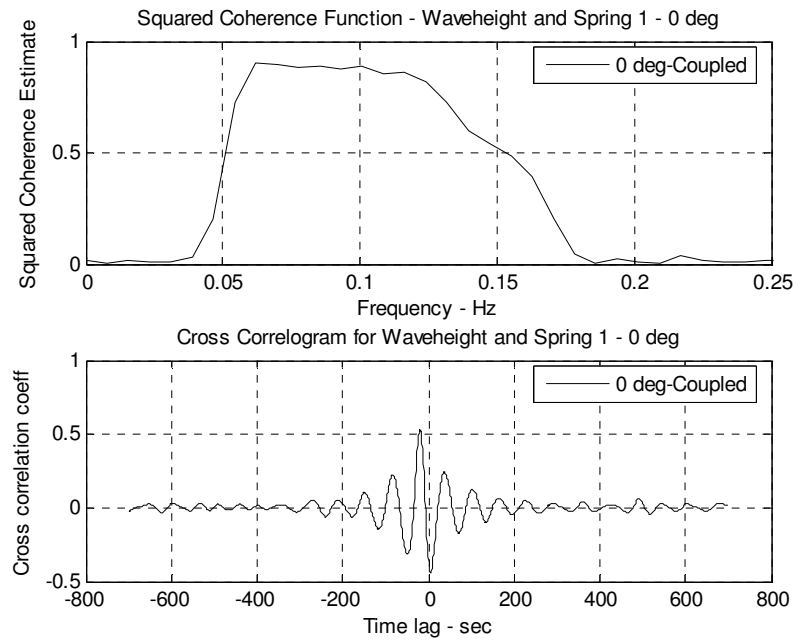
Fig. 5-62. Cross correlation: waveheight and spring 1 force for 0 degree heading
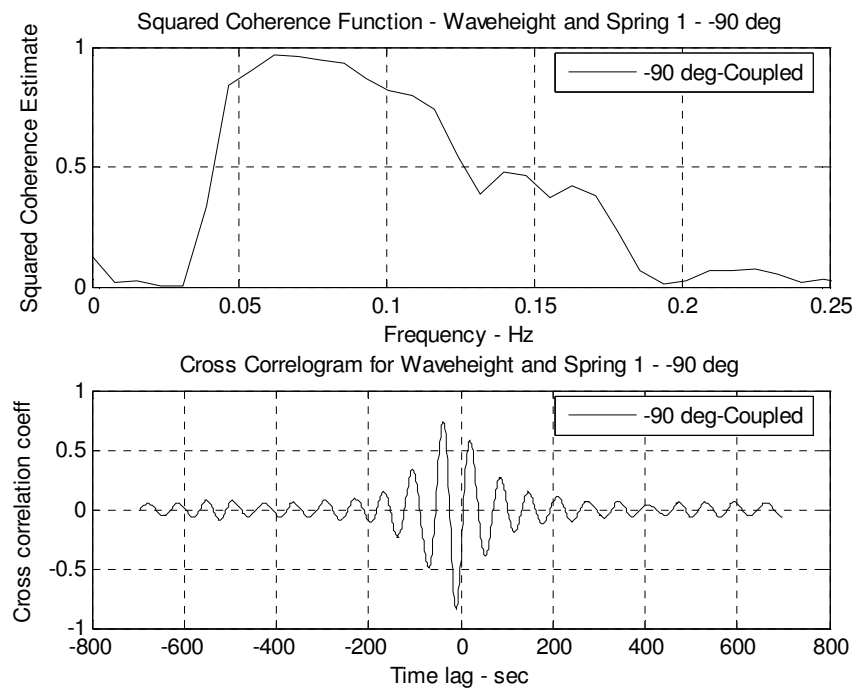
Fig. 5-63. Waveheight and spring 1 force for -90 degree heading

6. CONCLUSIONS

The focus of this thesis was in the use of statistical analysis methods to determine the characteristics of mooring line tensions, tendon tensions and fender forces for a mini-TLP – barge experiment for 0 degree and -90 degree environment headings. Two different cases were considered. In the first case, the response of the uncoupled platforms was investigated. In the second case, the vessels were coupled to each other with a fender – breast line soft connection. The cross correlations and interference / coupling effects of the mini-TLP and barge motions with these parameters were studied to assess the degree of non-linearity in this two-body hydrodynamic system.

The analyses of the data distribution patterns show that the mooring line tensions, tendon tensions and the fender forces closely follow a broad banded Gaussian distribution pattern for most cases. Although the broad – banded processes analyzed tend to follow a Gaussian pattern, the extreme values do not necessarily conform to a Gaussian distribution which implies non-linearity in the system. The extreme values for several key parameters were identified in the appropriate data sets and then modeled using a Weibull distribution. In particular, probability of exceedance plots were developed using the maxima and when compared with an ideal two-parameter Weibull distribution, it was shown that the Weibull distribution fits the low to moderate extreme responses very well, but tends to overestimate the largest values. The mooring line tensions, tendon tensions and fender forces show a very high degree of non-linearity as indicated by the high MPM values.

The sensitivity of the Fourier transforms used to evaluate the spectral density was investigated. It was illustrated that the 512 point Fourier transform best fits the JONSWAP wave spectrum with a peakedness factor of 2. Moreover, it was shown that the 512 point Fourier transform poorly resolves the low frequency response components for mooring line tensions and tendon tensions. However, spectral densities using higher number of points result in plots which were more complicated.

Comparison of the spectral density plots and transfer functions for mooring line tensions, tendon tensions, fender forces, coupling spring tensions and the mini-TLP /

barge motions for the 0 degree and -90 degree environment headings, for both coupled and uncoupled cases, lead to some interesting results. An inspection of the mini-TLP and barge motions show that the mini-TLP motions are generally not influenced by coupling between the bodies. However, the barge surge, sway, roll and yaw motions are significantly reduced when the vessels are coupled. The exceptions are the barge heave and pitch motion which are found to be independent and controlled by the barge and its mooring system design. It is clearly evident that the high tendon tensions keep the mini-TLP relatively stiff while the barge is more compliant as its catenary mooring system is less stiff. Also, the mooring system mostly provides stiffness in the horizontal plane and hence the vertical motions for both the vessels largely remain unaffected by coupling. For the -90 degree heading, the barge is partially masked by the mini-TLP and this affects the coupling influence on barge sway motion. For the most part, both coupled and uncoupled configurations show similar values for barge sway. The coupling resulting from the fender – breast line system reduces the barge horizontal plane motions significantly and is influenced by the masking effects of the TLP for the -90 degree case.

The spectrum of the mooring line tension shows two distinct peaks with the first peak corresponding to the low frequency resonance effects of the barge surge and sway motions and the next peak resulting from wave frequency effects. It was observed that when the two bodies are coupled, the mooring line tensions fall significantly as the coupling system takes a part of the load. Interestingly, the coupling effects are visible only in the low frequency resonant range as the coupling directly influences the barge surge and sway motions. The second peak corresponding to the wave excitation remains unchanged and hence the wave frequency range mooring tensions remain unaffected by coupling effects. Further, it was observed that the low frequency mooring tension effects dominate for the 0 degree heading case while for the -90 degree heading, the wave frequency effects dominate.

The spectrum of tendon tension shows three distinct peaks. The first corresponds to the low frequency resonance effects of TLP surge and sway motions. The second is again associated with the wave frequency effects and the third peak is associated with the high

frequency effects corresponding to TLP heave, roll and pitch. The tendons are very taut unlike the catenary mooring lines and hence the coupling effects between the two vessels do not change the tendon tensions significantly. The important effects are noticeable in the high frequency ranges for the -90 degree heading. The fender forces and the coupling spring forces are more significant in the -90 degree heading when the environment hits the vessels from the beam pushing the vessels against each other. The -90 degree case has a more linear relationship between the incident environment and the fender / spring forces. But the 0 degree case shows a high degree of non-linear interaction between the incident environment and fender / spring forces.

For the -90 degree headings, the TLP masks the barge and hence it can be assumed that this masking effect causes a significant reduction in the barge motions. For the -90 degree case, it was anticipated that reflected waves from the barge should cause higher TLP heave motions. However, measurements for the mini-TLP alone and barge alone cases were not available to confirm this assumption.

The cross spectral analysis was used to determine the degree of linear coherence and correlations between the different parameters for the wave frequency range. The complex cross spectrum between two parameters yields the amplitude and phase spectrum. The coherence spectrum is then derived as a normalized version of the amplitude spectrum and measures the correlation between two processes at each frequency. The correlogram is used to determine the correlation coefficient between two processes for the corresponding time lags. Both the cross spectrum and coherence spectrum are represented in the frequency domain while the correlogram is plotted against the process time lags.

The cross spectral analysis shows that TLP surge has a strong linear correlation with the mooring line tension. The coherence is stronger for the coupled case. TLP sway motion has no correlation with the mooring line tensions while TLP heave shows a strong linear correlation. The relation between the mooring line tensions and the fender forces and between mooring line tensions and the coupling spring forces shows a strong linear correlation for the -90 degree heading alone (when the environment is beam side). Highly

linear interaction effects are also noticed between mooring and tendon tensions irrespective of the direction of environment heading and whether the vessels are coupled or not. The waveheight also has a strong linear coherence with the mooring line tensions for both coupled and uncoupled cases.

The tendon tensions show a strong linear correlation with barge surge motion for both 0 and -90 degree headings. However, the uncoupled case shows a higher correlation for the 0 degree heading. The barge sway has no interaction with the tendon tensions while the barge heave linearly influences the tendon tensions over a small range of frequencies only. But in the barge heave – tendon tension correlation, uncoupled case shows a much stronger correlation than the coupled case for the 0 degree heading. Barge roll shows no correlation with the tendon tensions for 0 degree heading; however the correlation is very strong for the -90 degree case. Coupled and uncoupled cases show similar effects. Barge pitch shows a strong linear coherence with tendon tension for the 0 degree heading and almost no coherence for the -90 degree heading. Barge yaw does not show a very strong linear coherence with the tendon tension. Tendon tensions also show a strong linear coherence with waveheight for both 0 and -90 degree cases. However, the uncoupled case shows a higher correlation for the 0 degree case.

Fender forces show a good linear correlation with the other parameters only for the -90 degree heading as in this case, the incident environment pushes the vessels against each other and fender forces are large. TLP and barge surge motions show a high degree of linear correlation with fender forces over a wide band of frequencies for the -90 degree heading. TLP sway shows no correlation for either 0 or -90 degree cases. Barge sway motion shows a correlation over a small band of frequencies for the 0 degree heading while there is no coherence for the -90 degree heading. TLP and barge heave show linear correlation with the fender forces for a very narrow band of frequencies only. For 0 degree heading, barge heave shows no correlation. Barge roll again shows a strong linear coherence for the -90 degree heading only. Barge pitch and yaw motions have no influence on the fender forces for both headings. Tendon tensions and the waveheights show a strong linear coherence with the fender forces for the -90 degree heading. Since

the fender forms a part of the coupling system with the breast line springs, they are correlated linearly for both 0 and -90 degree cases, but the -90 degree heading shows a much stronger correlation.

The forces on the springs forming the coupling breast lines show strong linear coherences with TLP and barge surge motions for both 0 and -90 degree headings. TLP and barge sway motions show no coherence for any of the headings while TLP heave shows a linear correlation for a very narrow band of frequencies. But barge heave motion has a much larger magnitude and influences the spring motion a lot more for both 0 and -90 degree heading. Barge roll motion shows a much stronger correlation with the spring forces for the -90 degree heading than the 0 degree heading. However, both barge pitch and yaw show a strong linear correlation with the spring forces for the 0 degree heading only. The tendon tensions and waveheights also are linearly related to the spring forces for both 0 and -90 degree headings.

The mini-TLP and barge motions for the two wave headings were shown to influence the mooring line tensions, tendon tensions and fender forces. In this study, the characteristics of the response behavior were shown to change appreciably when the vessels are coupled to each other and when the environment headings change. The study illustrates the importance and complexity of these factors which have to be kept in mind when designing the coupled multi-body system. The amount of data involved is quite significant and it is not possible to present all the information in the main text and hence only the most important findings were included. However, additional information is provided in the appendices.

REFERENCES

[1] Wren T, Fawcett JN, Burdess JS. Application of extensible catenary theory to determine the displacement of a moored ship. Mech. Mach. Theory, 1989; 24: 207-12.

[2] Smith RJ, MacFarlane CJ. Statics of a three component mooring line. Journal of Ocean Engineering, 2001; 28: 899-914.

[3] Niedzwecki JM, Casarella MJ. On the design of mooring lines for deep water applications. ASME Journal of Engineering for Industry, 1976; 98: 514-522.

[4] Moe G, Arnsten O. An analytic model for static analysis of catenary risers. In: Proc. Eleventh Offshore and Polar Engineering Conference, Stavanger, Norway , 2001; 2: 248-53.

[5] Recommended practice for design and analysis of stationkeeping systems for floating structures, first ed. Washington: American Petroleum Institute, 1995.

[6] Chakrabarti P, Chandwani R, Larsen I. Analyzing the effects of integrating riser / mooring design. OMAE'96 Conference, Florence, Italy, 1996.

[7] Portella RB. Mooring system: From initial design to offshore installation. Offshore Technology conference, Houston, Texas, 2000; 12174: 1-12.

[8] Fender system design. Transport Canada (http://www.tc.gc.ca/marinesafety)

[9] Mini-TLP – Barge experiment. OTRC Report, 2000.

[10] Newton JH. Timeslab: A time series analysis laboratory. Pacific Grove, California: Wadsworth & Brooks/Cole, 1988.

[11] MATLAB – Version 7.0.0.19920 (R 14). May 06, 2004.

[12] Ochi MK. On prediction of extreme values. Journal of Ship Research, 1973; 17(1): 29-37.

[13] Teigen P, Niedzwecki JM. Experiments and analysis with fully coupled Mini-TLP/ Barge system. Ninth International Offshore and Polar Engineering Conference, Brest, France, 1999; 1: 339-47.

[14] Bendat JS, Piersol AG. Random data: Analysis and measurement procedures. Third ed. New York: John Wiley & Sons Inc., 2000.

[15] Mercier RS, Schott WE, Howell CT, Denison EB, Gopalakrishnan R, Ekvall AGC. Mars tension leg platform – use of scale model testing in the global design. Offshore Technology Conference, Houston, Texas, 1997; 8354: 11-21.

APPENDIX A

SPECTRAL DENSITY AND TRANSFER FUNCTION PLOTS

A large amount of data has been analyzed and it is not possible to present all the plots in the main text. Hence, the spectral density and corresponding transfer functions for all parameters are summarized here in Appendix A so that the data trends for all the parameters can be identified. The spectral density plots for all the TLP and barge motions, mooring line tensions, tendon tensions, fender forces and the coupling spring forces are represented along with the corresponding transfer functions.
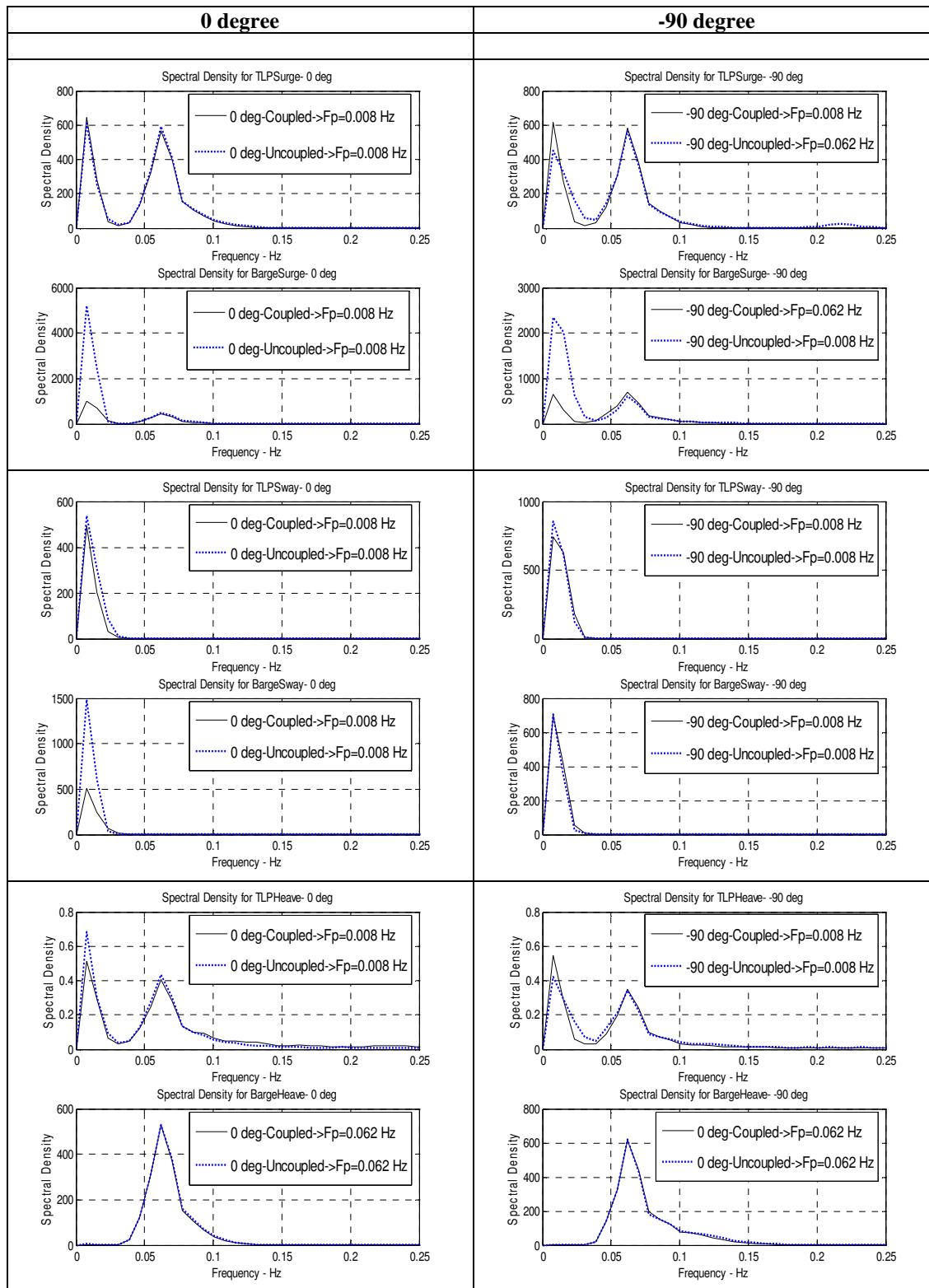
Fig. A-1. Spectral densities for TLP and barge surge, sway and heave
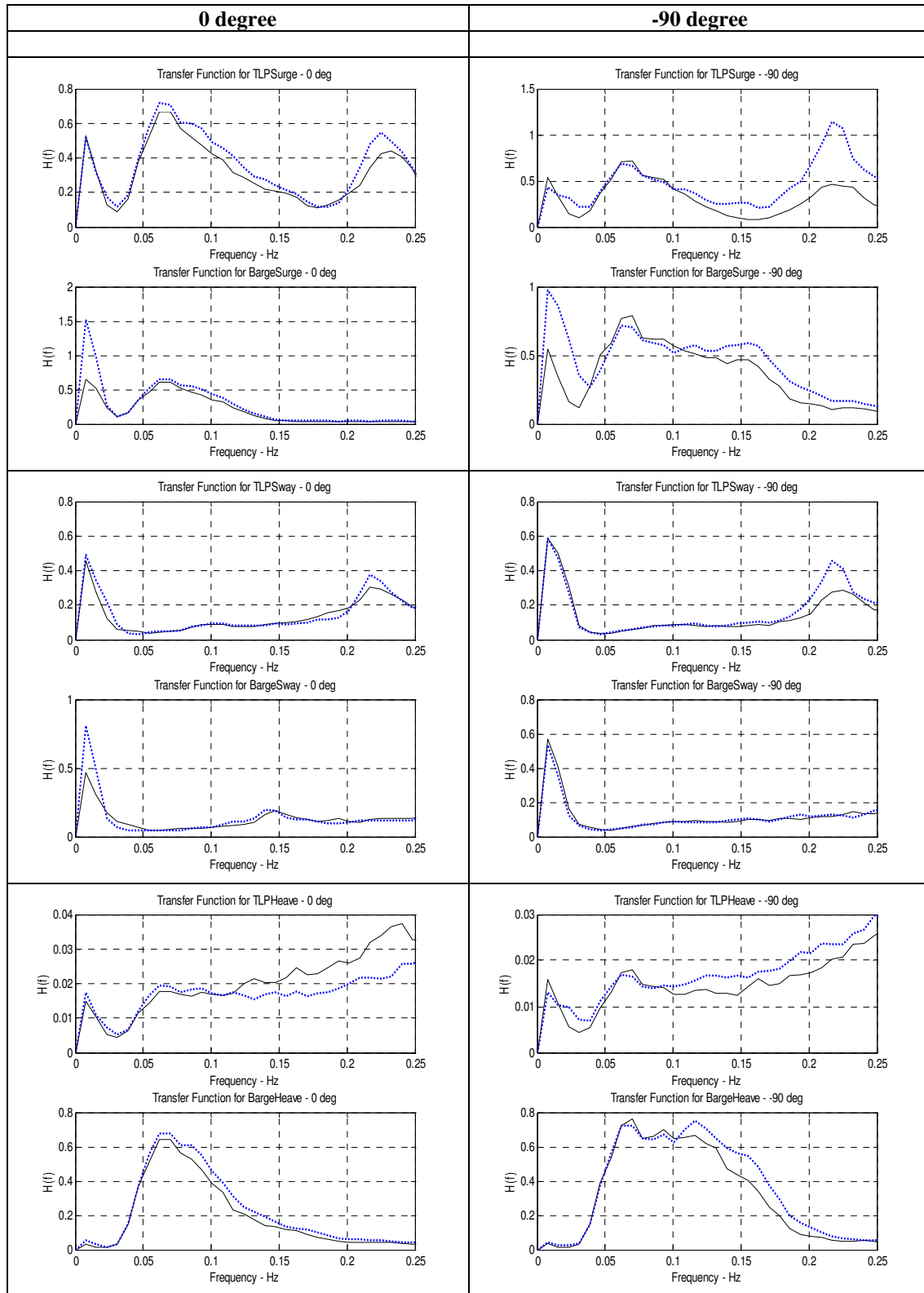
0 degree	-90 degree

Fig. A-2. Transfer functions for TLP and barge surge, sway and heave
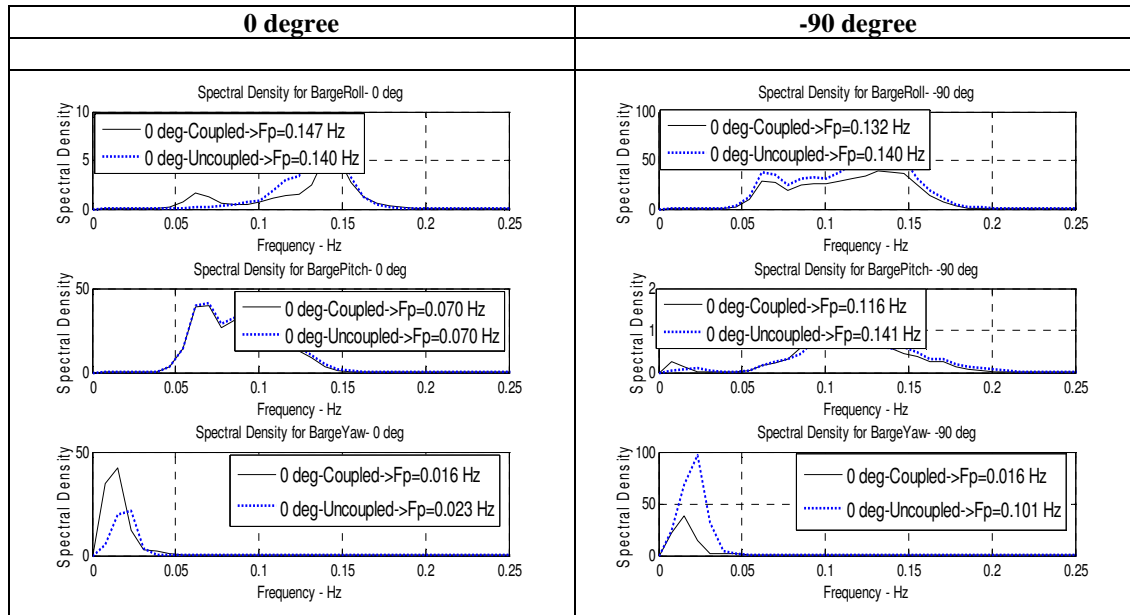
0 degree	-90 degree

Fig. A-3. Spectral densities for barge roll, pitch and yaw
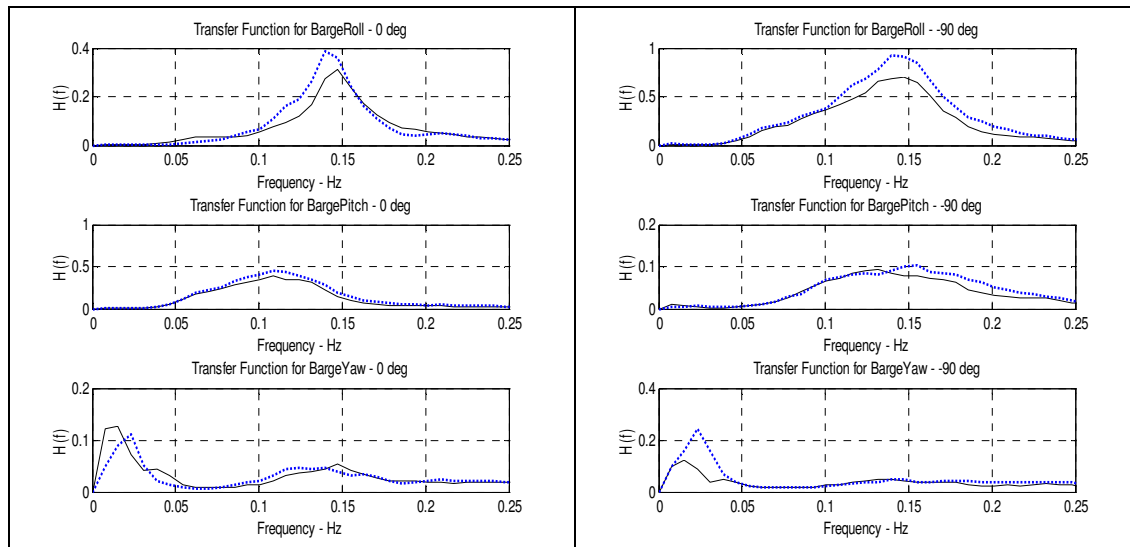
Fig. A-4. Transfer functions for barge roll, pitch and yaw
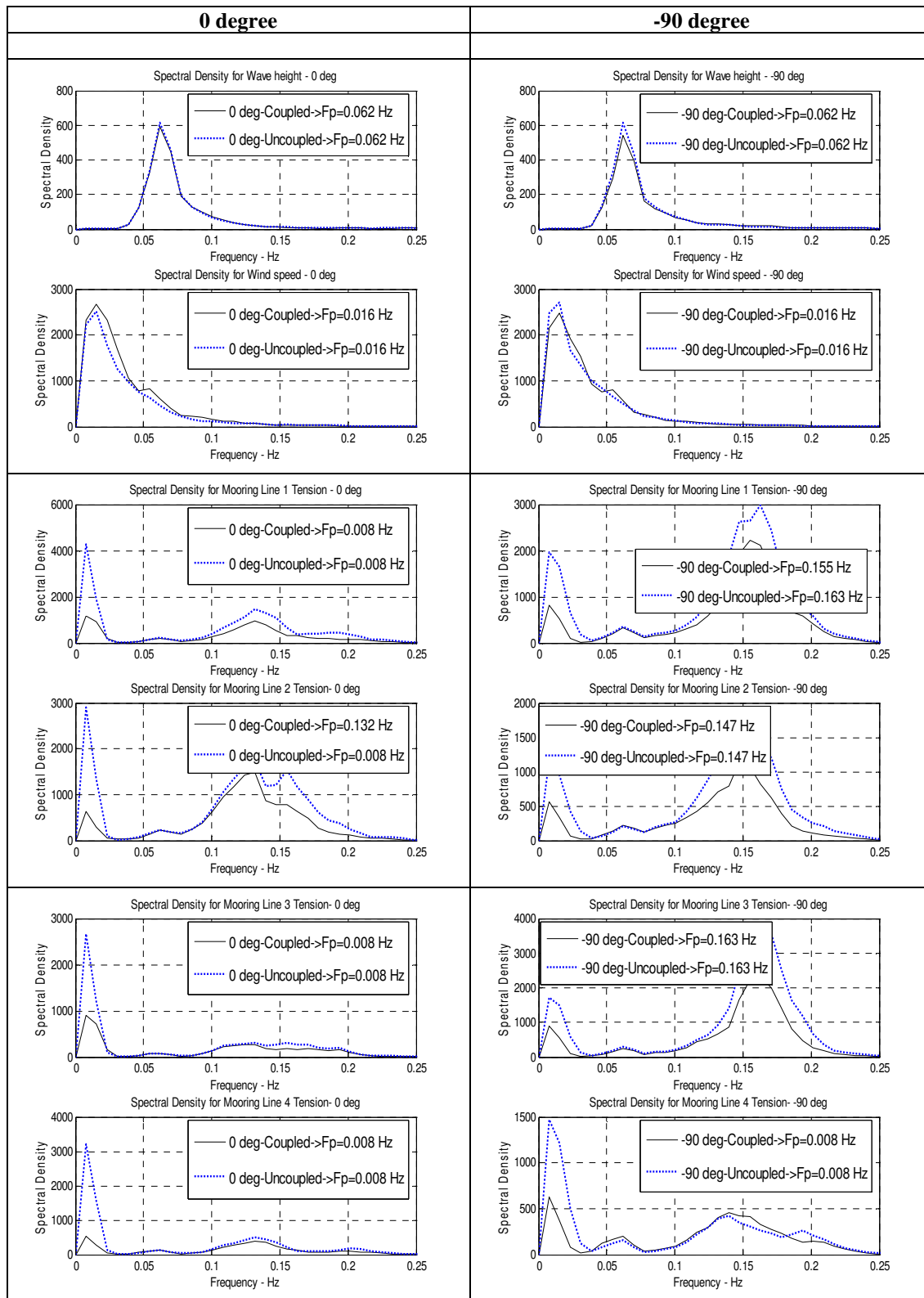
Fig. A-5. Spectral densities for mooring line tensions for 0 degree and -90 degree

0 degree	-90 degree
Transfer Function for Mooring Line 1 Tension - 0 deg	Transfer Function for Mooring Line 1 Tension - -90 deg
Transfer Function for Mooring Line 2 Tension - 0 deg	Transfer Function for Mooring Line 2 Tension - -90 deg
Transfer Function for Mooring Line 3 Tension - 0 deg	Transfer Function for Mooring Line 3 Tension - -90 deg
Transfer Function for Mooring Line 4 Tension - 0 deg	Transfer Function for Mooring Line 4 Tension - -90 deg

Fig. A-6. Transfer functions for mooring line tensions for 0 degree and -90 degree
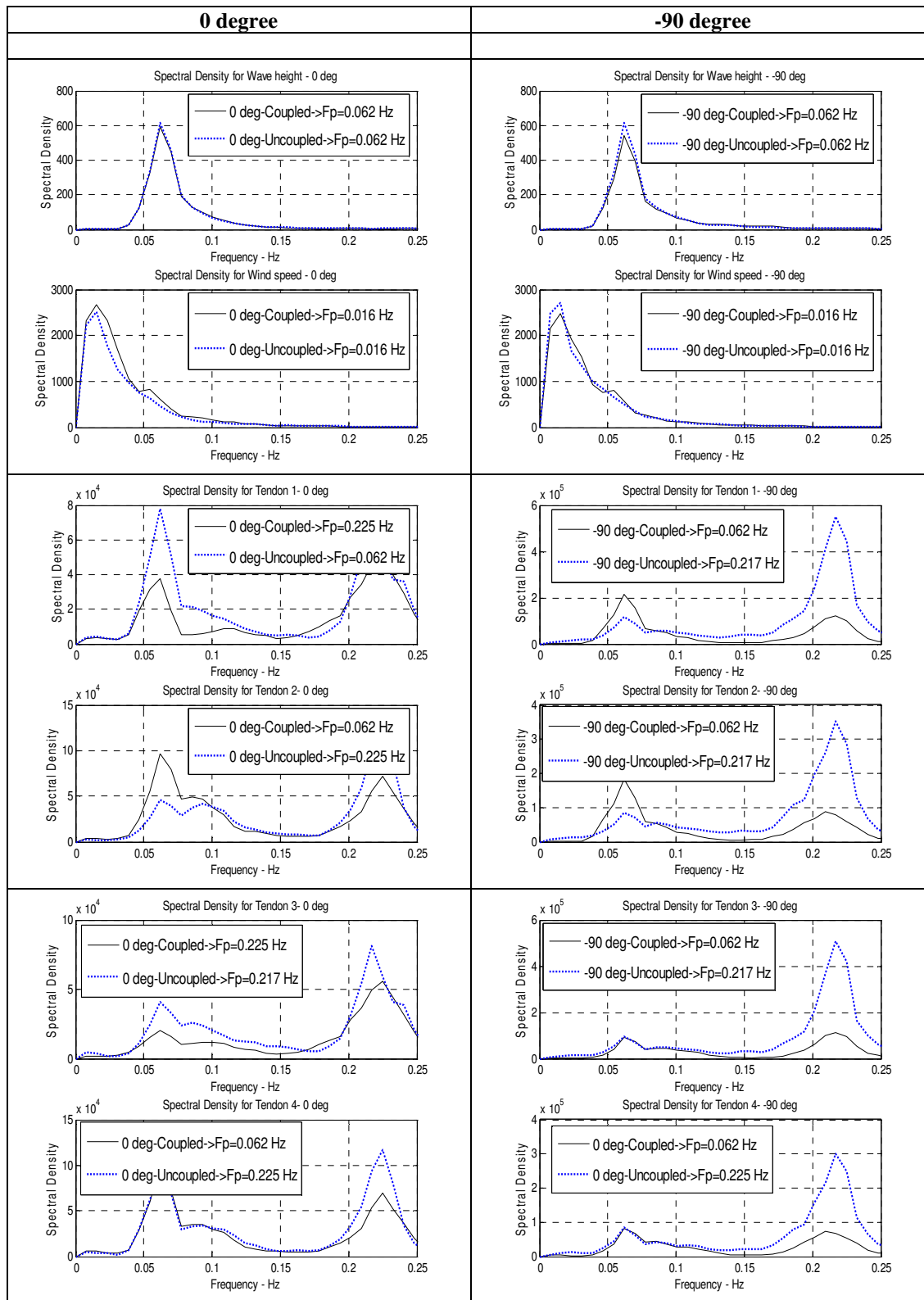
Fig. A-7. Spectral densities for tendon tensions for 0 degree and -90 degree
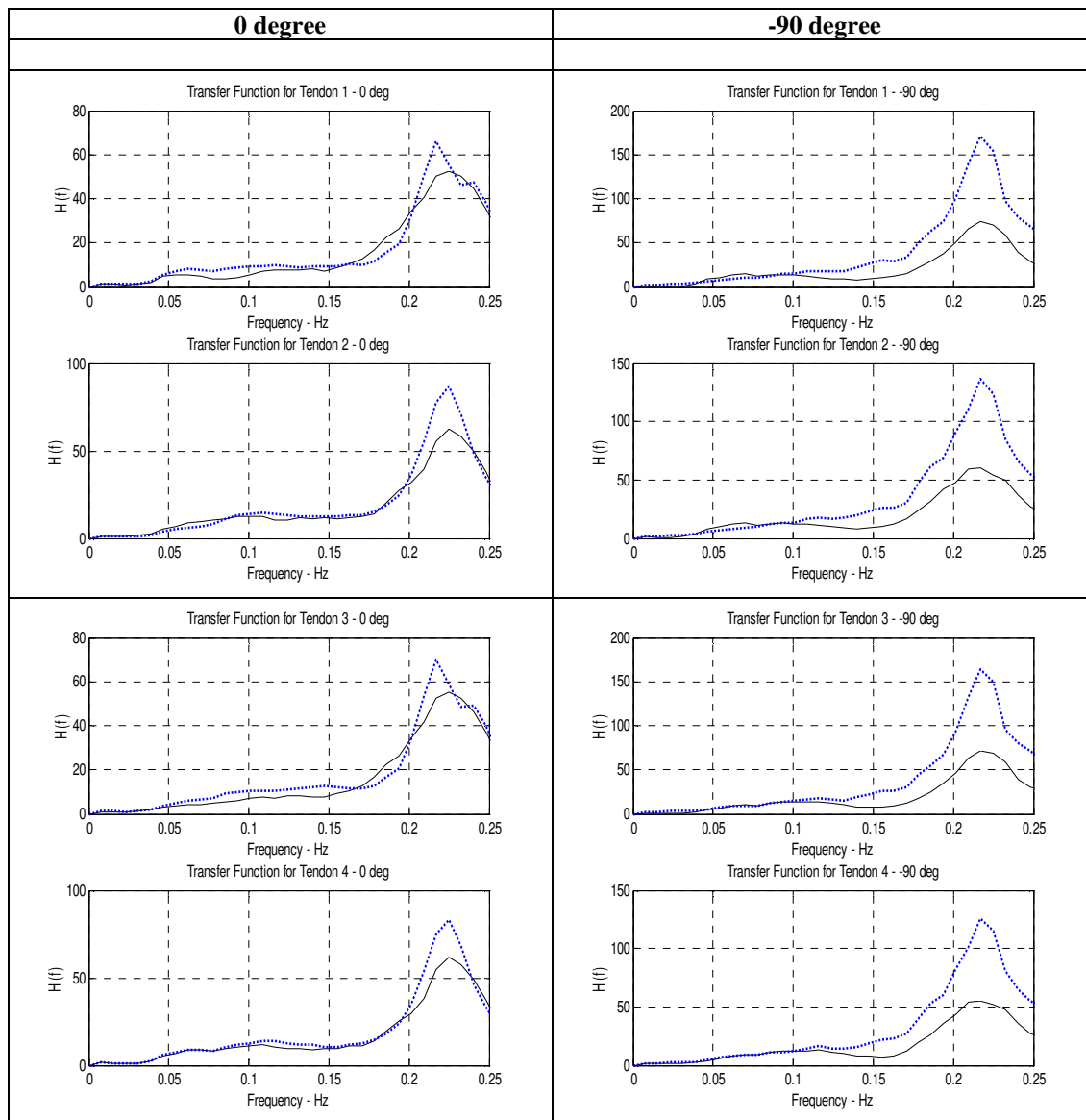
0 degree	-90 degree

Fig. A-8. Transfer functions for tendon tensions for 0 degree and -90 degree
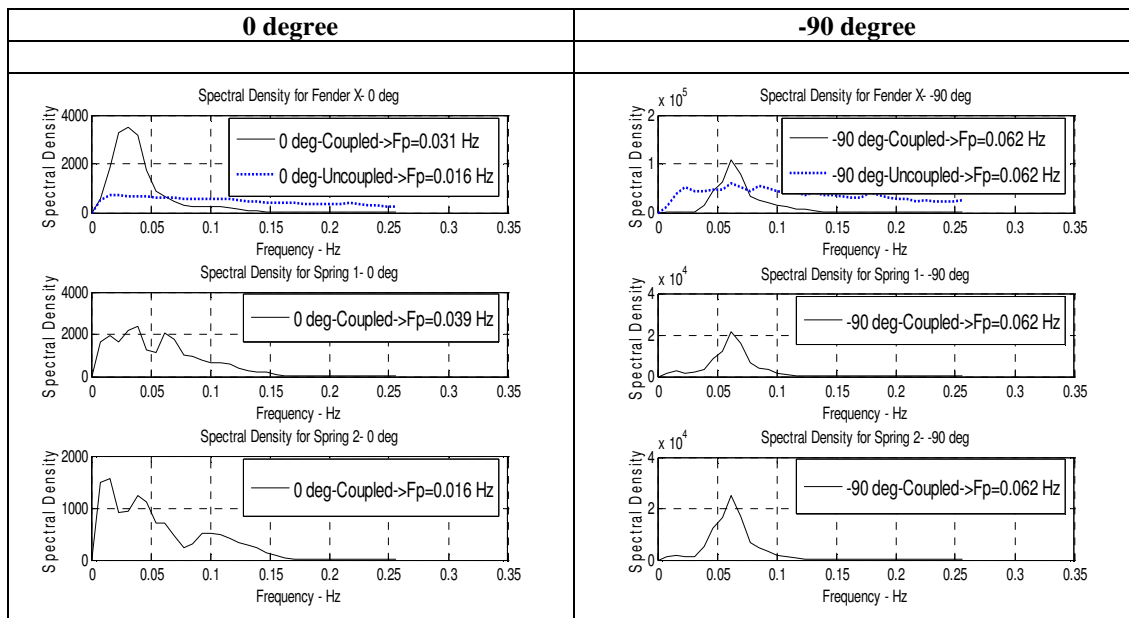
Fig. A-9. Spectral densities for fender X and spring forces for 0 degree and -90 degree
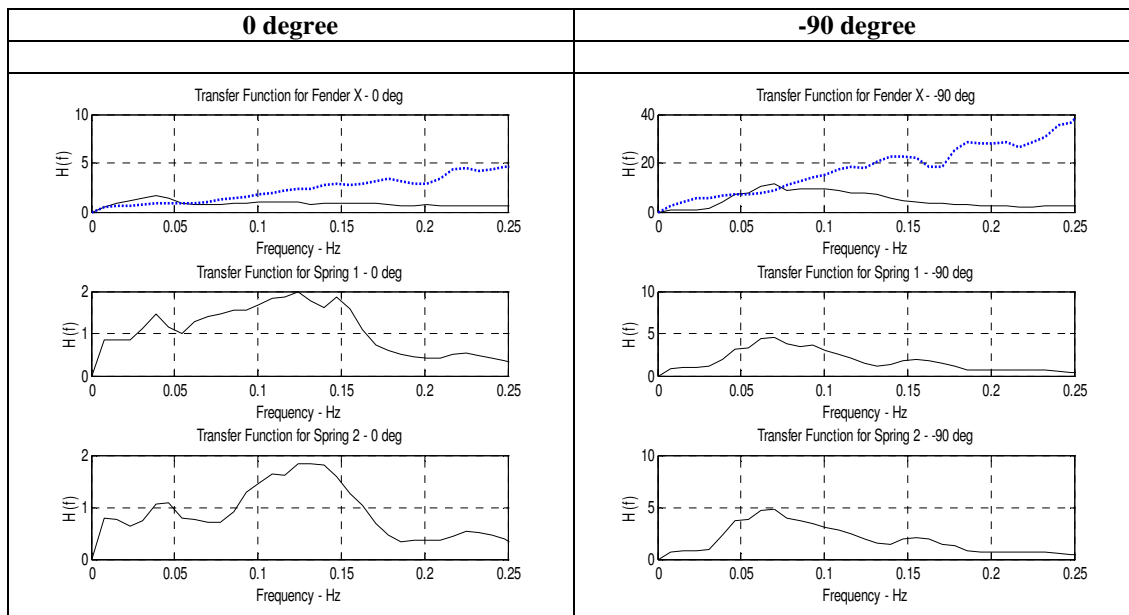
Fig. A-10. Transfer functions for fender X and spring forces for 0 degree and -90 degree

APPENDIX B
CROSS SPECTRUM AND COHERENCE SPECTRUM

The cross spectrum, coherence spectrum and the cross correlogram to determine the correlations between the different parameters are shown in the following plots. The influence of TLP motions on the barge mooring and fender system and the influence of the barge motions on the tendons and fenders are shown. The cross correlation between waveheight and the line tensions and fender forces are also investigated.
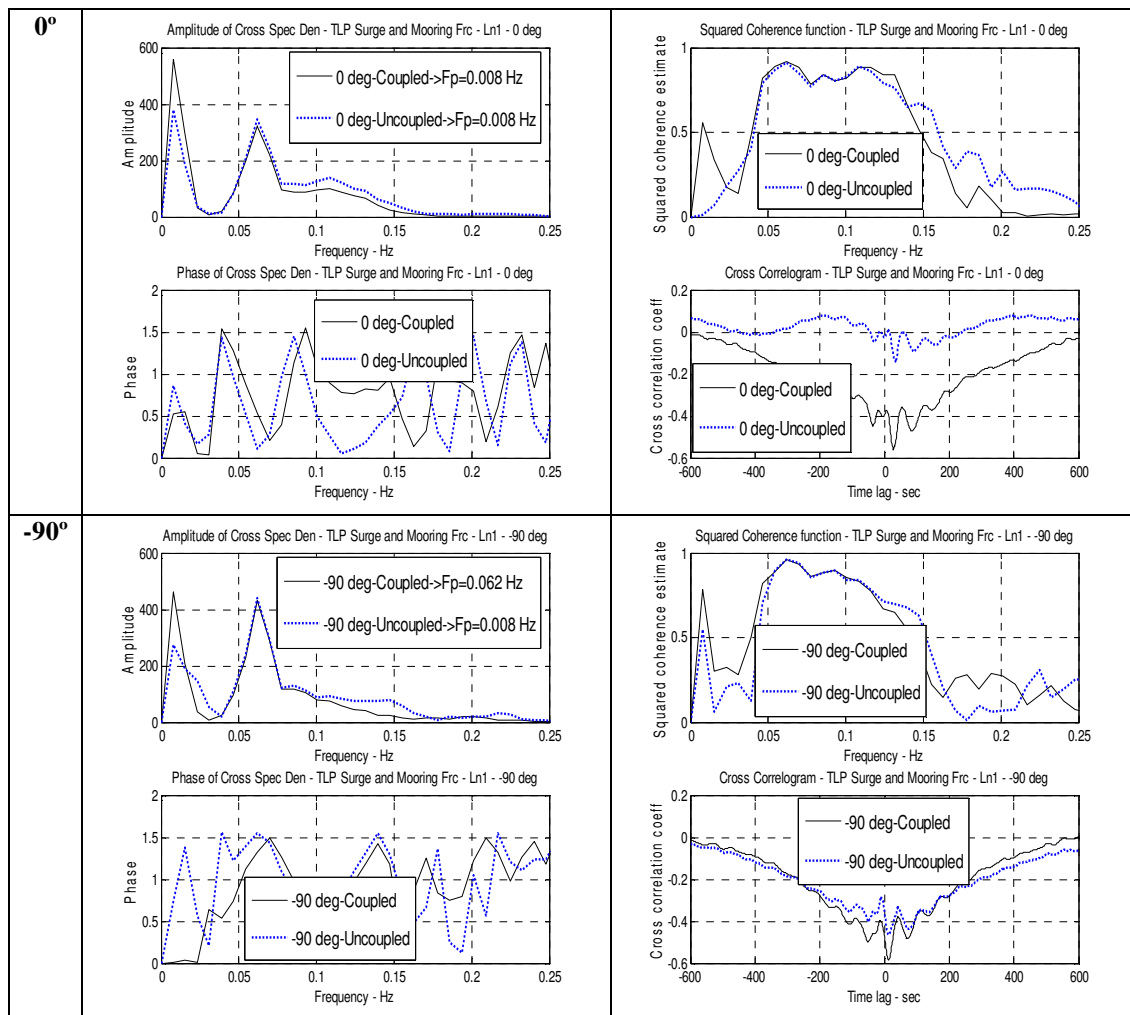
Fig. B-1. Cross spectral analysis: TLP surge and mooring line 1 tension
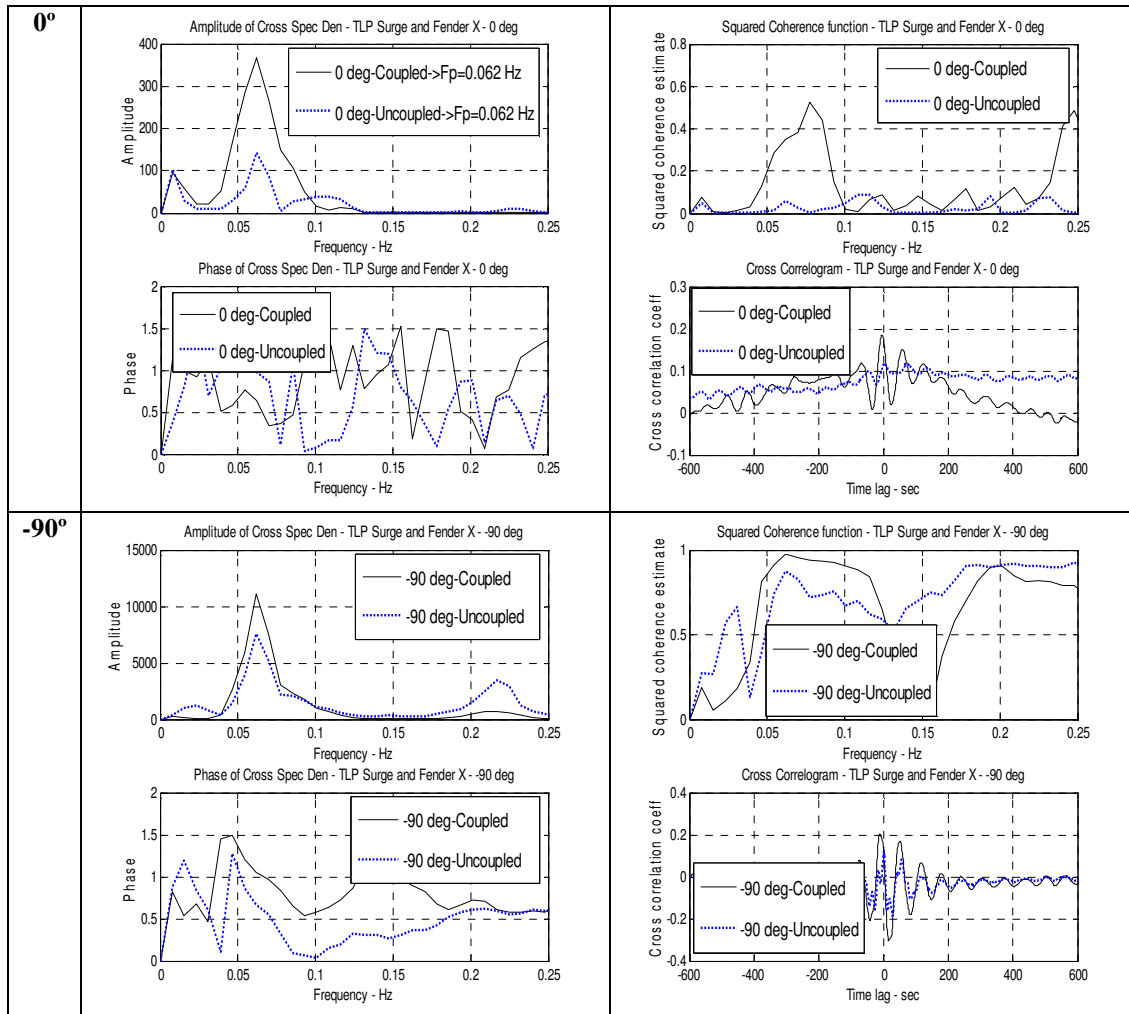
Fig. B-2. Cross spectral analysis: TLP surge and fender X force
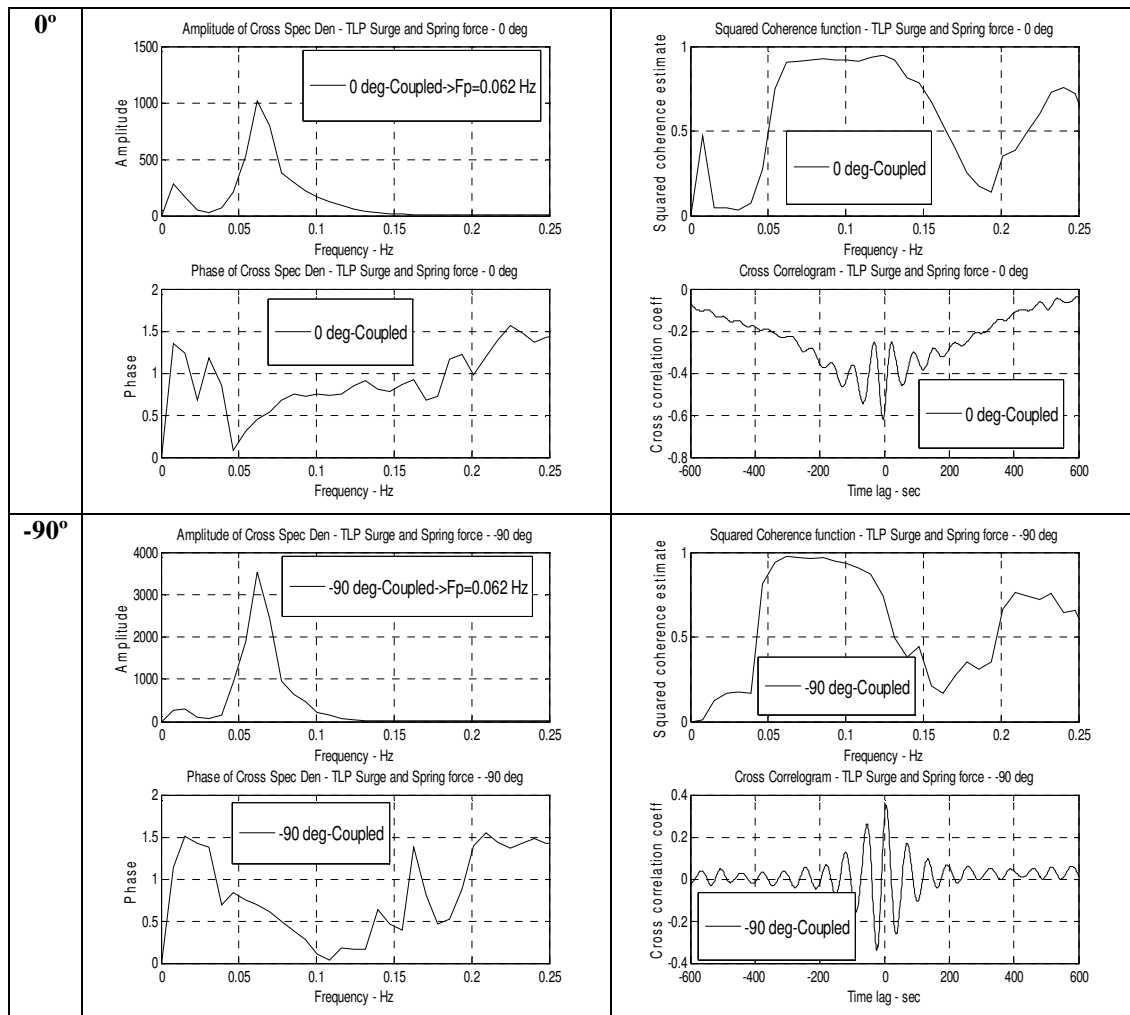
Fig. B-3. Cross spectral analysis: TLP surge and spring 1 force
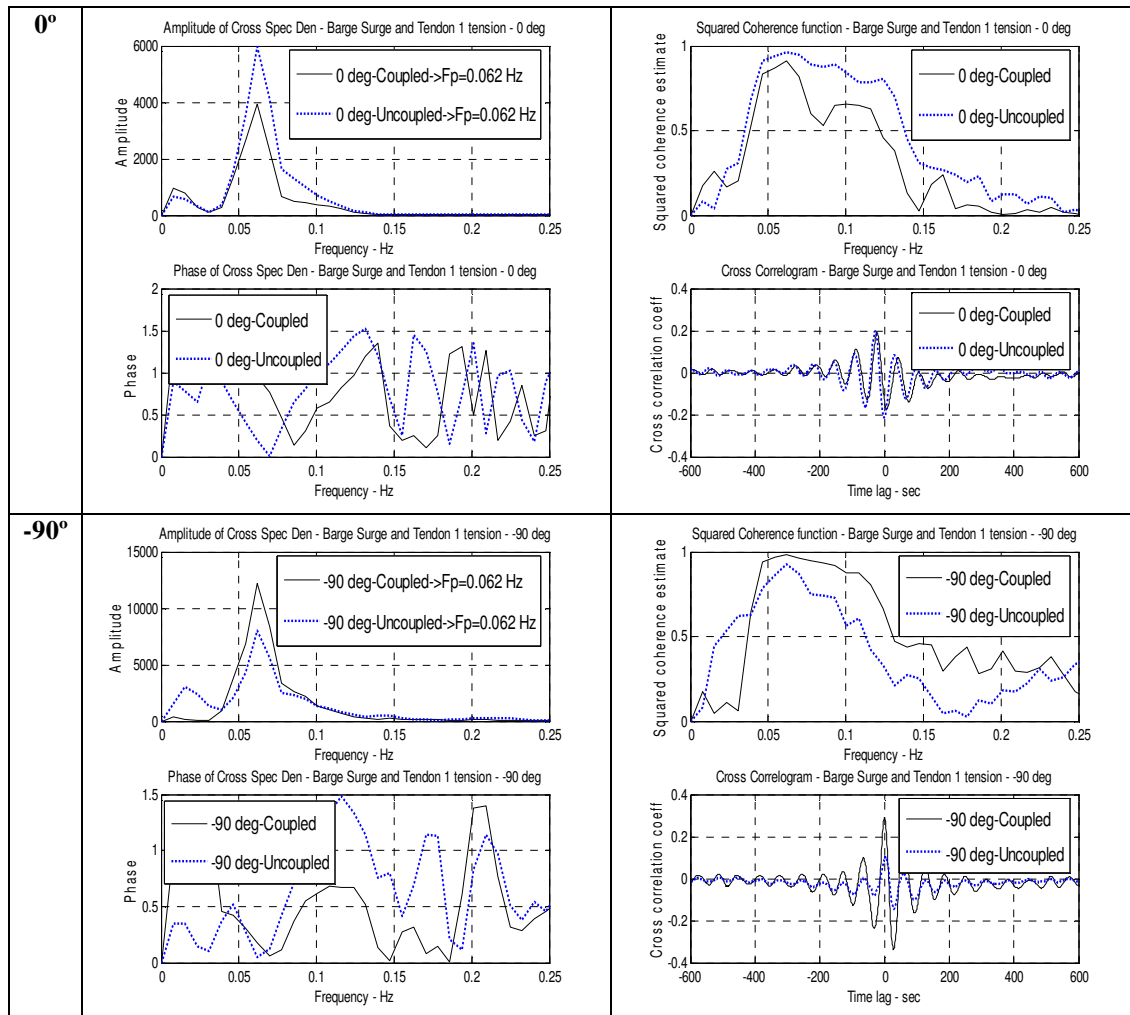
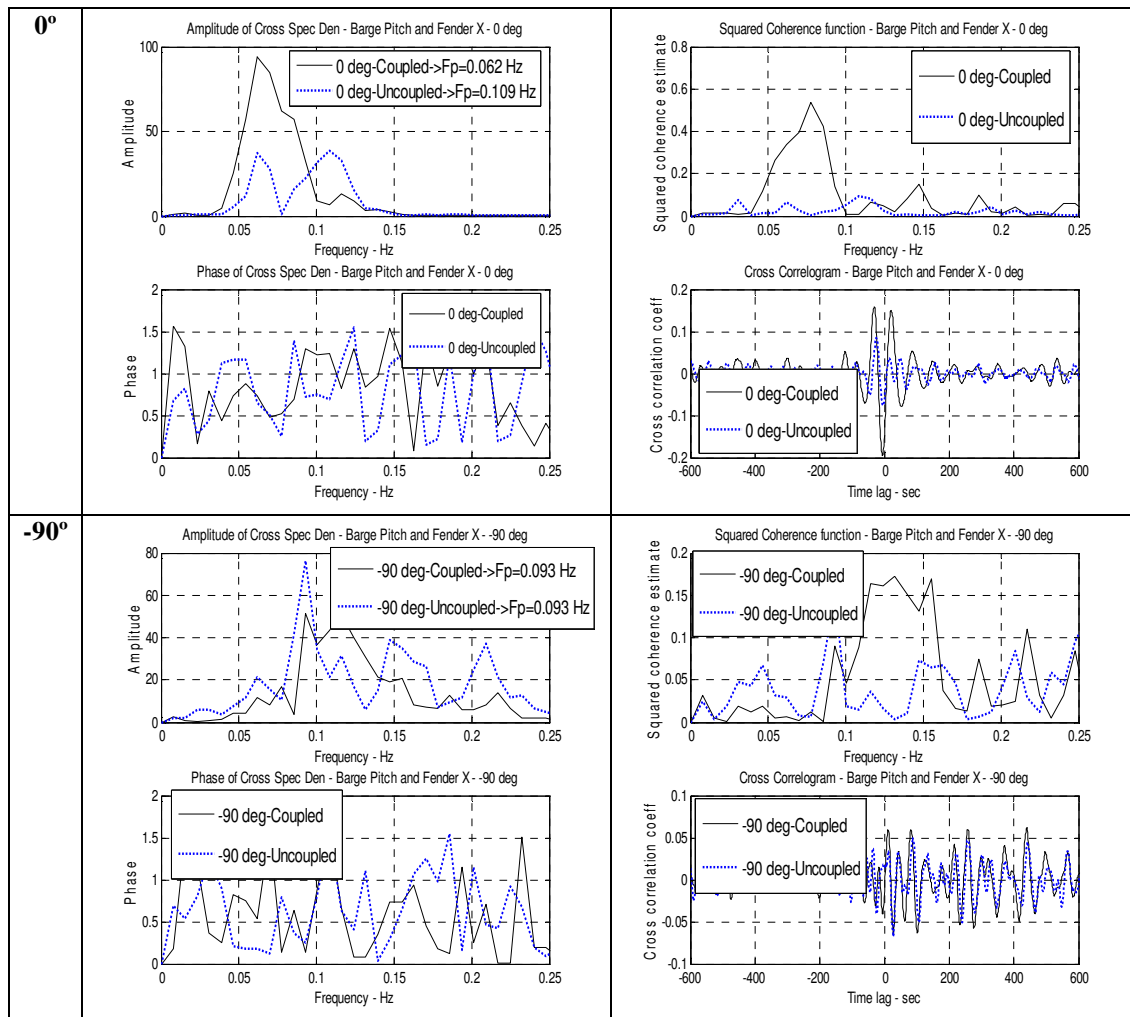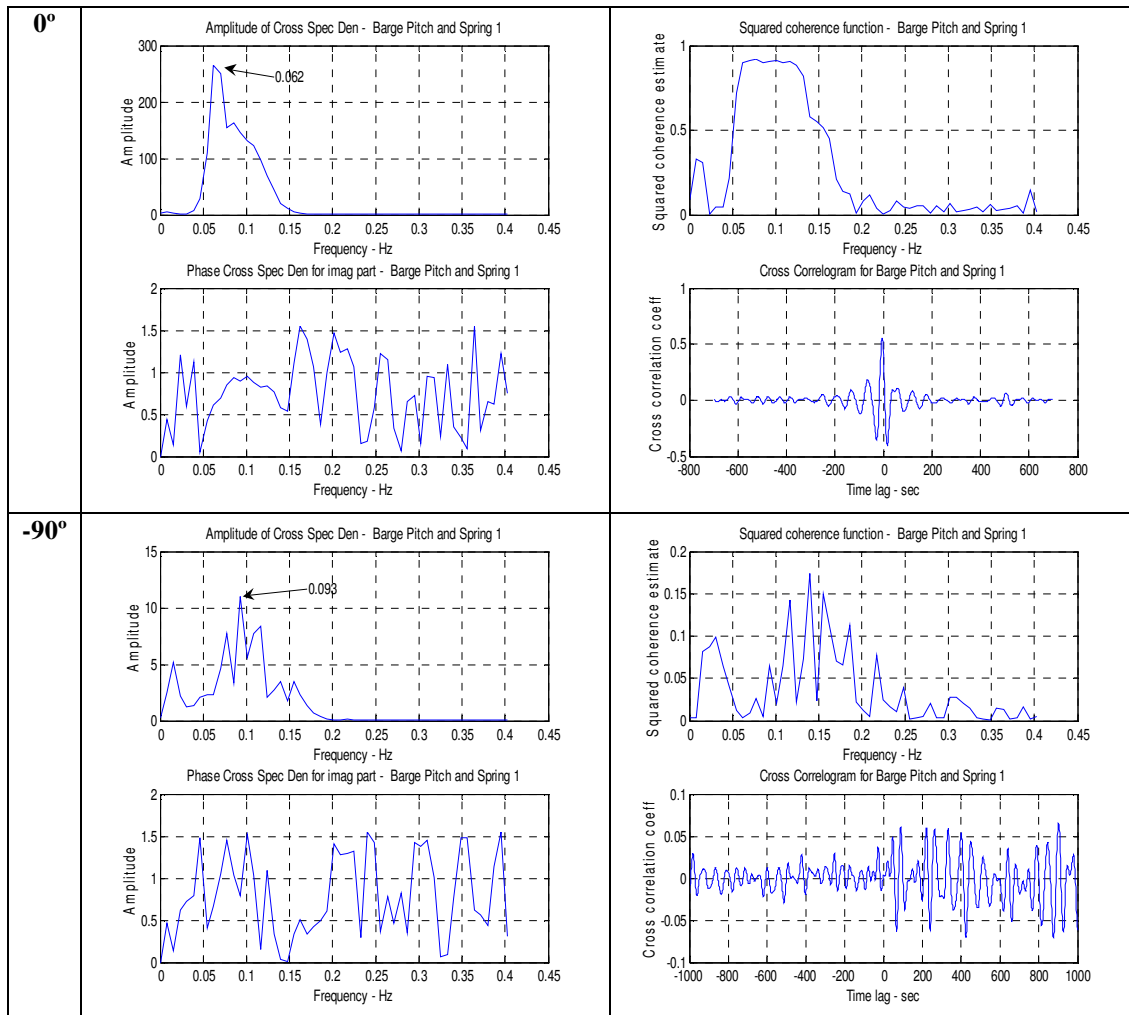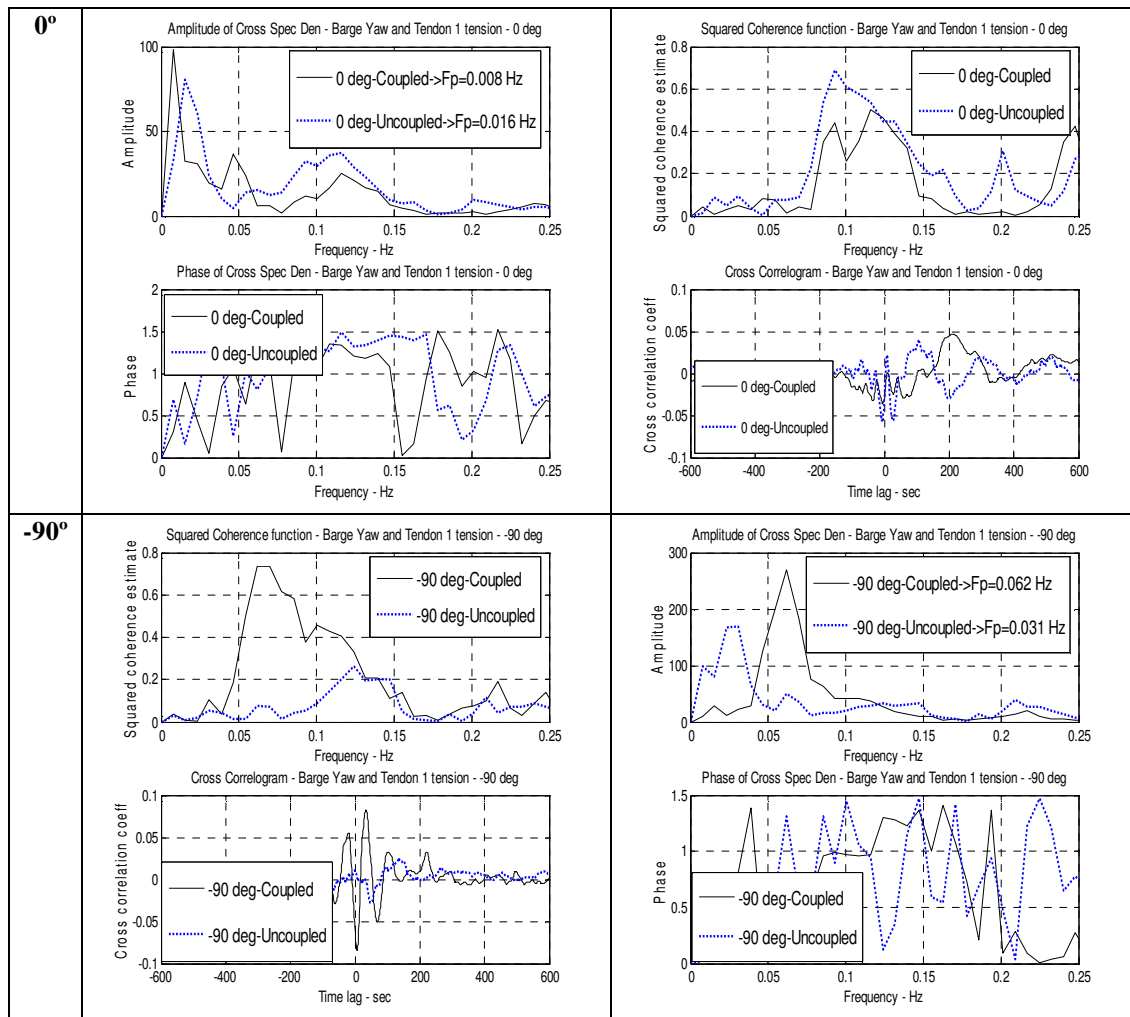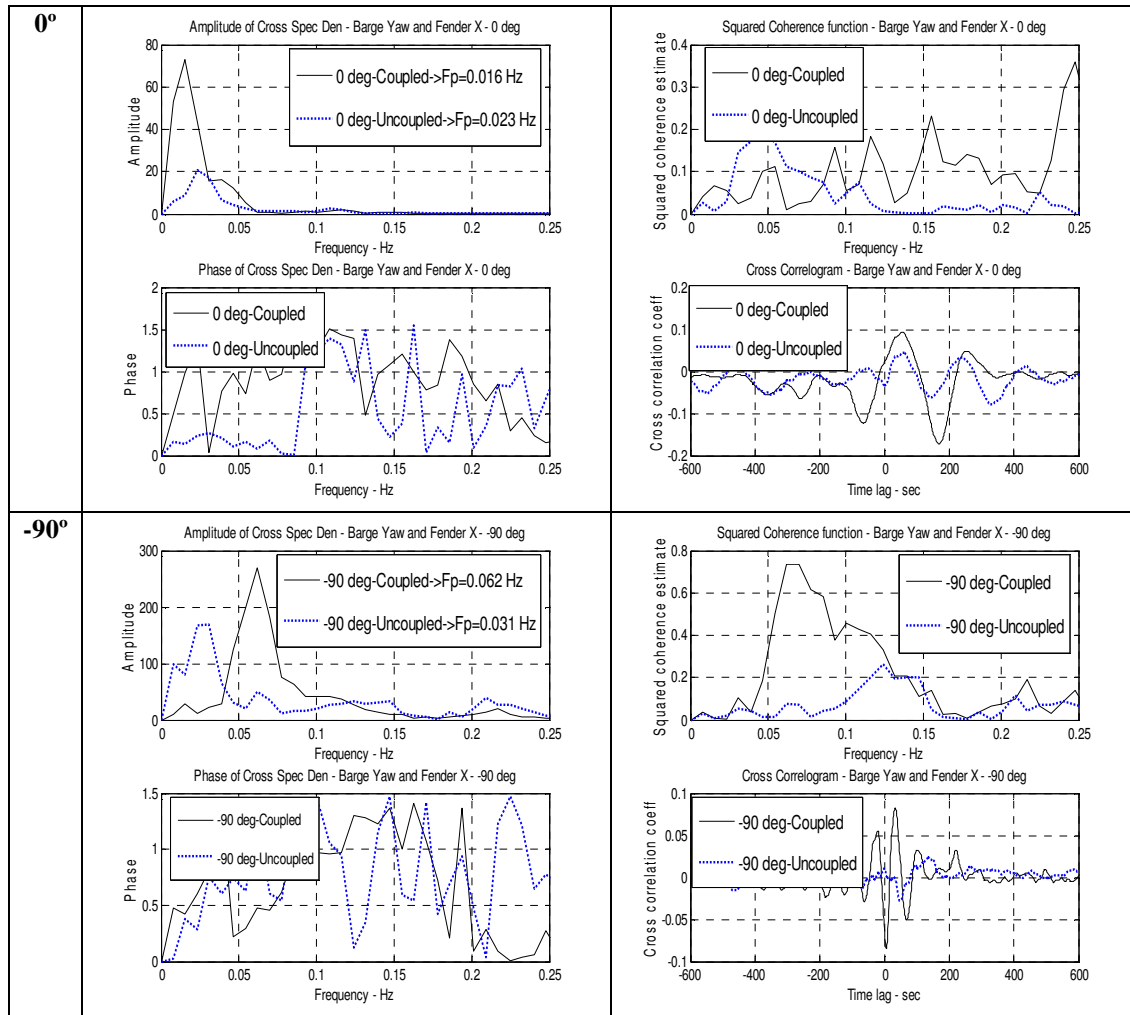Fig. B-4. Cross spectral analysis: barge surge and tendon 1 tension
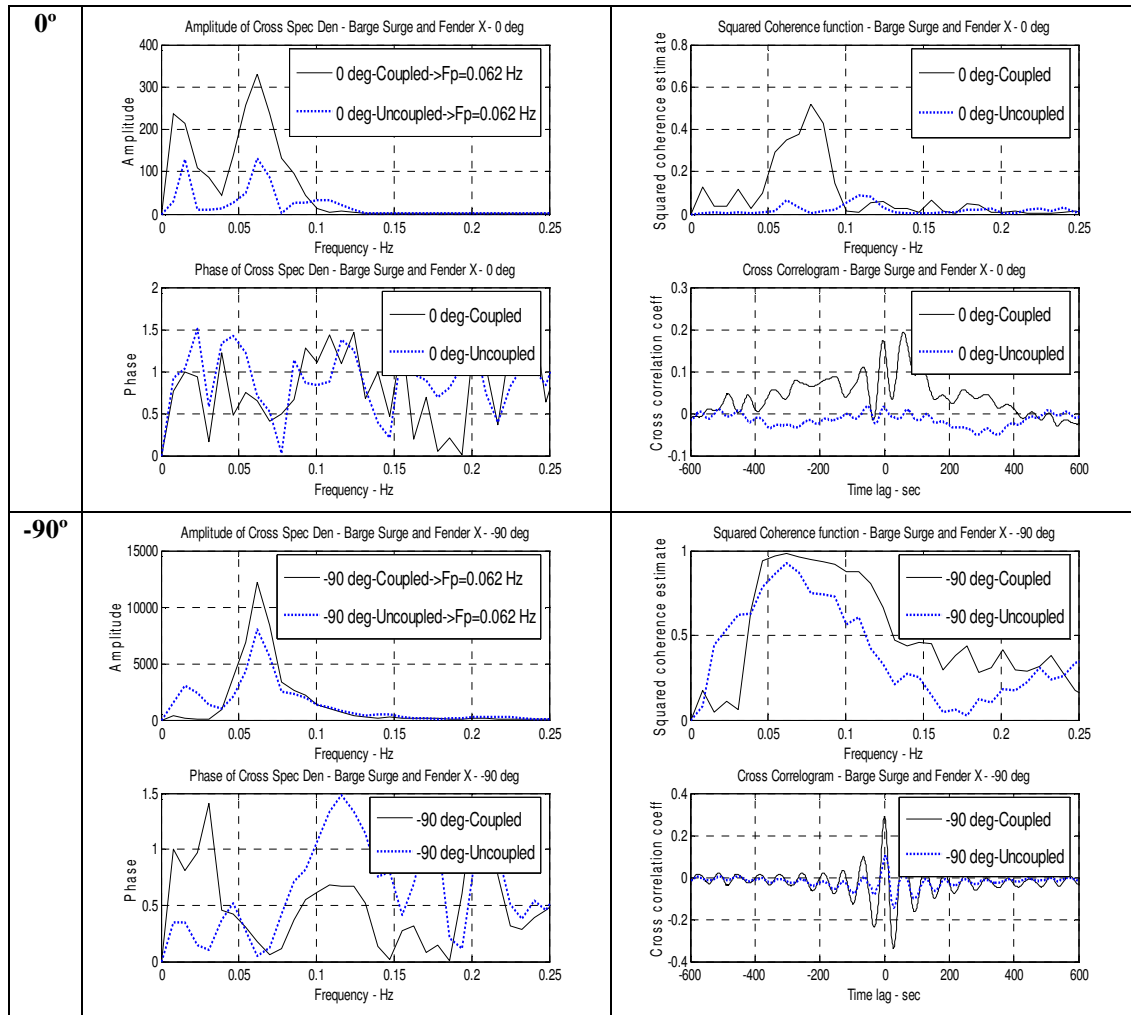
Fig. B-5. Cross spectral analysis: barge surge and fender X force
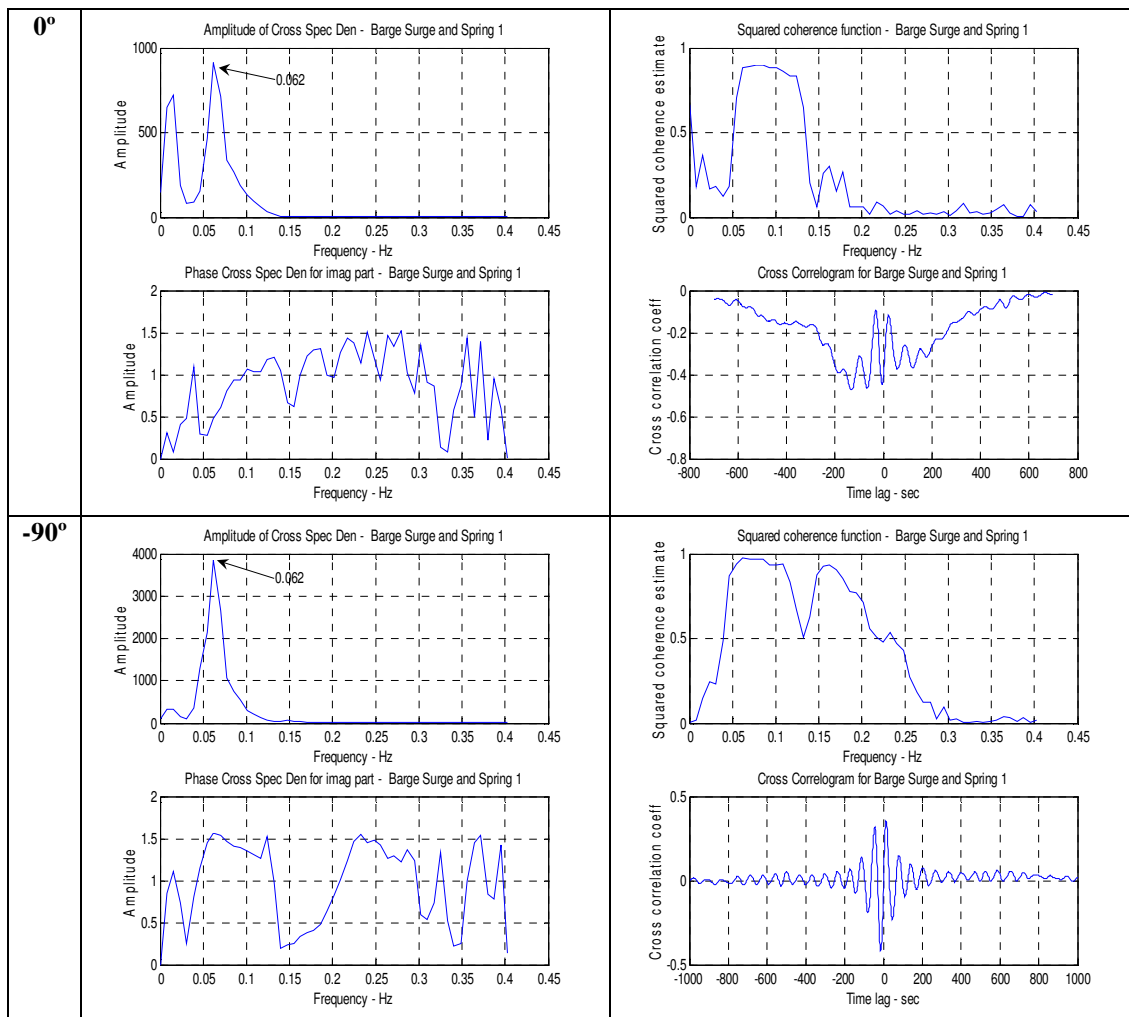
Fig. B-6. Cross spectral analysis: barge surge and spring 1 force
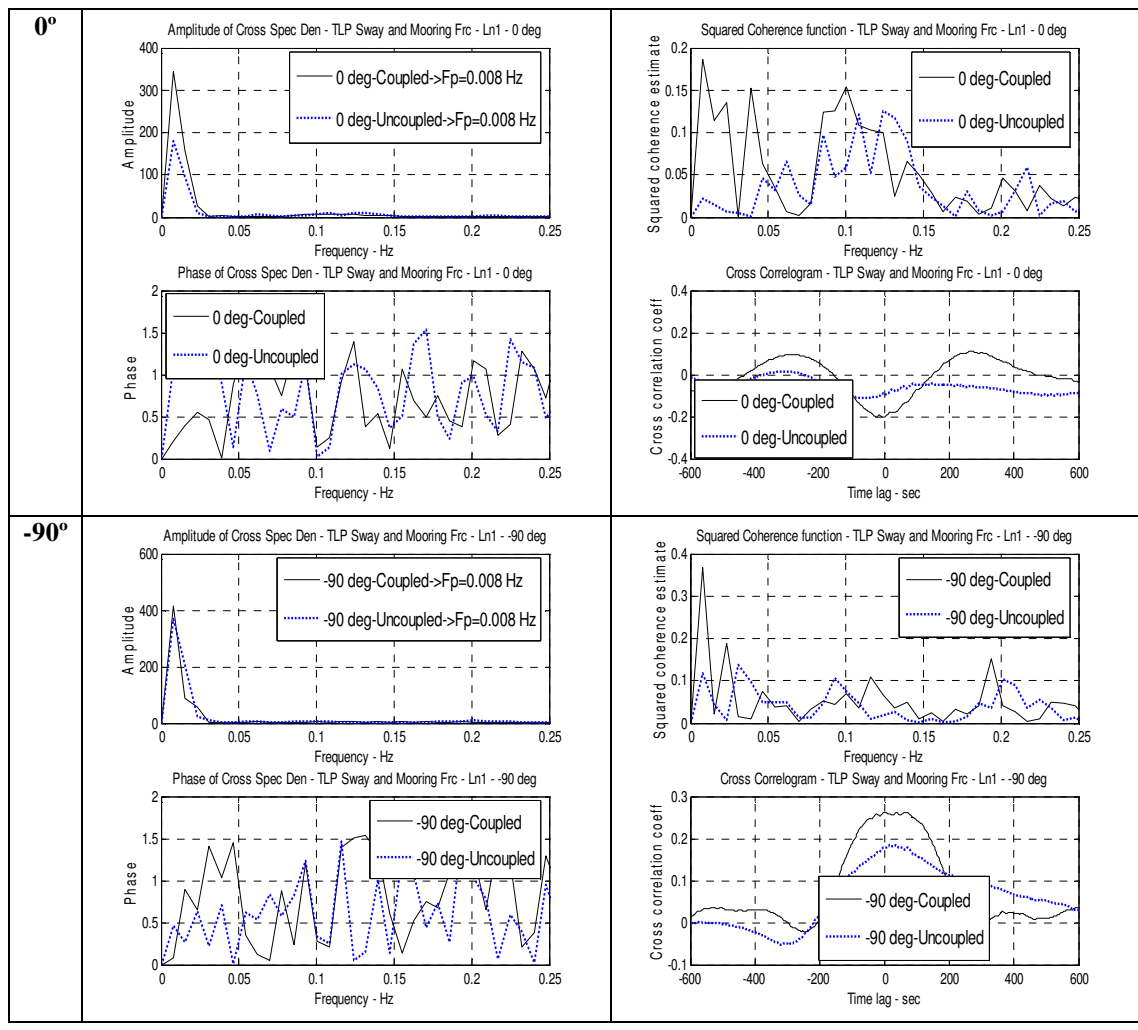
Fig. B-7. Cross spectral analysis: TLP sway and mooring line 1 tension
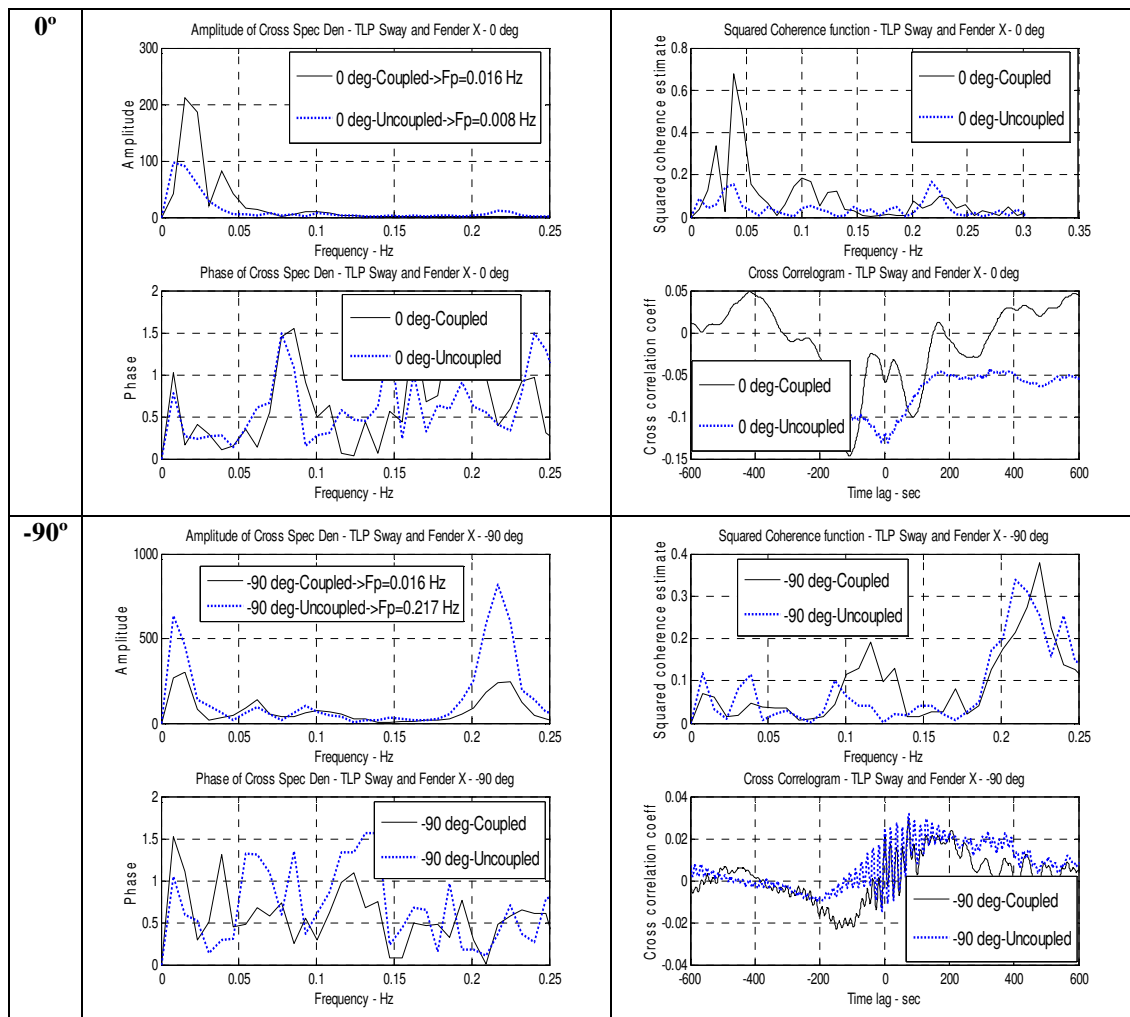
Fig. B-8. Cross spectral analysis: TLP sway and fender X force

119
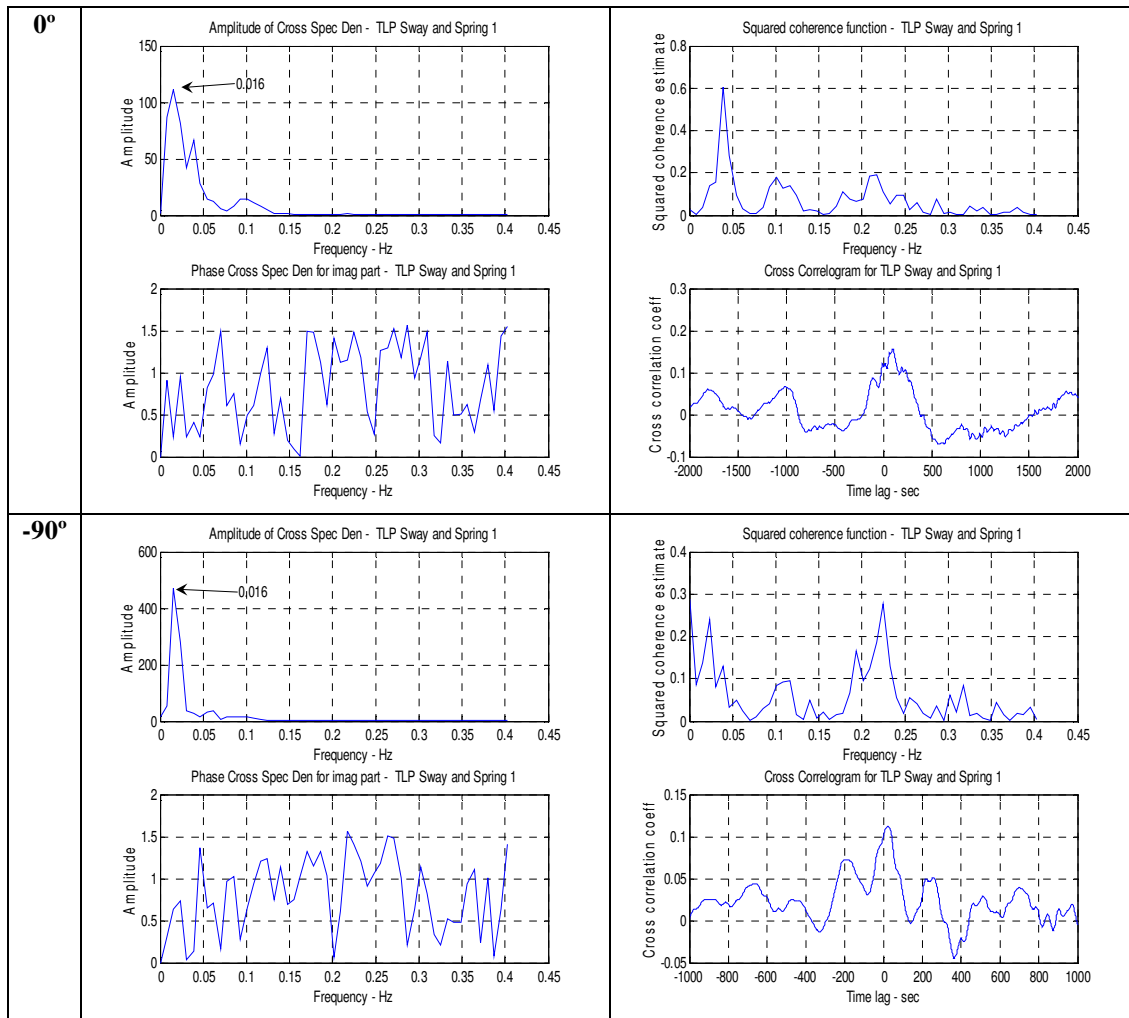
Fig. B-9. Cross spectral analysis: TLP sway and spring 1 force
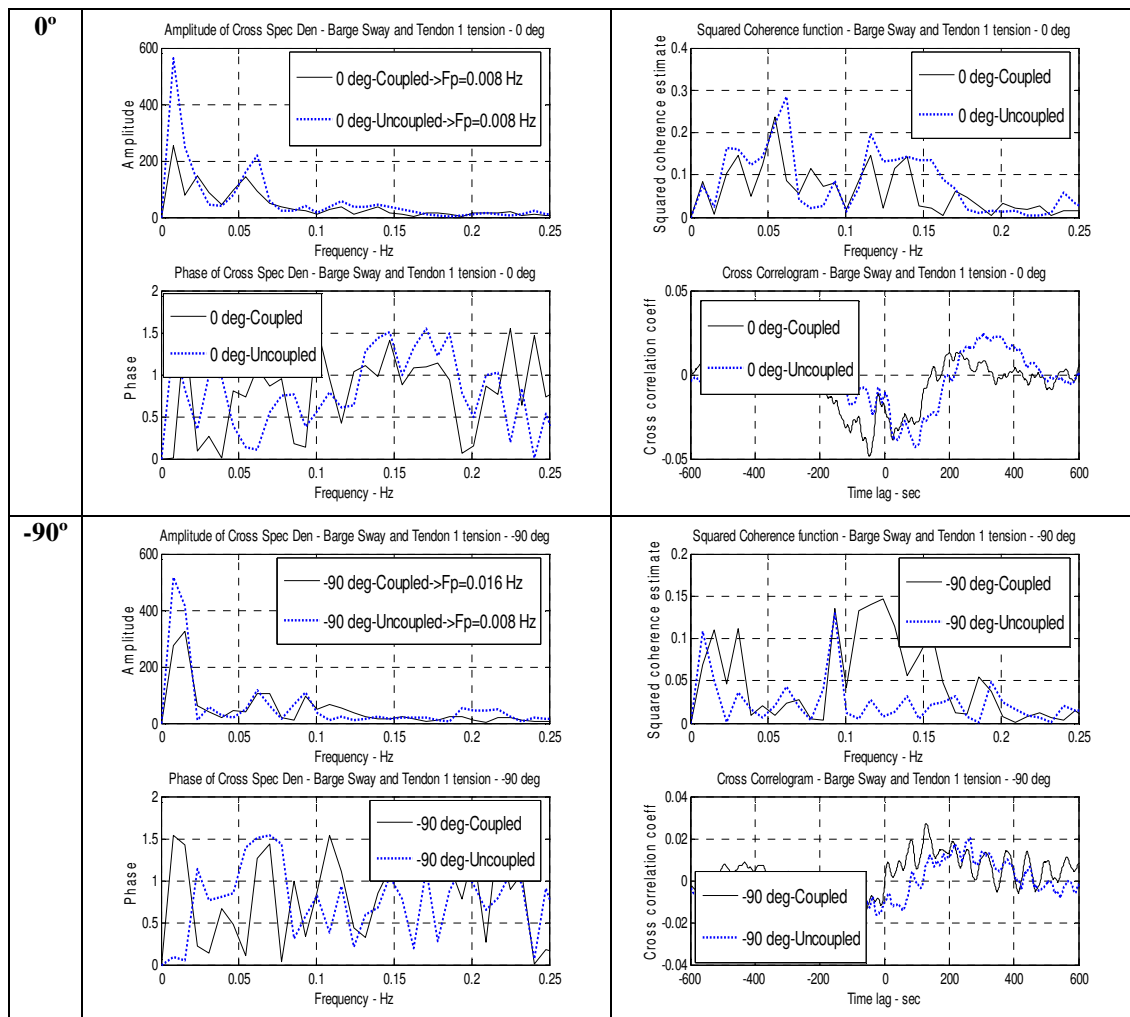
Fig. B-10. Cross spectral analysis: barge sway and tendon 1 tension
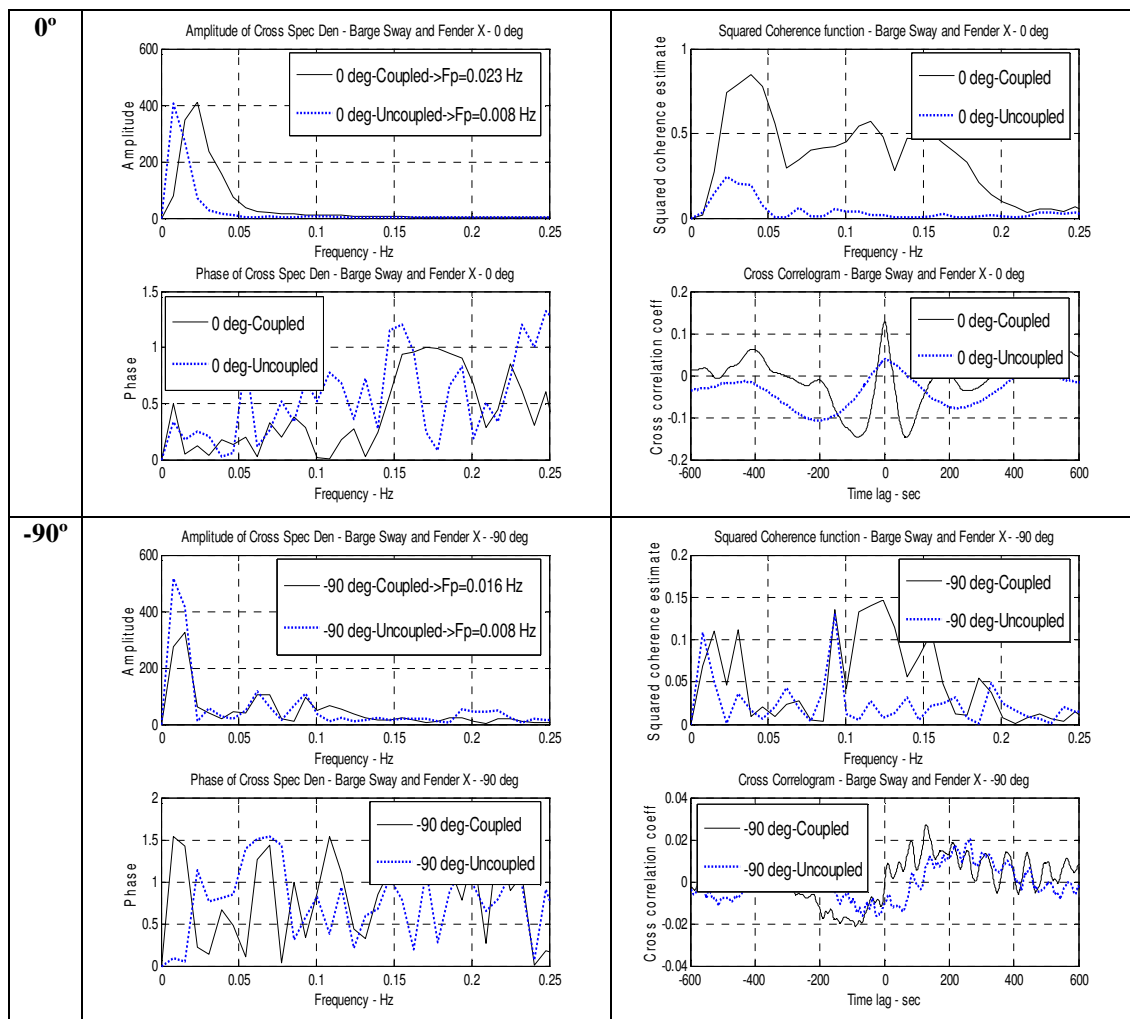
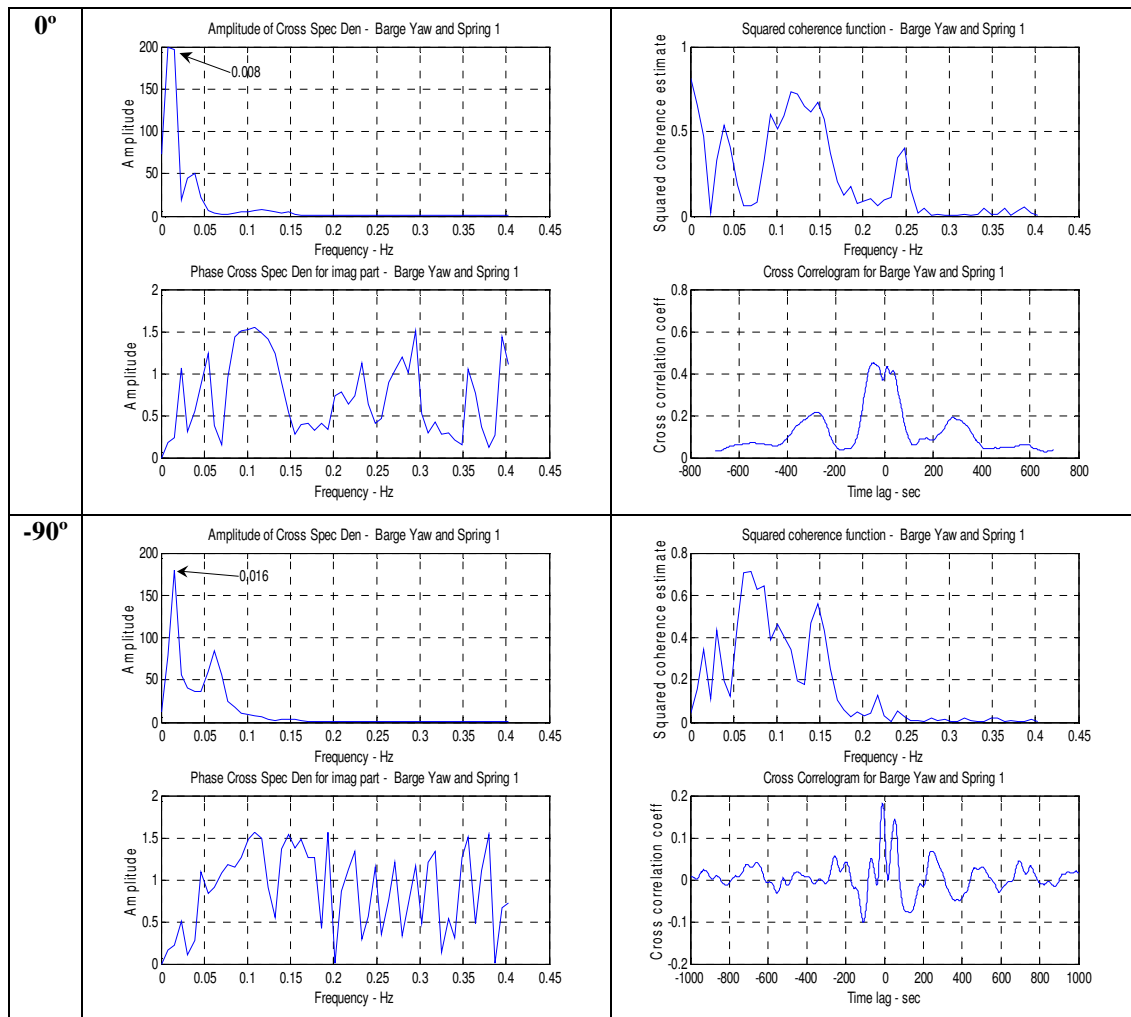Fig. B-11. Cross spectral analysis: barge sway and fender X force
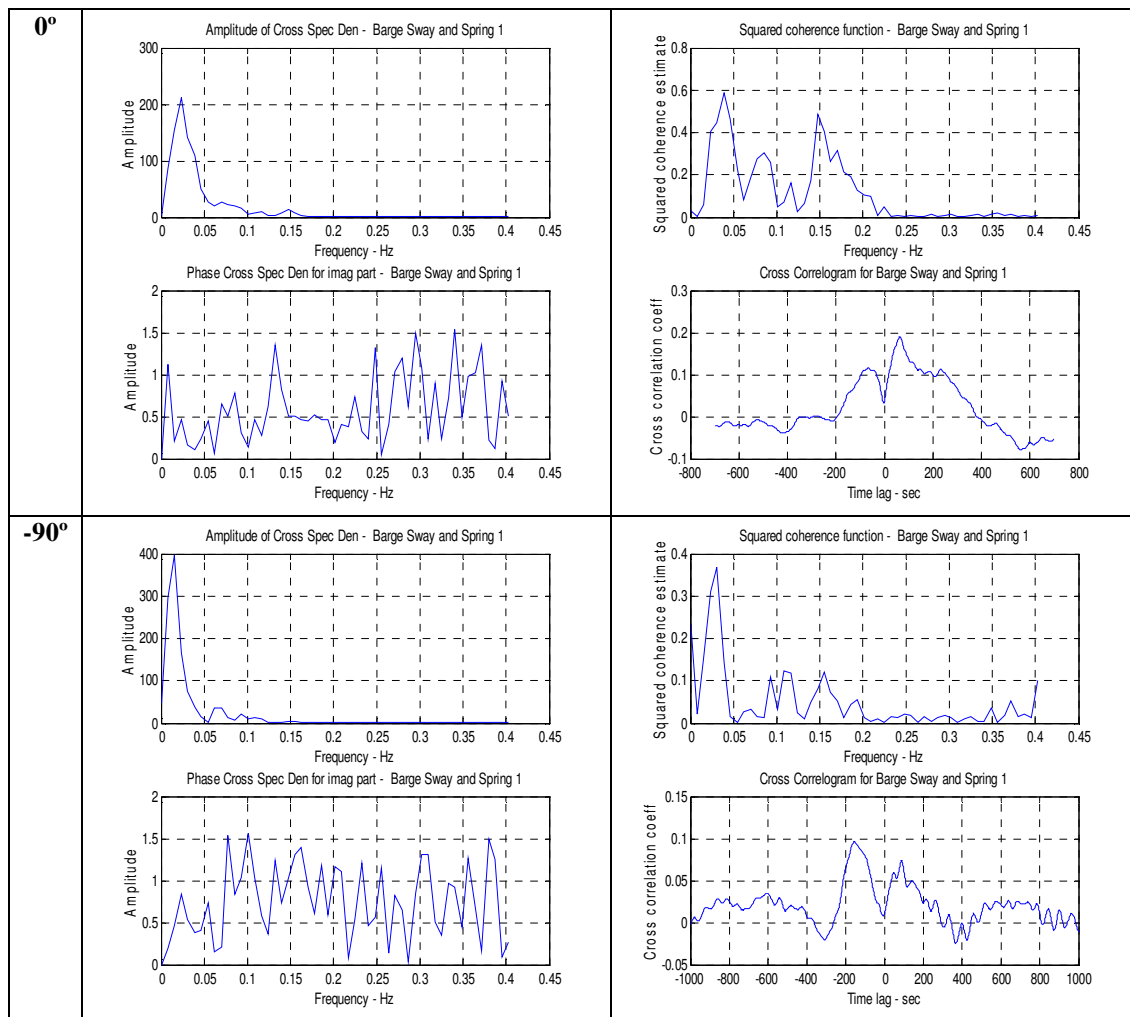
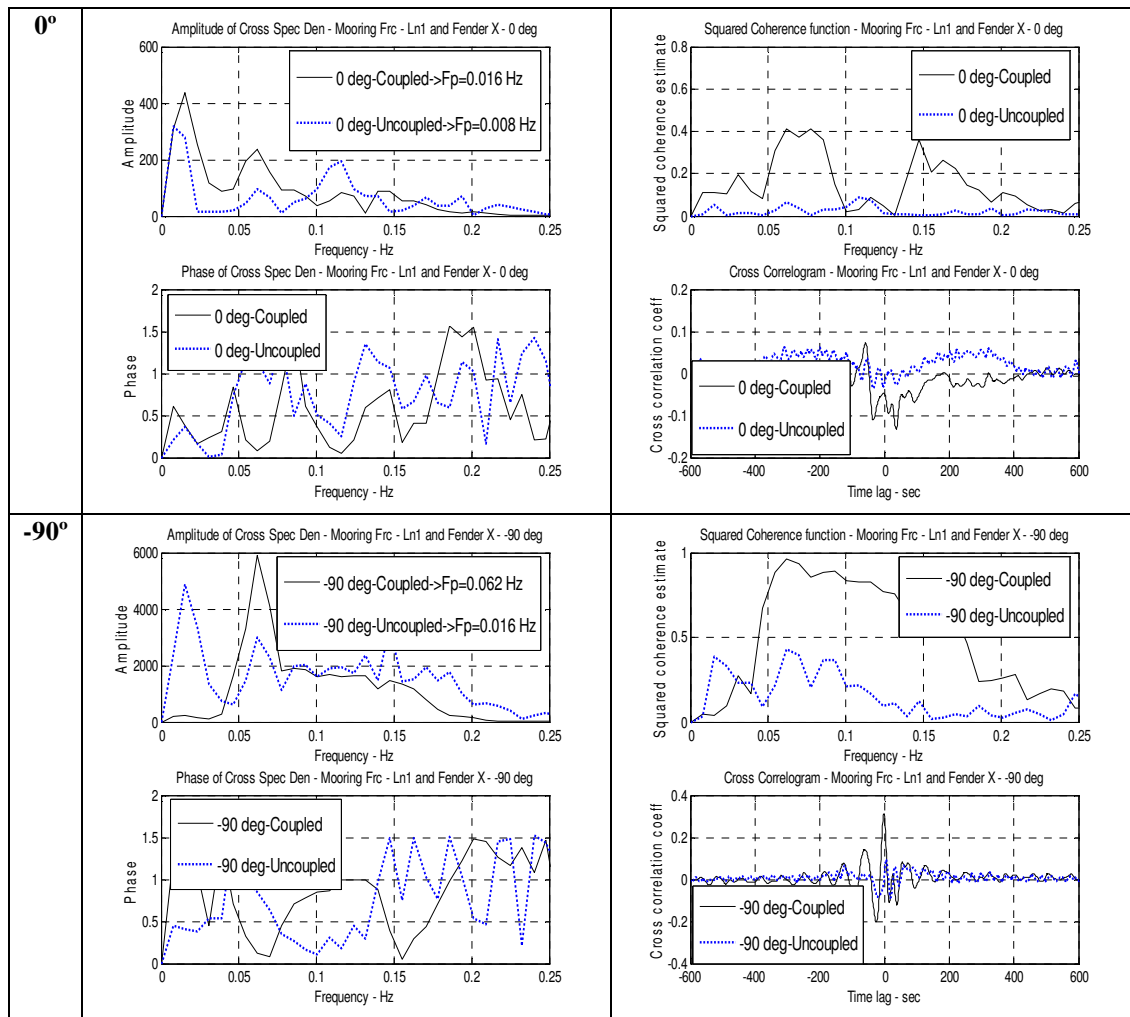Fig. B-12. Cross spectral analysis: barge sway and spring 1 force
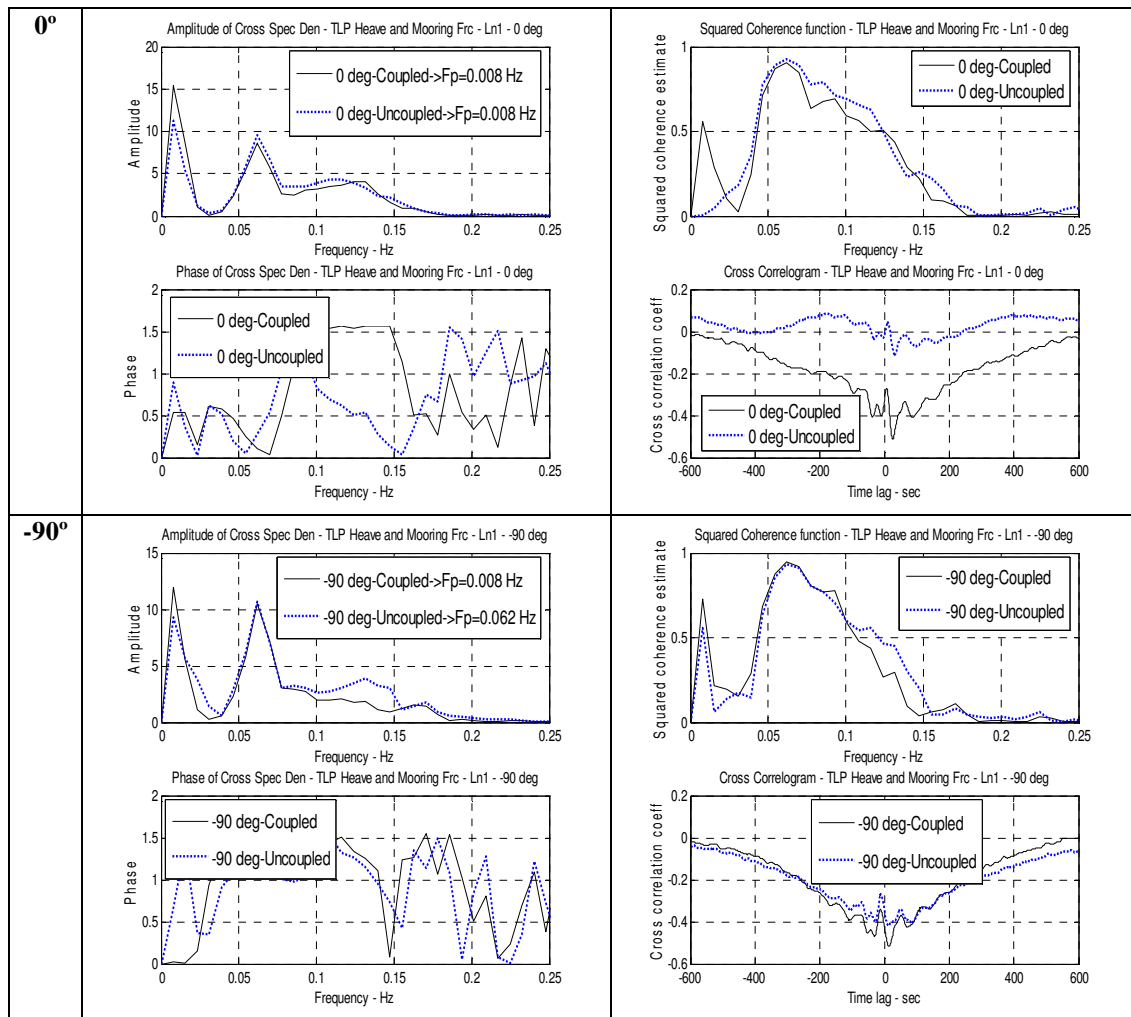
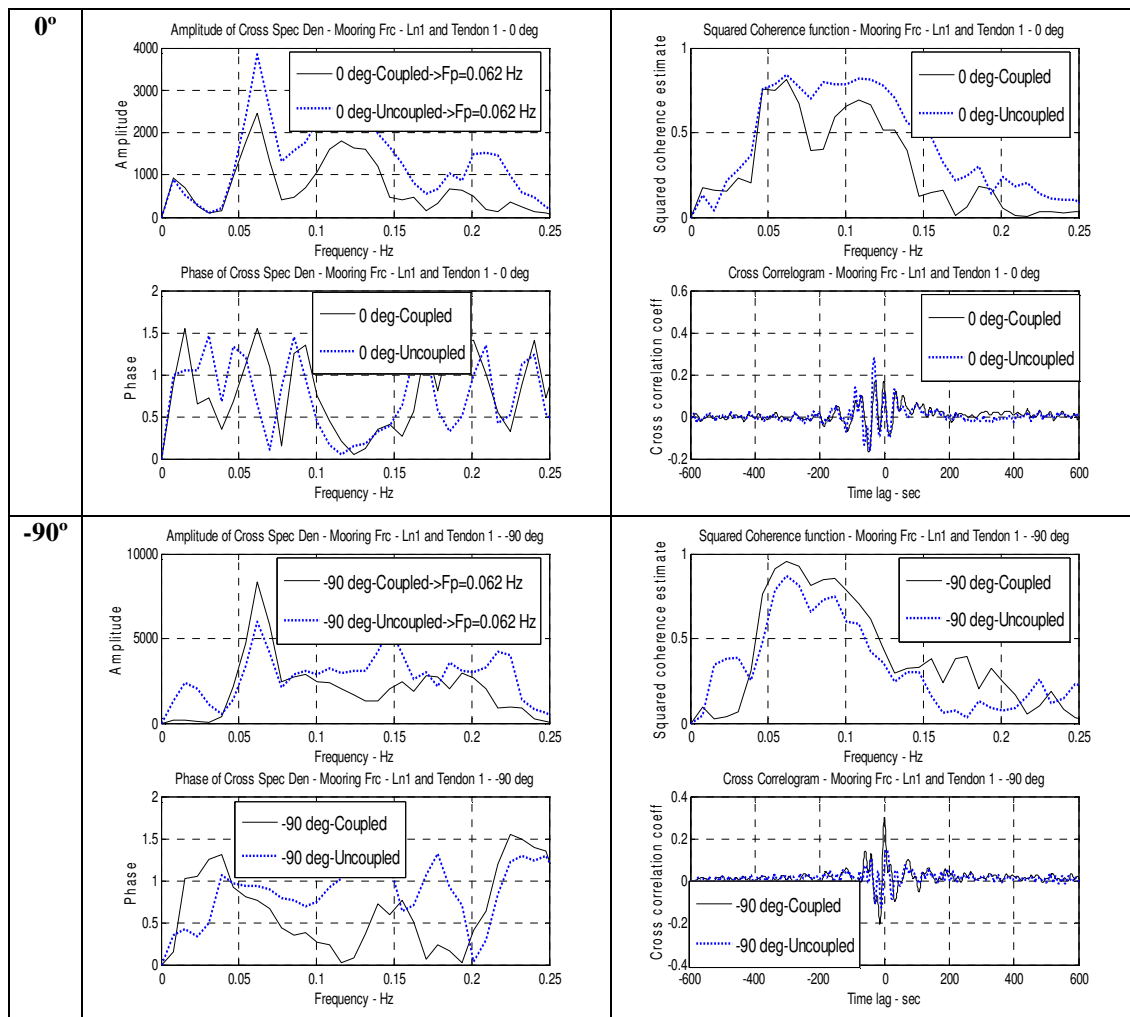Fig. B-13. Cross spectral analysis: TLP heave and mooring line 1 tension
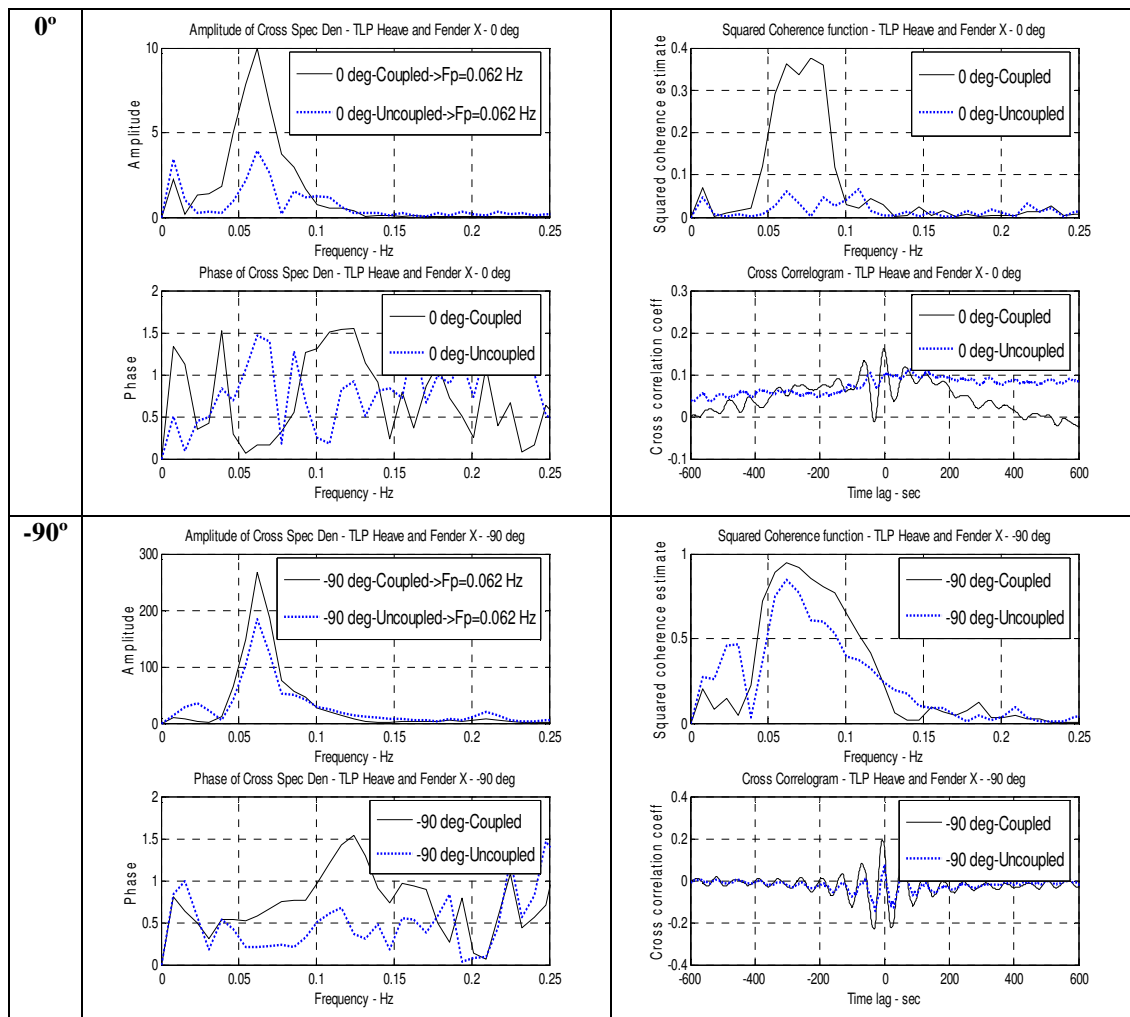
Fig. B-14. Cross spectral analysis: TLP heave and fender X force
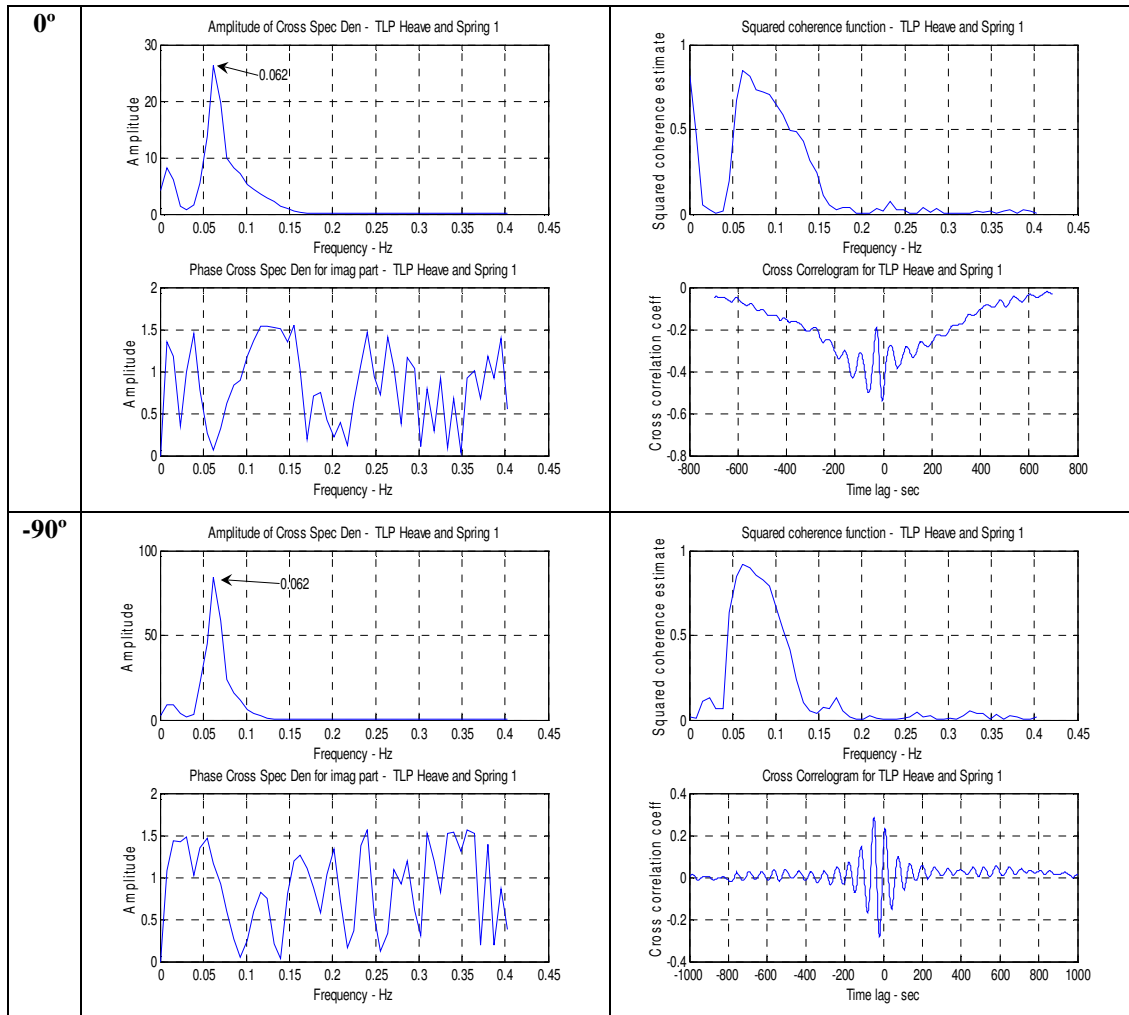
Fig. B-15. Cross spectral analysis: TLP heave and spring 1 force
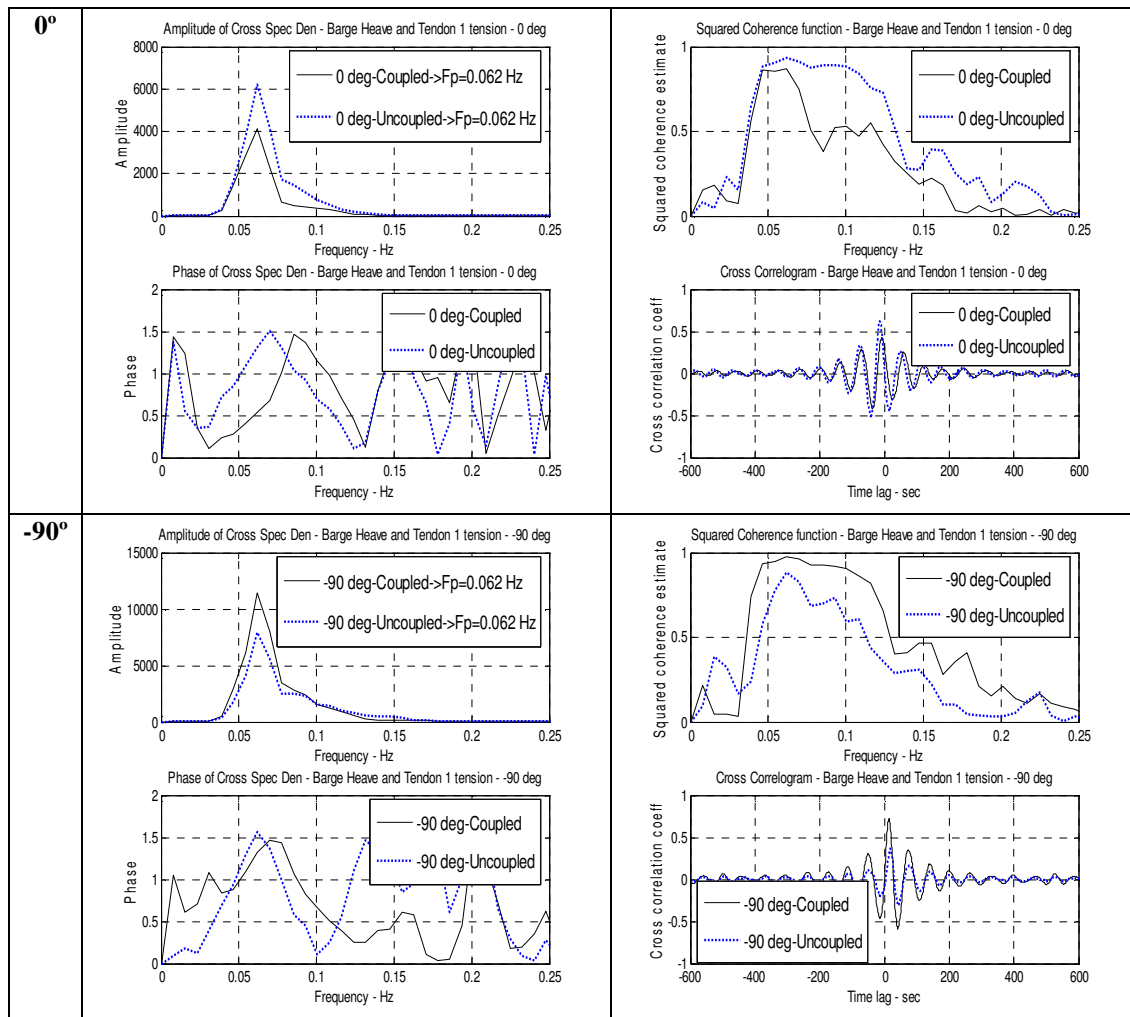
Fig. B-16. Cross spectral analysis: barge heave and tendon 1 tension
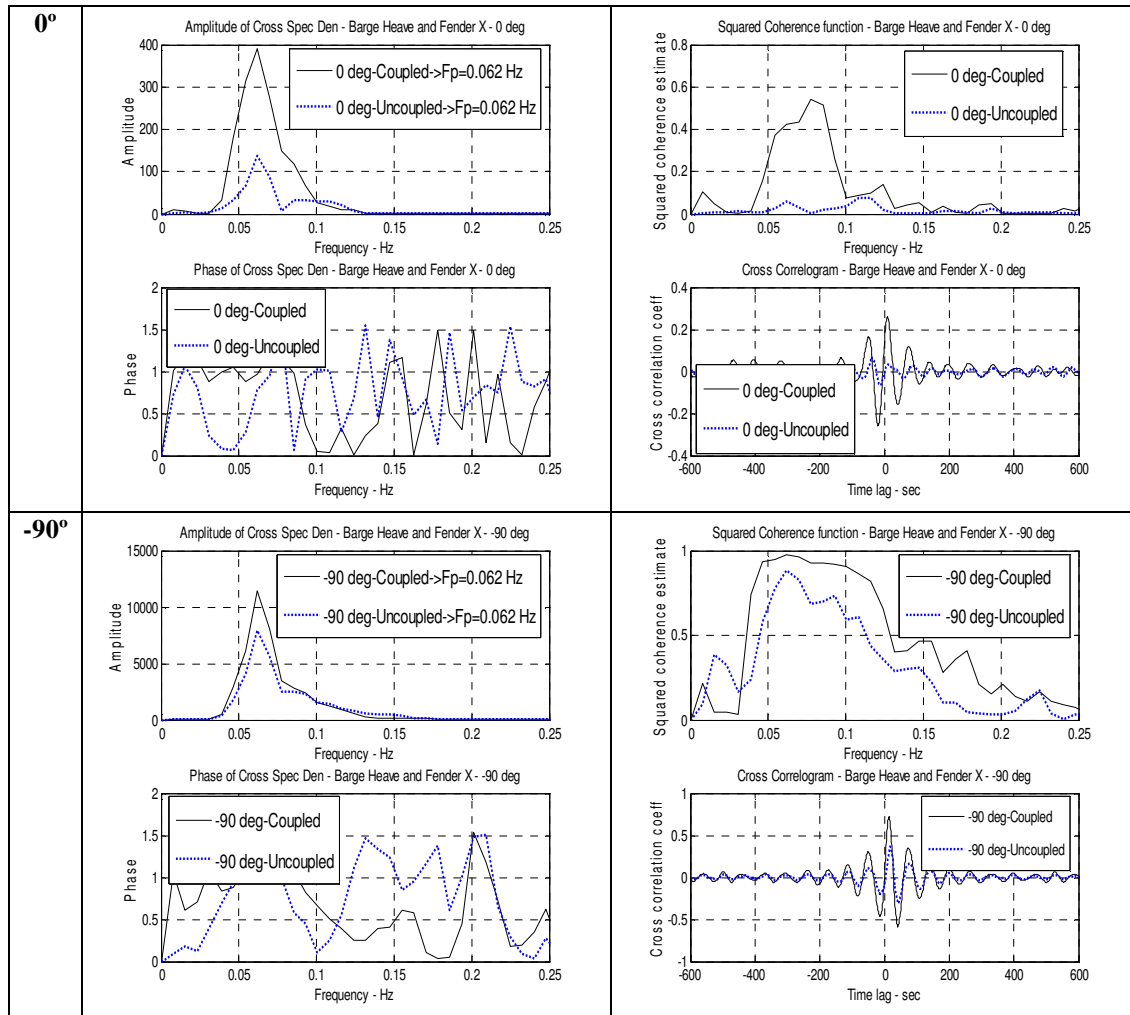
Fig. B-17. Cross spectral analysis: barge heave and fender X force
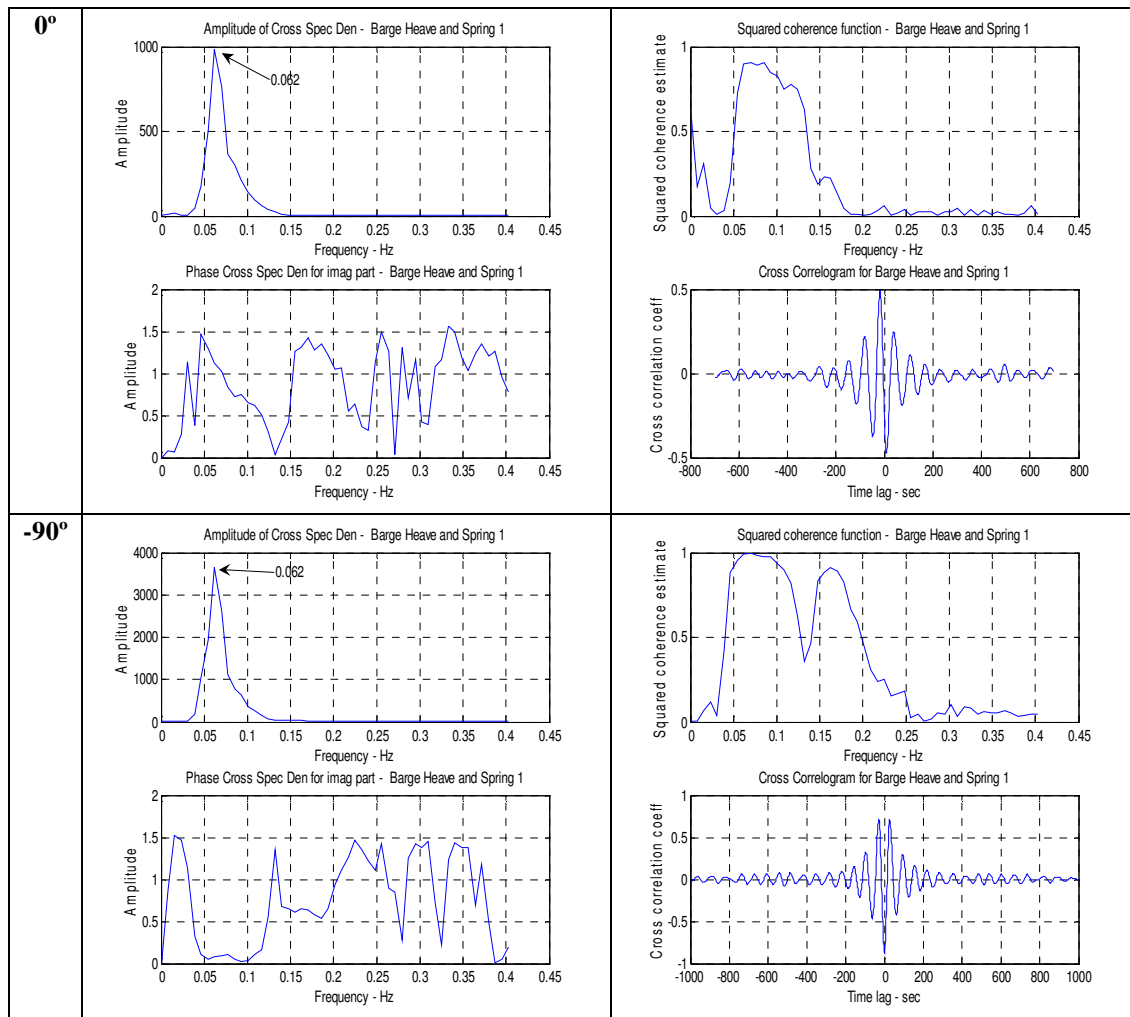
Fig. B-18. Cross spectral analysis: barge heave and spring 1 force
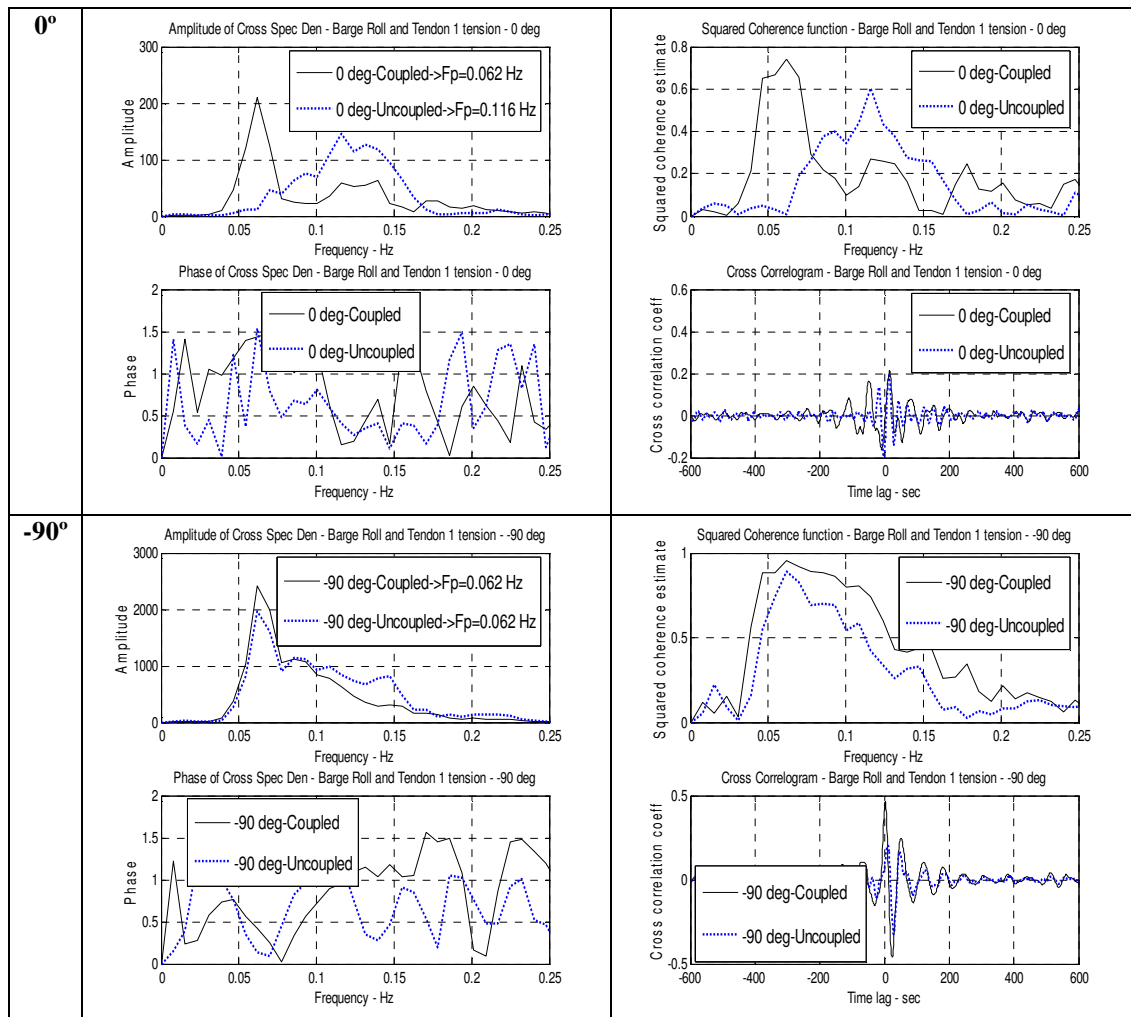
Fig. B-19. Cross spectral analysis: barge roll and tendon 1 tension
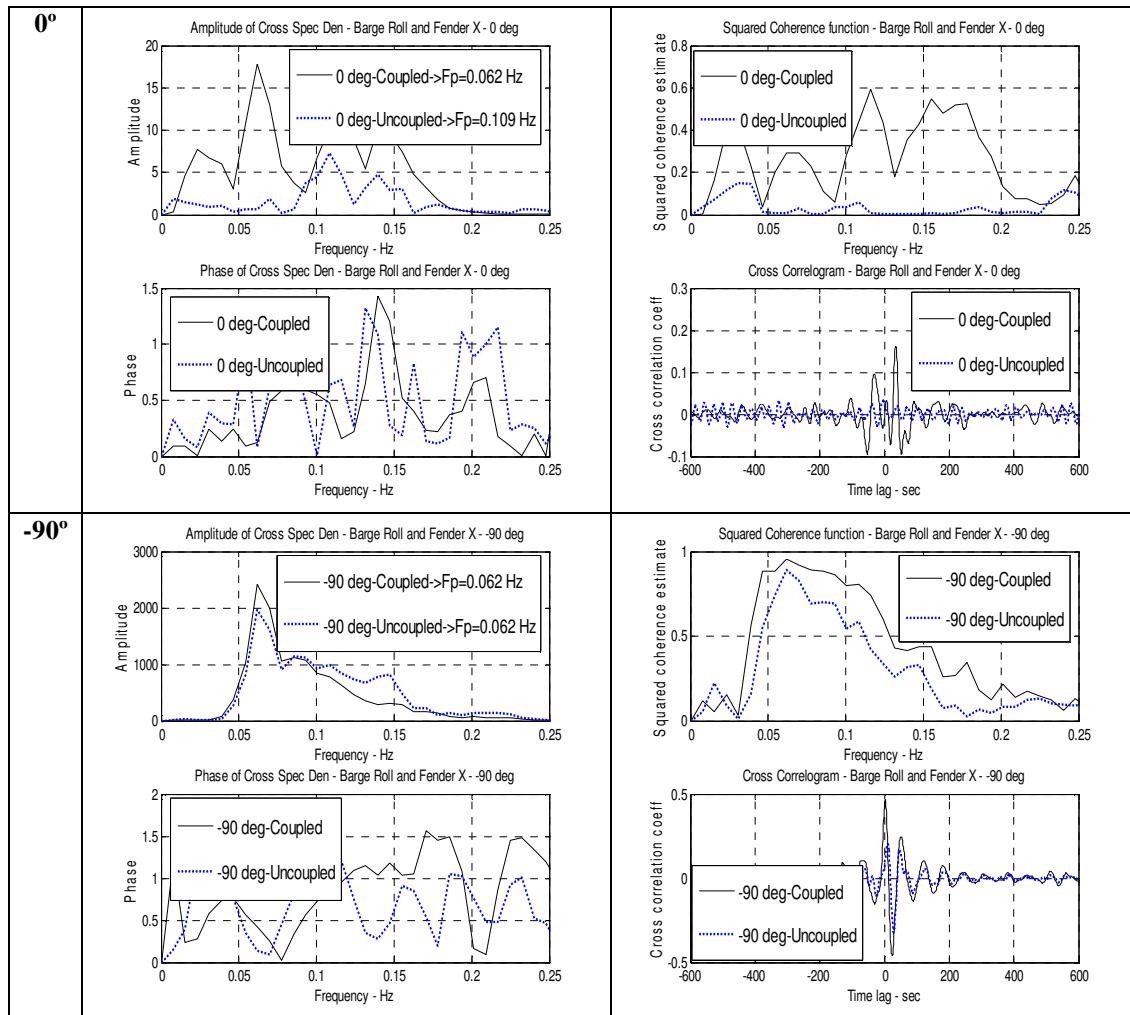
Fig. B-20. Cross spectral analysis: barge roll and fender X force
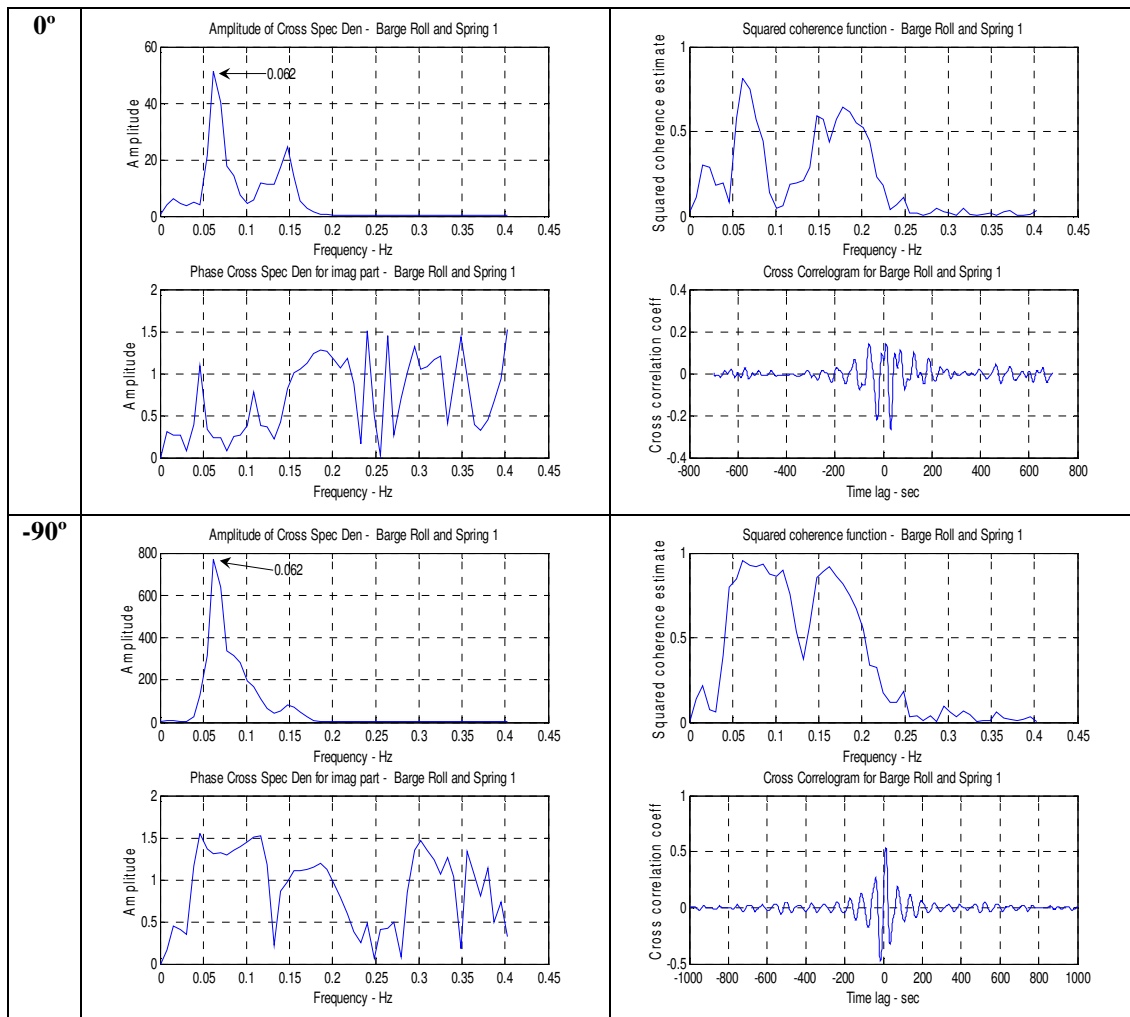
Fig. B-21. Cross spectral analysis: barge roll and spring 1 tension
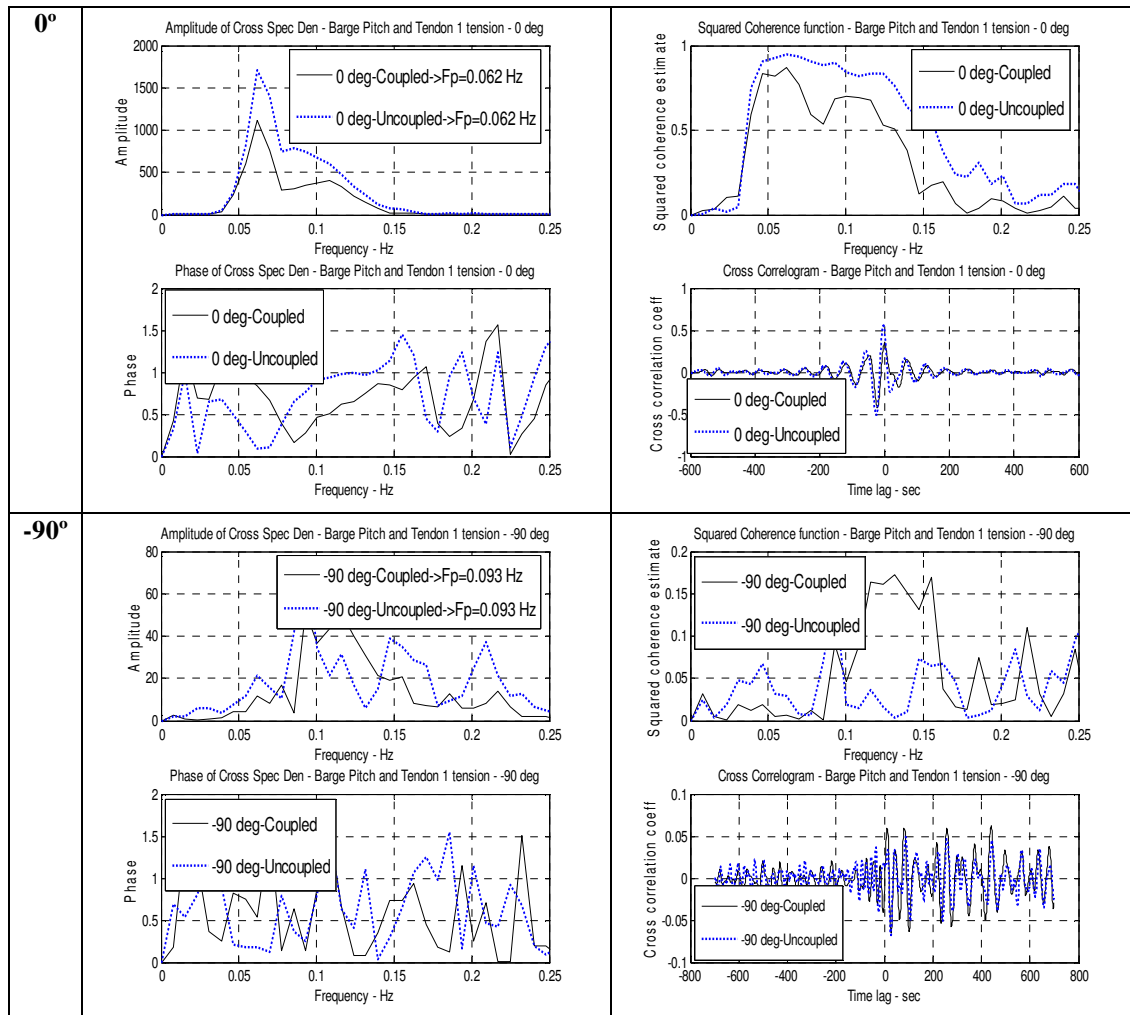
Fig. B-22. Cross spectral analysis: barge pitch and tendon 1 tension

Fig. B-23. Cross spectral analysis: barge pitch and fender X force

Fig. B-24. Cross spectral analysis: barge pitch and spring 1 force

Fig. B-25. Cross spectral analysis: barge yaw and tendon 1 tension

Fig. B-26. Cross spectral analysis: barge yaw and fender X force

Fig. B-27. Cross spectral analysis: barge yaw and spring 1 force

Fig. B-28. Cross spectral analysis: mooring line 1 tensions and fender X force

Fig. B-29. Cross spectral analysis: mooring line 1 and tendon tensions
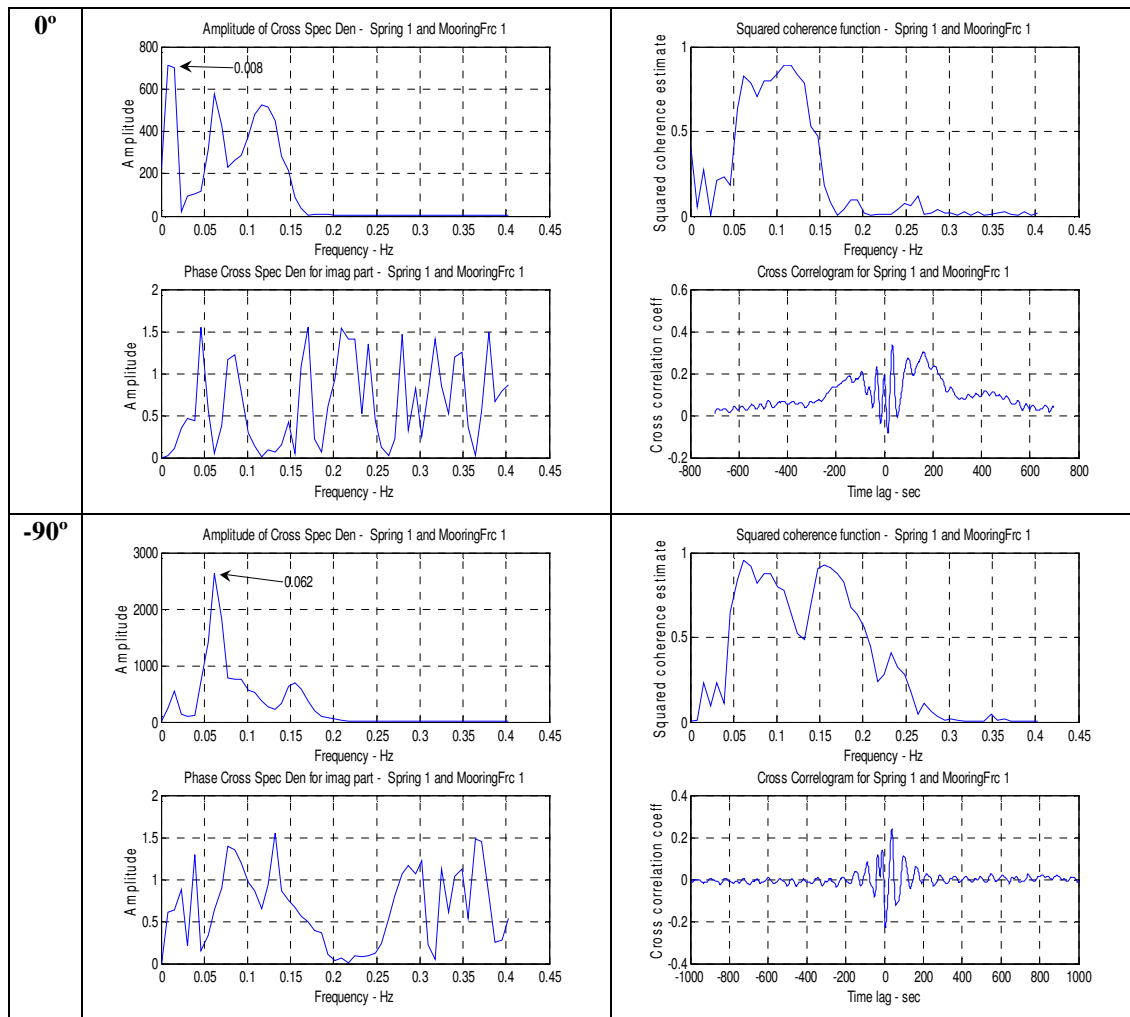
Fig. B-30. Cross spectral analysis: spring 1 force and mooring line 1 tension
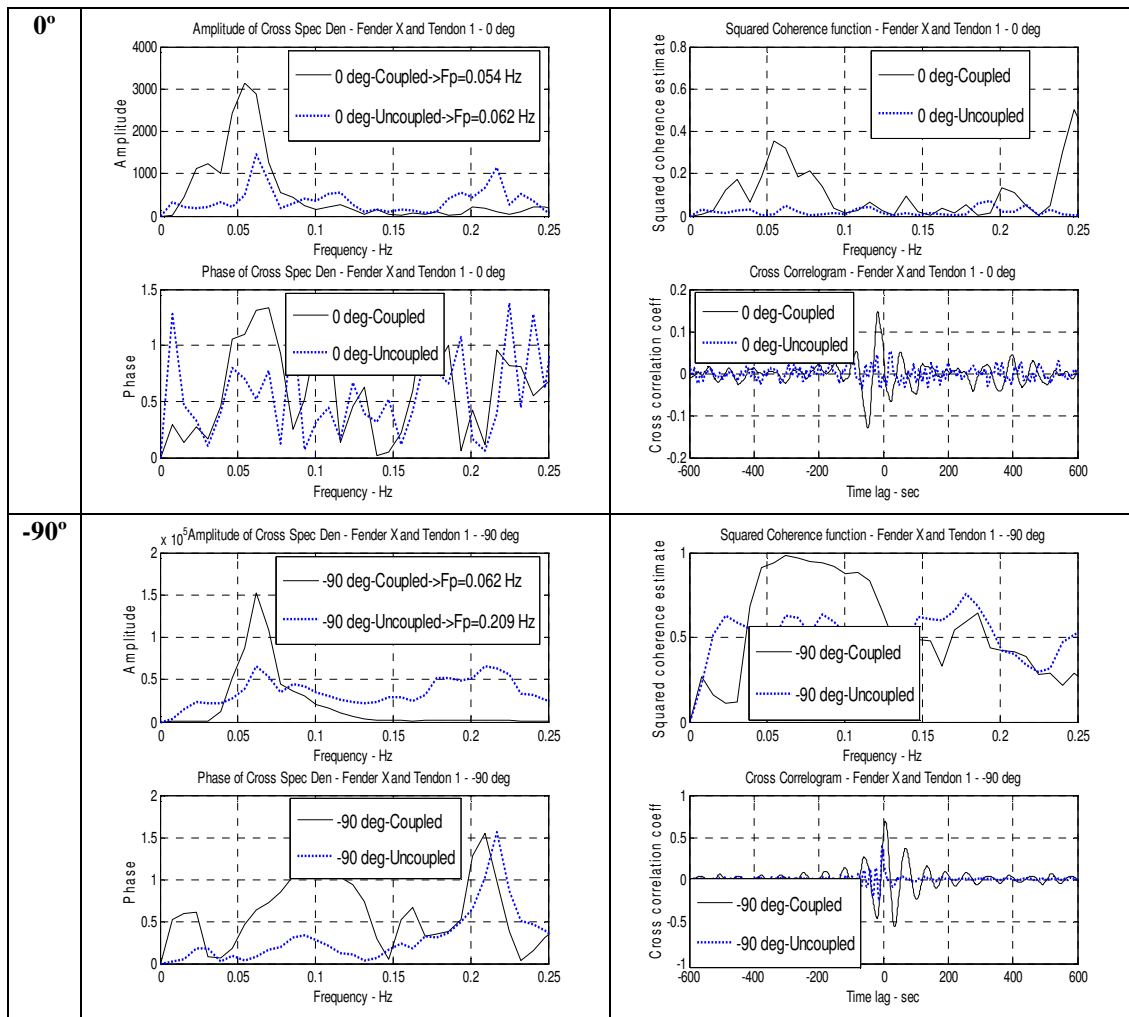
Fig. B-31. Cross spectral analysis: fender X force and tendon 1 tension
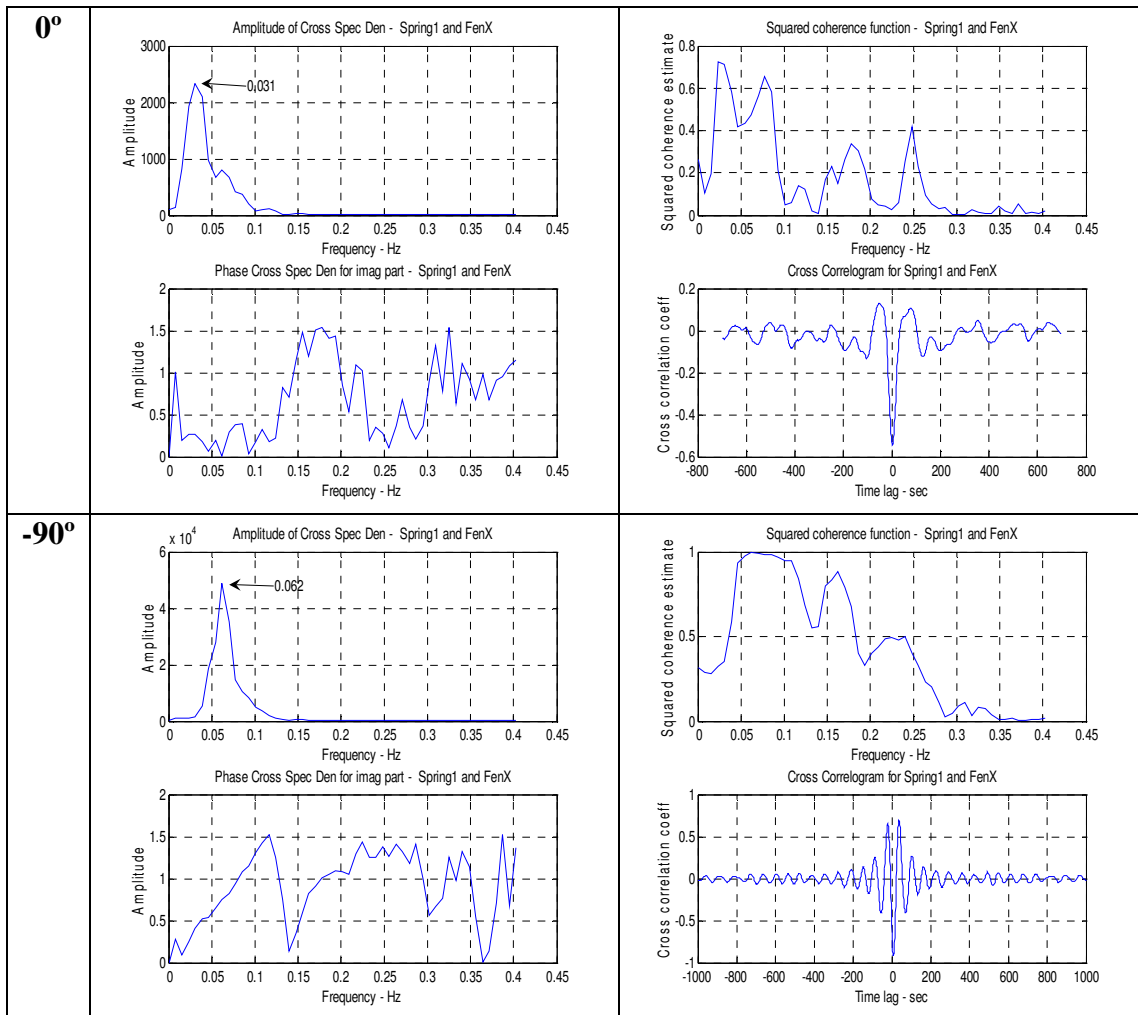
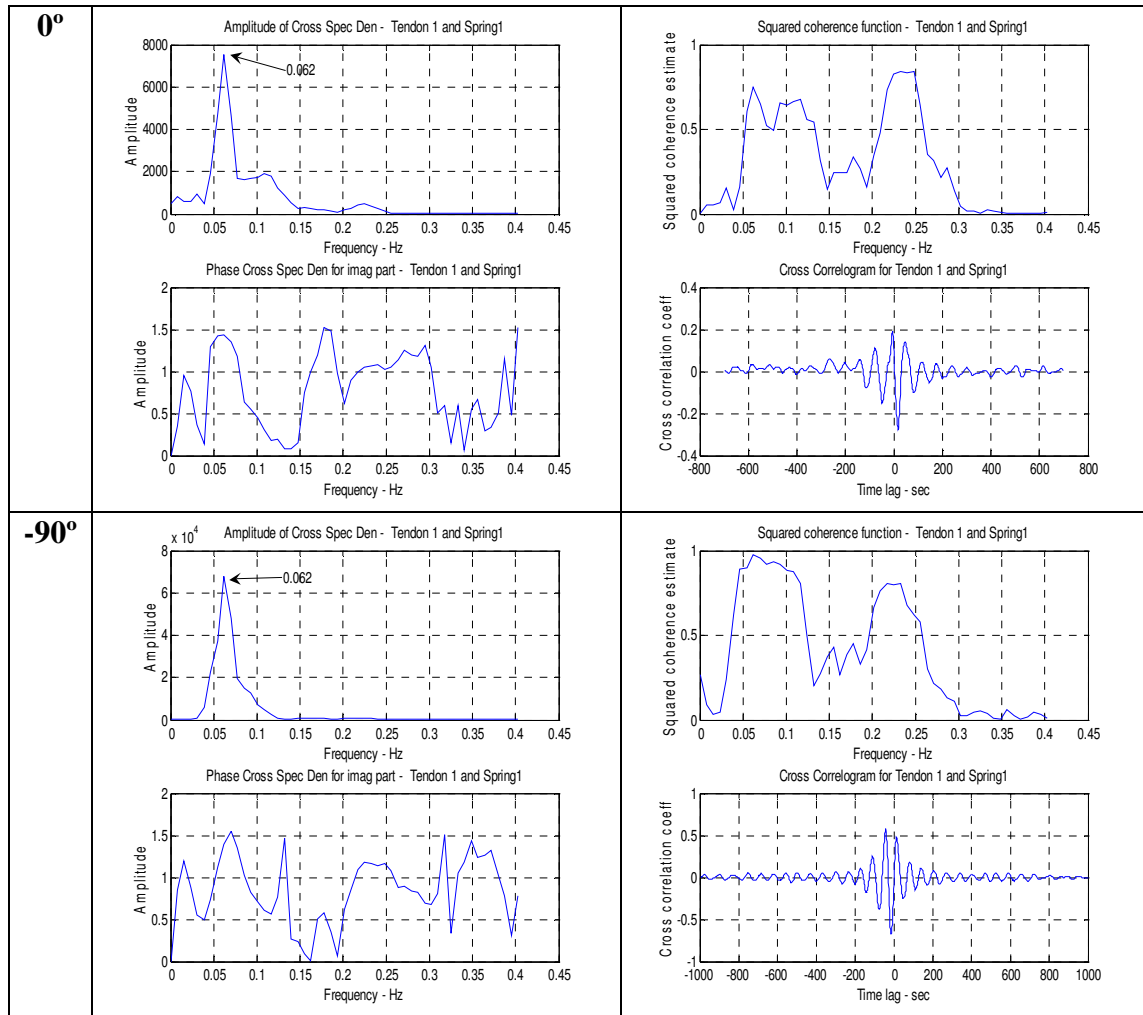Fig. B-32. Cross spectral analysis: fender X force and spring 1 force

Fig. B-33. Cross spectral analysis: tendon 1 tension and spring 1 force
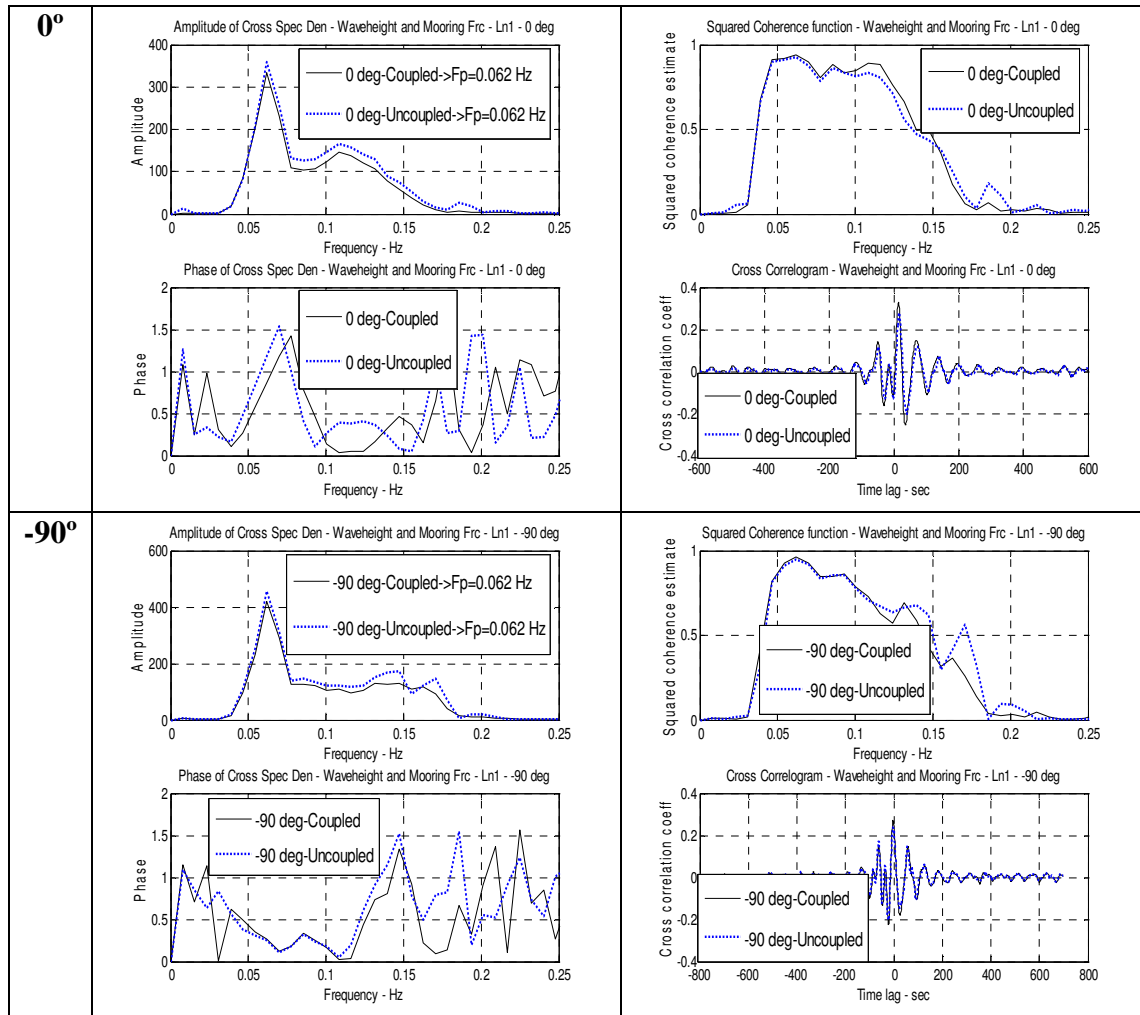
Fig. B-34. Cross spectral analysis: waveheight and mooring line 1 tension
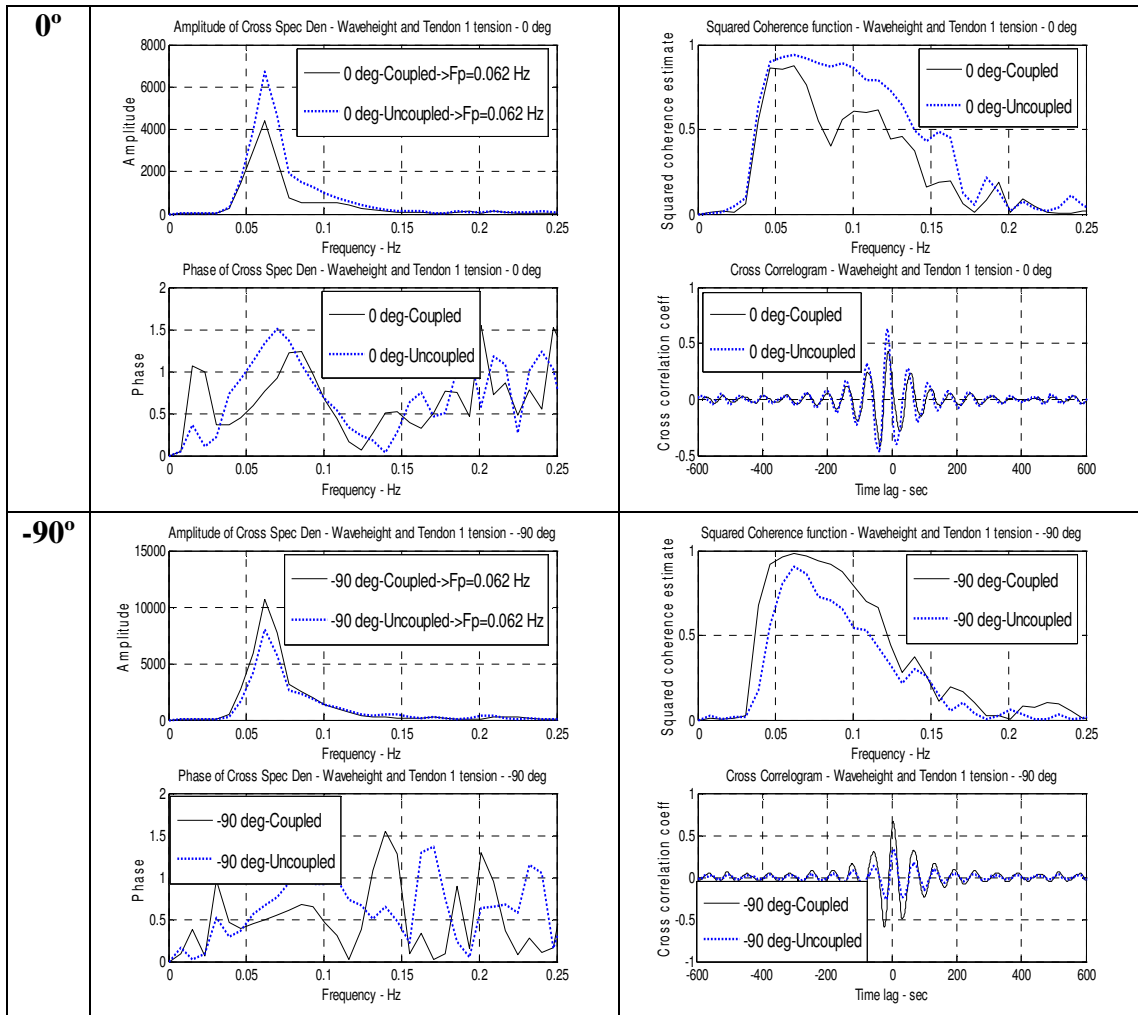
Fig. B-35. Cross spectral analysis: waveheight and tendon 1 tension
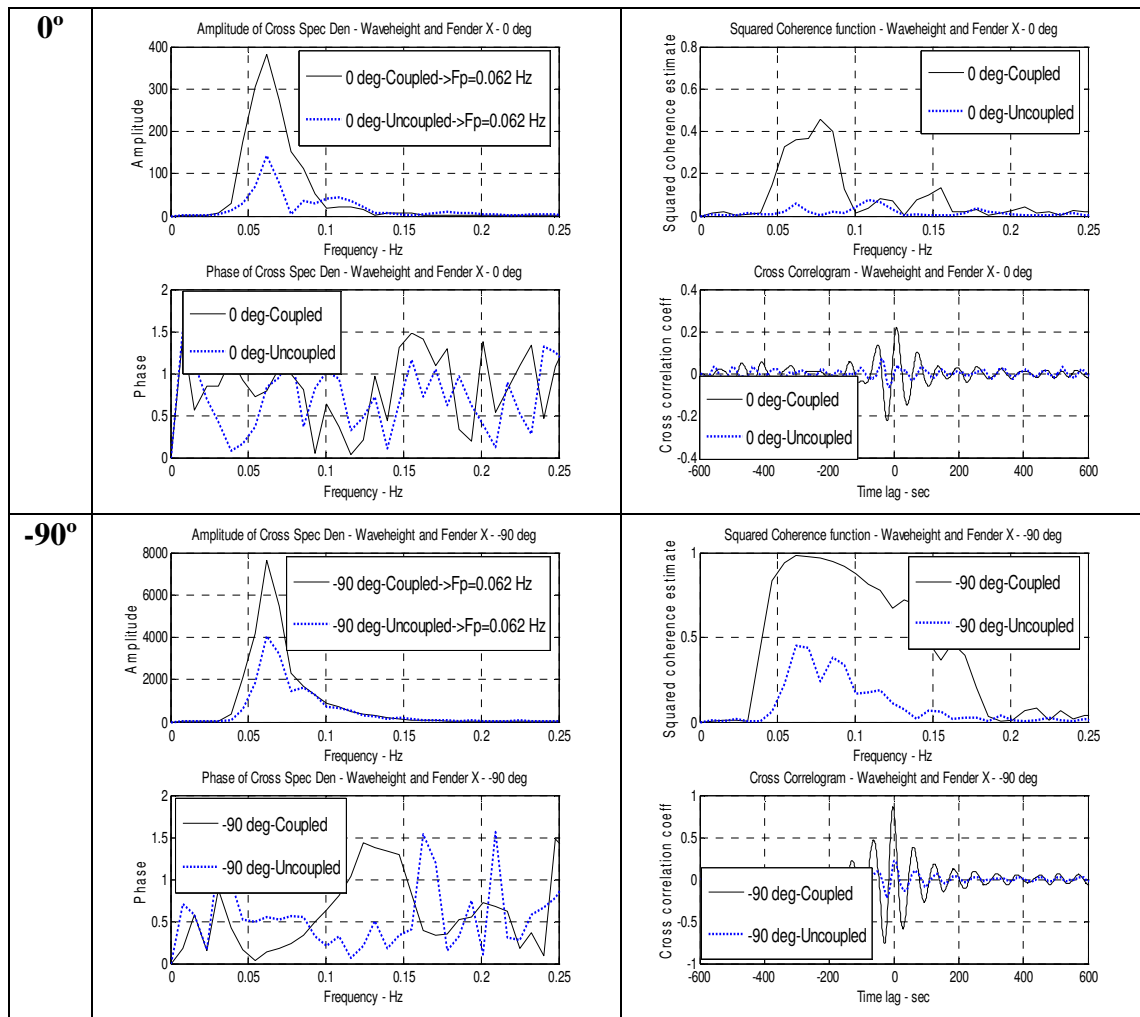
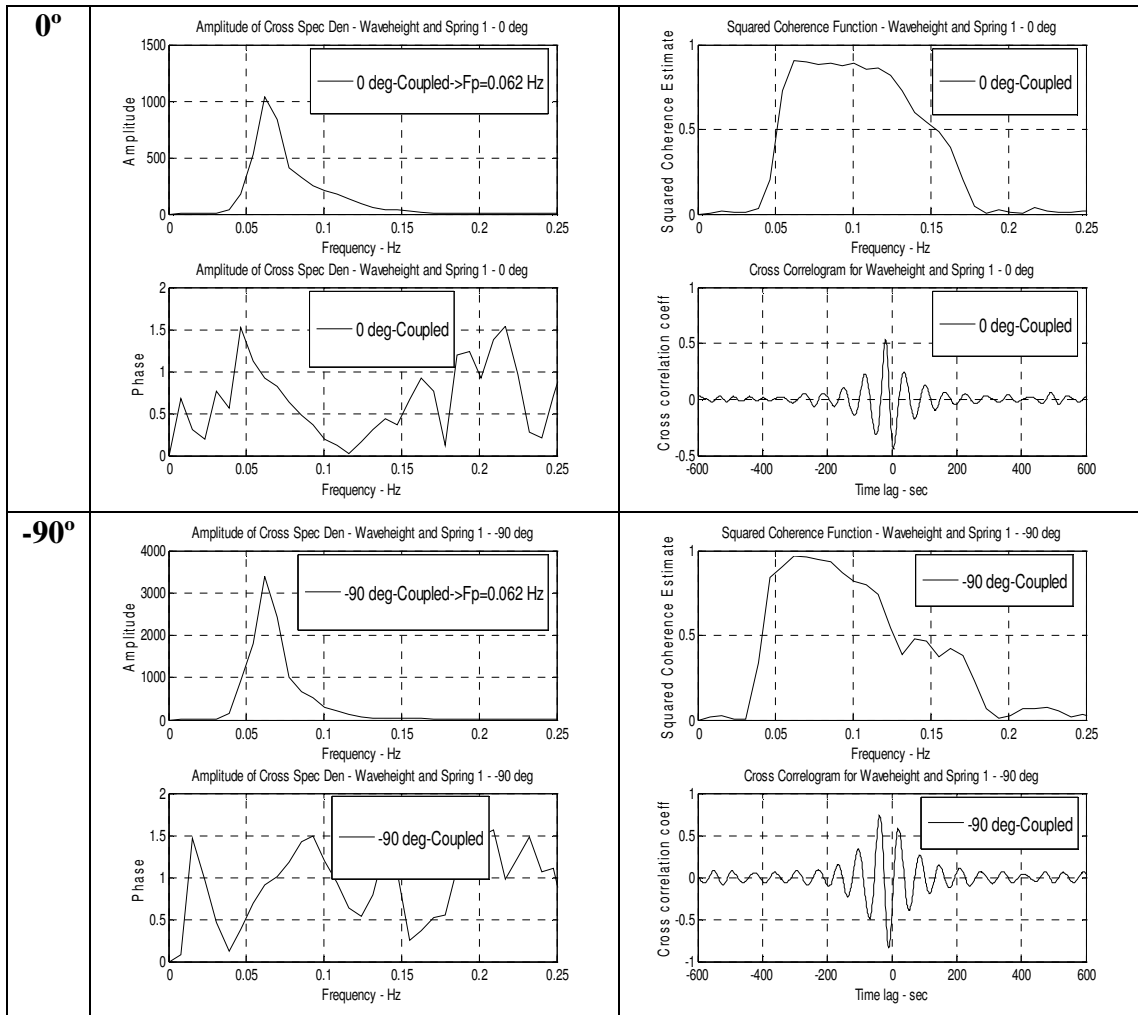Fig. B-36. Cross spectral analysis: waveheight and fender X force

Fig. B-37. Cross spectral analysis: waveheight and spring 1 force

VITA

Harish Girija Sasidharan Pillai

ADDRESS

15211 Park Row, Apartment #1322
Houston, TX 77084

Email: harishspillay@yahoo.co.in

EDUCATION

- Master of Science. Graduation date: August 2005
  Major: Ocean engineering
  Texas A&M University

- Bachelor of Technology. Graduation date: June 2001
  Major: Naval architecture and ship building
  Cochin University of Science and Technology

EXPERIENCE

- Texas A&M University, College Station, Texas (December 2002 - August 2003)
  Research Assistant for Dr. John Niedzwecki

- Zentech Inc., Mumbai (June 2002 – December 2003)
  Naval Architect

- Tata Consultancy Services (December 2001 – June 2002)
  Software Engineer